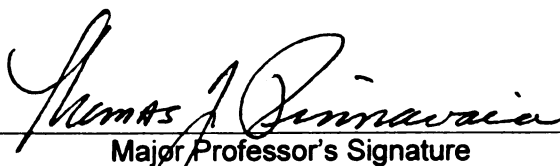This is to certify that the
dissertation entitled

ORGANIC-MODIFIER-FREE PATHWAYS FOR THE
PREPARATION OF POLYMER – METAL OXIDE
NANOCOMPOSITES

presented by
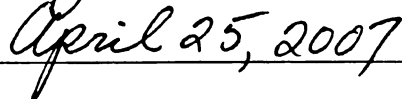
SIQI XUE

has been accepted towards fulfillment
of the requirements for the

Ph.D.   degree in   Chemistry

_____
Major Professor's Signature

April 25, 2007
_____
Date

PLACE IN RETURN BOX to remove this checkout from your record.
TO AVOID FINES return on or before date due.
MAY BE RECALLED with earlier due date if requested.

DATE DUE	DATE DUE	DATE DUE

ORGANIC-MODIFIER-FREE PATHWAYS FOR THE PREPARATION OF POLYMER – METAL OXIDE NANOCOMPOSITES

By

Siqi Xue

A DISSERTATION

Submitted to
Michigan State University
in partial fulfillment of the requirements
for the degree of

DOCTOR OF PHILOSOPHY

Department of Chemistry

2007

ABSTRACT

ORGANIC-MODIFIER-FREE PATHWAYS FOR THE PREPARATION OF POLYMER – METAL OXIDE NANOCOMPOSITES

By

Siqi Xue

Novel preparation strategies for the formation of polymer – metal oxide nanocomposites have been developed to eliminate the need for surface organic-modifiers and thereby to avoid the disadvantages of the modifiers, such as their plasticizer effects and low thermal stabilities. The success of these strategies relies on the smart design of the synthetic or naturally occurring metal oxides and the composite preparation methodology.

Synthetic clay materials exhibit high purity, uniform surface properties and composition, and are promising substitutes for natural clay minerals with more variable properties. We synthesized three types of saponite-like silicates with different octahedral sheet compositions and different layer stacking orders depending on synthesis methodology. When bis(triethoxylsilyl) methane was used as the Si source, an inorganic-organic hybrid clay material, which had $-CH_2-$ tetrahedra bridging groups in the basal plane, was achieved.

Among the synthetic saponites, an irregularly stacked derivative (denoted SAP) was examined as an epoxy polymer reinforcing agent. SAP exhibited a large surface area (920 m^2/g), small lateral dimension (20 - 30 nm), irregularly stacked layered morphology with porous surfaces, which allowed polymer

intercalation without any surface modifications. A Uniform dispersion of SAP nano-aggregates was achieved for the epoxy – SAP nanocomposites, providing improved strength, modulus and toughness of the polymer. For example, for a glassy epoxy system, a 10% by weight loading of SAP provided a 10% increase in strength, 30% increase in modulus and 45% increase in toughness, compared with the pristine polymer. In addition, the nanocomposites had the same glass transition temperature as the pristine epoxy, because the plasticizer effects of the organic modifiers were avoided.

Palygorskite, a silicate clay with a pleated 2:1 layered structure, has a lath-like particle morphology, and low surface charges that make it an attractive candidate for the formation of polymer nanocomposites. The pristine clay mineral provided reinforcement to epoxy matrix without organic modification. The silylated derivatives of palygorskite provided better dispersions in rubbery epoxy matricx than the pristine mineral, affording further improvements in mechanical properties, especially at low loadings levels of 2 and 5 % (w/w).

Mesostructured silicas with pore sizes larger than 20 nm allowed polyethylene intercalation in the porous regions without silica surface modifications. Even with an inhomogeneous dispersion of mesoporous silica, the polymer mesocomposites exhibited improvement in tensile strength and modulus that were analogous with those achieved in polyethylene – clay systems where extensive modifications were required.

ACKNOWLEDGEMENT

I would first like to express my appreciation to Prof. Thomas J. Pinnavaia for his thoughtful guidance during the five years of my Ph.D. study. Prof. Pinnavaia has been my role model of not only an erudite scientist, but also a great person. I feel extremely lucky to be his student.

I would also like to thank former and current group members. Discussions with Dr. Kim, Dr. Liu, Dr. Reinholdt and Dr. Zhang have always been very inspiring and helpful whenever I met problems during research. Dr. Park had great patience in teaching me various techniques to get started in research when I just joined the group. My friendship with Emily, Hua, Jainisha and Xin extended outside the lab, and we went for movies, dinners and shopping together. Christian, D.K., Hui, Joel are all great person to work with. My close friend Shujuan has been like my sister. I am also very grateful for the staff members in the Composite Materials and Structure Center and Microcopy Center at Michigan State University for teaching me how to use their facilities.

I would like to dedicate this humble thesis to my parents, Mr. Ligen Xue and Mrs. Xue, Xiuhua Shi. I could not have completed my Ph.D. degree without their love and support.

TABLE OF CONTENTS

CHAPTER 1
AN OVERVIEW OF POLYMER – CLAY NANOCOMPOSITES

CHAPTER 2
SYNTHESIS OF SAPONITE-LIKE PLATEY SILICATES AND THEIR
INORGANIC-ORGANIC HYBRID DERIVATIVES

CHAPTER 3
Porous Synthetic Smectic Clay for the Reinforcement of Epoxy Polymers

CHAPTER 6
CONCLUSIONS AND FUTURE DIRECTIONS

LIST OF TABLES

LIST OF FIGURES

CHAPTER 1

AN OVERVIEW OF POLYMER – CLAY NANOCOMPOSITES

1.1 Introduction

When a polymer materials is reinforced by a particle that is nanometric in at least one dimension, the resulting polymer composite usually exhibits remarkable improvements in material properties relative to the pristine polymers or conventional composites. Nanocomposites can be divided into three categories depending on whether the filler has one, two, or three dimensions in the nanometer range. Smectic clay minerals in exfoliated form are representative of the first type of nanoparticle filler, since the silicate sheets are 1-nm thickness, but up to several microns in diameter.

Polymer - clay nanocomposites (PCNs) have been extensively studied ever since Toyota researchers first reported the nylon - exfoliated montmorillonite (MMT) nanocomposites with improved mechanical properties (Figure 1.1) [1-14]. What makes clay minerals promising fillers to complement the drawbacks of conventional polymer materials is the unique combination of the properties of clay, such as the high stiffness and modulus, thermal stabilities, and low gas permeabilities. Additionally, clays are inexpensive and abundant natural minerals. The unique properties of clay can be transferred into polymer

1

composites only when clay sheets are uniformly dispersed in polymer materials on a nanometer length scale. The resulting nanocomposites usually exhibit improved mechanical properties, better thermal stabilities, reduced gas permeability and flammability at clay loadings below 10 wt%, and even below 5 wt%.
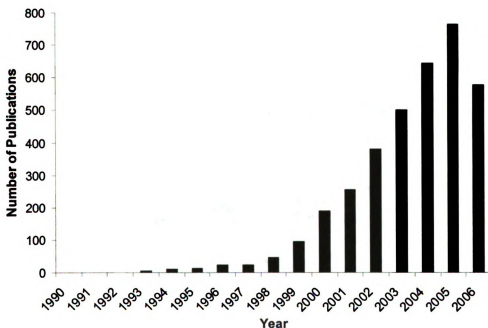
Figure 1.1 The number of publications on "polymer – clay/layered silicate composites" from the year 1990 to 2006.

The commonly used clays for the preparation of PCNs belong to the smectite family, which possesses a layered structure where silicate sheets stack due to the electrostatic interactions between negatively charged silicate sheets

2

and exchangeable gallery alkaline or alkaline earth cations (Figure 1.2). Simply adding clays to polymers results in the formation of conventional composites (or microcomposites) that have micrometer-sized clay tactoids dispersed in the polymer phase. However, when clay surfaces are modified and made compatible with polymers, the polymer chains can wet the clay basal surfaces, penetrate into clay galleries and exfoliate the tactoids into nanolayers, forming nanocomposites.

$M^{n+} \bullet nH_2O$

○   Oxygen atoms
●   Hydroxyl atoms
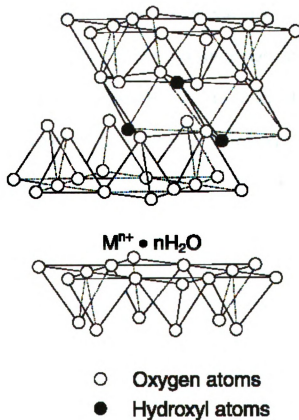
Figure 1.2 Structure of 2:1 phyllosilicates [14].

Two types of dispersed clay structures have been recognized in PCN formation. One is the intercalated state, where the clay gallery heights are expanded to a substantial extend (usually 10 Å or more) by the polymer, but the parallel orientation of the silicate layer, which is characteristic of the initial tactoids, remains in registry upon composites. Such composites generally are referred to as "intercalated nanocomposites", particularly if the clay phase in the nanocomposite exhibits a 001 X-ray reflection indicative of layer stacking. Even when Bragg scattering is not observed due to irregular or very large spacings between nanolayers, transmission electron microscopy can reveal the parallel orientation of the expanded clay galleries, in which case the term "intercalated nanocomposite" may still be appropriate. The other state of clay particle dispersion is the exfoliated state, in which the average separation between nanolayers is very large, usually up to 100 Å or more. An exfoliated clay nanocomposite does not exhibit any X-ray evidence for layer stacking and, ideally, the parallel registry of the nanolayers is lost upon nanocomposites formation, as evidenced by transmission electron microscopy. That is, there are no remnants of the initial tactoid structure of the clay. The distinction between intercalated and exfoliated states is difficult to establish, much less quantify, particularly if the composite provides no X-ray diffraction evidence for layer stacking. In many PCN systems that do not exhibit Bragg scattering for clay, a combination of intercalated and exfoliated clay structures usually are present.

4

Vaia has suggested an expanded classification to describe PCN morphologies on the basis of (1) relative changes in layer spacing and correlation (d and δd, respectively); (2) the relative volume fraction of single layers and layer stacks; (3) the dependence of single-layer separation on silicate volume fraction (φ) above a critical volume fraction for ordering (φ^*) (Figure 1.3) [19]. However, quantifying these states of clay particle dispersion for a particular polymer-clay generally is experimentally difficult, though some progress is being made in this direction.

Extensive experimental and theoretic studies have been carried out on PCNs for engineering applications. The most successful examples of exfoliated PCN are for nylon-6 and epoxy clay nanocomposites prepared via in-situ polymerization [2, 3]. Nylon-clay nanocomposites have been used in under the hood applications in Toyota automobiles. Although great improvements have been made in PCN performance properties, realizing the full potential of these remarkable materials and achieving their commercialization are still challenging tasks. For some non-polar polymers, such as polyolefins, achieving facile exfoliation of clay nanoparticles in the polymer matrix on a commercial scale still is a challenging problem [15-18]. The complexity of PCN systems and the limitations of quantitative structural characterization methods make it difficult to establish morphology – processing – structure – property relationships [1]. Nevertheless, researchers have been developing new strategies in PCN

Unintercalated

Ordered
$d/d_0 < 2\text{-}3$
$\delta d/\delta d_0 \approx 1$

$d_0 \delta d_0$

Intercalated

Disordered
major: $d/d_0 < 2\text{-}3$
$\delta d/\delta d_0 > 1$
minor: $d/d_0 > 3$

Exfoliated

Partically
major: $d/d_0 > 3$
minor: $d/d_0 < 3$
$\delta d/\delta d_0 > 1$

Ordered
$\phi > \phi$
$d \infty \phi^{-1}$

Ordered
$\phi < \phi$
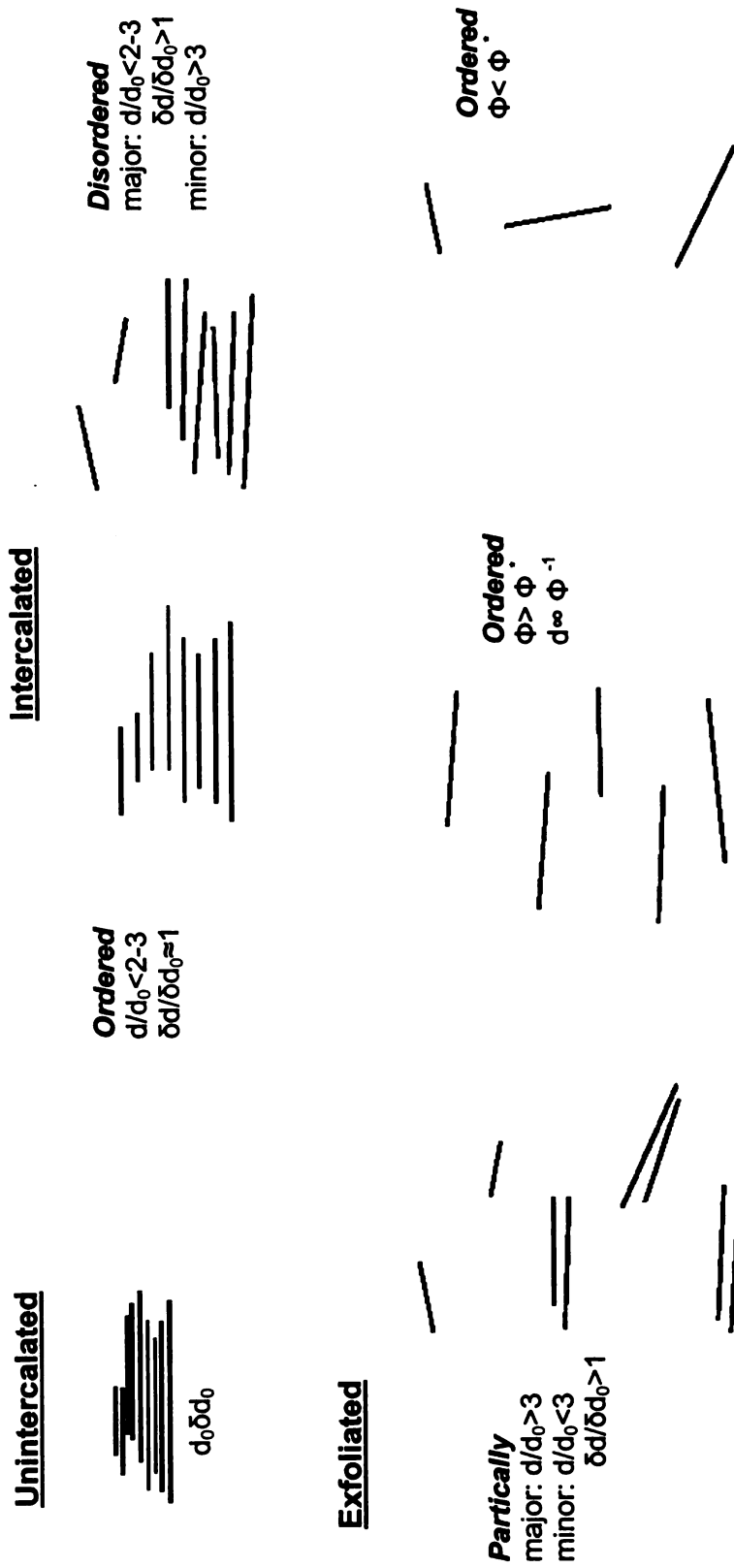
Figure 1.3 Nanoscale arrangements of layered silicates in polymer nanocomposites [19].

6

chemistry to reach a better understanding in this field. Several of these emerging advances, along with additional technical problems facing the field, are outlined below.

1.2 Clay Surface Modification

Smectites are hydrophilic materials, immiscible with most of engineering polymers that are hydrophobic. Additionally, clay layers are closely stacked through electrostatic interactions, with galleries occupied by hydrated alkaline or alkaline earth cations, making it difficult for macromolecule diffusion. Therefore, clays usually require organic modifications prior to the preparation of PCNs. The most commonly used modification method is alkyl-ammonium-ion-exchange. When the inorganic gallery cations are replaced by long-chain alkyl-ammonium cations, not only the clay surfaces become more hydrophobic and, consequently, more compatible with polymers, but also the gallery spaces expand, readily for the intercalation of polymer chains. Depending on the cation exchange capacities (CEC) of clays, the alkyl chain length, alkyl ammonium cations in clay galleries may adopt structures that vary from lateral monolayer-, lateral bilayer-, paraffin-, or lipid-type orientations, in the order of increasing gallery height [20].

While the onium-ion-exchange is widely used as a convenient and effective clay surface modification method, it has several disadvantages. First, the plasticizing effect of the alkylammonium cations may compromise the

benefits of clay nanolayer reinforcement [21, 22]. Second, ammonium cations are susceptible to thermal decompose via Hoffmann degradation mechanism at temperatures above 200 °C, which ares the processing temperature of some engineering polymers, such as polyamide. The degradation of the organic cation will cause the re-stacking of clay nanolayers and a loss of potential benefits [23, 24]. Third, during the preparation of PCN, the gallery alkyl ammonium cations interact with the polymer matrices and clay layers, adding complexicity to the nanocomposite systems [25]. Okamoto and coworkers argued that, in a polylactide (PLA) – clay system that involves organo-clay with a large platelet diameter and CEC value, the alkylammonium surfactant ions on the basal surfaces of the clay form a restricted conformation due to steric limitations and, consequently, hinder polymer intercalation [26].

Alkylimidazolium, alkylphosphonium and alkylpyridinum ions have been used as clay modifiers for the reinforcement of high-melt-temperature engineering polymers, such as polyamide-6 (PA-6), PA-6,6, polyethylene terephthalate (PET) and polycarbonate (PC), as well as polymers bearing medium-melt temperatures, such as polystyrene (PS) and polypropylene (PP) [27-36]. Gilman and coworkers have used different dimethyl alkylimidazolium salts to modify MMT, proving a higher thermal stability of the alkylimidazolium-MMTs compared with alkylammonium-MMTs (Table 1) [34, 36]. The 1,2-dimethyl-3-hexadecyl-imidazolium-MMT was exfoliated in PA-6 via melt-blending

Table 1.1 Thermal stability date for imidazolium- and alkylammonium-MMT [34]

Sample	Organic fraction (±0.05)	Onset decomposition temp (TGA) (°C)	Peak decomposition temp (DTA) (°C)	Change in d-spacing vs NaMMT (nm)
1,2-dimethyl-3-hexadecylimidazolium-MMT	0.25	343	406	0.72
1-decyl-2,3-dimethylimidazolium-MMT	0.17	320	432	0.49
1-butyl-2,3-dimethylimidazolium-MMT	0.13	340	448	0.16
1,2-dimethyl-3-propylimidazolium-MMT	0.13	340	445	0.20
1,2-dimethyl-3-hexadecylimidazolium-FSM	0.24	392	400	0.63
Dimethyldioctadecylammonium bromide	-	221	233	-
Dimehyldioctadecylammonium bromide-MMT	0.36	280	308	1.49
Dimethyl-di(hydrogenated tallow)ammonium-MMT	0.35	200	310	2.00

processes at 300 °C. Dong and coworkers compared the stability of imidazolium-MMT (I-MMT) and ammonium-MMT (A-MMT) as reinforcement agents for PP [29]. Both I-MMT and A-MMT exfoliated in PP upon in-situ polymerization. However, I-MMT exhibited higher thermal stability than A-MMT, whether analyzed as the pristine clay or as the composite form. The phase-structure stability of the nanocomposite was investigated by melt-extrusion at 200 °C for durations varying from 2-10 min. Re-stacking of clay layers was observed for PP – A-MMT nanocomposites, due to the decomposition of alkylammonium modifier, leading to inferior incompatibility between PP and MMT. The structure integrity of PP – I-MMT nanocomposites was maintained during the extrusion. Pyridinium- and imidazolium-based ionic liquids also have been used to modify clay [37, 38].

Silylation of surface silanol groups is a common method to modify glasses and silicates for use in polymer composite formulations. Silylation has also been used for the polymer compatiblilization of smectite clays, layered silicic acids, and silica materials [39, 40]. But this method is seldom used as the sole surface modification technique in PCN studies, because only a small fraction of the hydroxyl groups of a smectite clay are found at the surfaces of the platelet edges. The remaining hydroxyl groups are buried in the second and third atomic planes of the 2:1 layered structure and are unavailable for coupling reactions with silane modifiers. On the other hand, one of the advantages of silylation is that the

treated clay contains less organic components (less than 5 wt%) than organicly exchanged clay (25-45 wt%). Silylation has been used to graft functional groups to organo-clay to improve clay dispersion and material properties of the nanocomposites [40-45]. Bourgeat-Lami and coworkers synthesized organic-inorganic nanocomposite colloids containing Laponite, which was modified by either a monofunctional (γ-methacryloxy propyl dimethyl ethoxylsilane) or a trifunctional (γ-methacryloxy propyl trimethoxysilane) silane coupling agent, via emulsion polymerization [42]. Their results showed that trifunctional silane coupling agents chemically locked the clay platelets into irreversibly stacked nanolayers in tactoid form. However, the Laponite modified by monofunctional silane derivatives can be satisfactorily dispersed in water and was found to cover the styrene-butyl acrylate copolymer latex surface during the preparation of colloids, as shown in Figure 1.4.

It has been realized that unmodified, purely inorganic clays are able to disperse homogeneously in polymers and provide reinforcement, once the surface properties of clays are compatible with polymers. Synthetic clays are commonly used in this area since they usually possess lower aspect ratio than natural clays. Haraguchi and coworkers reported nanocomposite hydrogels containing rubbery poly(2-methoxyethyl acrylate) (PMEA), which is a biocompatible polymer material, and inorganic clay (Laponite) [46]. The composites were made via in-situ polymerization of MEA monomer and Laponite

11

in aqueous solution. The resulting composites were completely transparent and had unique mechanical properties that they can undergo reversible necking deformation of more than 1000%. The authors claimed that, during the polymerization, PMEA monomers aggregated and excluded the hydrophilic clay platelets so that the nanocomposite products were composed of PMEA nanospheres that were covered by clay from the outside. When the composites were under stress, the PMEA core provided the high elongation while clay provided stiffness. More recently, McKinley and coworkers reported high-performance elastomeric nanocomposites of polyurethane-polyether copolymer and Laponite via solvent exchange processing technique [47]. Laponite preferentially dispersed in and interact with the hard microdomains of polyurethane, and, consequently, improved stiff, toughness and heat distortion temperature of the polymer, especially when it reaches the weight loading to form a percolative network. Pinnavaia and coworkers developed a strategy to prepare a porous saponite-like silicate material and to use it to reinforce epoxy polymers [48]. Due to its porous surfaces and irregularly stacked morphology, the synthetic saponite dispersed uniformly in epoxy in the form of nanometric tactoids. The nanocomposites exhibited improved strength, modulus, elongation and toughness.
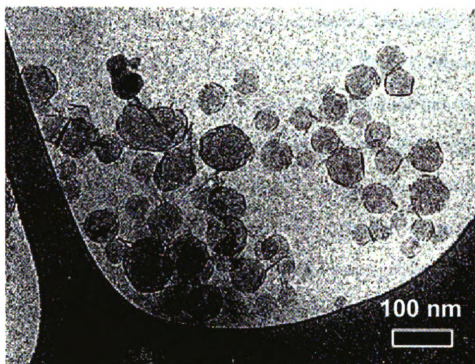
Figure 1.4 Cryo-TEM image of styrene-butyl acrylate particles coated by monofunctional silane-treated Laponite clay nanolayers, as obtained by emulsion polymerization in the presence of 10 wt% Laponite clay platelets [42].

1.3 PCN Preparation Technology

Three main methods have been used for the preparation of PCNs, namely, solvent intercalation, in-situ polymerization, and melt blending. The solvent intercalation method requires the polymer or pre-polymer to be soluble in a solvent that also is capable of swelling the clay galleries. Polymer chains are allowed to access the clay galleries, thereby, promoting the formation of either an intercalated or exfoliated nanocomposites upon the removal of the solvent. This method is commonly used for water-soluble polymers, and for composite film

fabrication [49-55]. For hydrophobic polymers, solvent intercalation methods require the use of organic solvents, such as chloroform [56, 57]. From practical point of view, organic solvent processing is environmentally challenging.

PCNs also can be prepared via in-situ polymerization of monomers in the presence of the modified clay. The in-situ polymerization methodology is particularly useful for the preparation of thermoset PCNs and for thermoplastics that can be readily prepared under near-ambient conditions. Nylon-6 – exfoliated MMT nanocomposites, the first example of an exfoliated PCN, were prepared by polymerization of a mixture of ε-caprolactam and MMT modified by the onium ion of a α, ω-amino acid [8, 9]. This method has also been applied to epoxy, polyolefin, PS, PA, and polyimides (PI) systems [22, 58-63]. The advantage of the in-situ polymerization approach is the ease of clay – pre-polymer processing. It is usually much easier to pre-intercalate or to pre-exfoliate a clay with a polymer precursor than the polymer itself.

The melt-blending method blends a mixture of polymer and clay at a temperature above the softening point of the polymer [34, 64-68]. This method has been identified as the most desired approach to the preparation of thermoplastic PCNs because it does not require the use of solvents or the re-tooling of processing equipment and conforms to standard industrial methods for polymer processing. However, thermoplastic polymers, especially non-polar polymers are not good wetting agents for organoclays. Moreover, many

14

organoclays are not stable under melt processing conditions due to the low thermal stability of the organic modifiers. Thus, it generally is difficult to achieve organoclay nanolayer exfoliation under common melt processing conditions. To overcome these limitations, extra modification of the polymer needs to be carried out to achieve compatibility with the clay and to facilitate intercalation. Commonly used technique in the preparation of polyolefin – clay nanocomposites is to incorporate maleic anhydride grafted polyolefin as a compatibilizer, although the addition of the lower molecular weight component lowers the mechanical properties of the polymer matrix [13-18, 69].

The mechanism of polymer intercalation in clay has been studied extensively. At thermodynamic equilibrium, the dispersion of the platelets in polymer matrix is favored only if the enthalpy changes overcome the entropy loss of the confined polymer chains within the clay galleries [70]. Vaia and Giannelis studied the polymer melt intercalation in organo-clay using a mean-field, lattice-based model, and pointed out that the entropic penalty of polymer confinement may be compensated by the increased conformational freedom of surfactant chains as the layers separate. The dispersion of clay was energy favored by maximizing the polymer-surface interactions and minimizing the unfavorable apolar interactions between polymer and surfactants [25].

Epoxy-based PCNs prepared via in-situ polymerization method provide examples for clay exfoliation mechanism research. Pinnavaia and coworkers

pointed out that the exfoliation of clay is possible when comparable intra- and extragallery polymerization rates were achieved by incorporating acidic exchange cation as both a clay surface modifier and a catalyst for intergallery epoxide polymerization [71]. Chen et al. divided the interlayer expansion process into three stages: initial interlayer expansion due to the monomer and curing agent diffusion, steady-state interlayer expansion due to the intergallery polymerization, and the cessation of interlayer expansion [72]. More recently, Jana and coworkers argued that the elastic force exerted by cross-linked epoxy molecules inside the clay galleries was the primary force for exfoliation [73]. The elastic force pushed the outermost clay layers out from the tactoids against the opposing forces arising from electrostatic and van der Waals attraction and shear until gelation of the system occurs (Figure 1.5). Complete exfoliation can occur if the ratio of shear modulus to complex viscosity was maintained at or above 2-4 1/s, so that the elastic forces inside the galleries outweighed the viscous forces of the extragallery epoxy.

Organic solvents have been used to assist in the preswelling of an organo-clay in the presence of a prepolymer [22, 74]. Hasegawa reported the preparation of a PCN by compounding nylon-6 with a Na^+-MMT aqueous slurry [75]. After the evaporation of water, Na^+-MMT layers were found to be exfoliated and dispersed homogeneously in the nanocomposites. The properties of these novel nanocomposites were nearly equal to those of conventional nylon-organo-

clay nanocomposites. Also, Mai and coworkers synthesized exfoliated silicone rubber – clay nanocomposites based on a siloxane surfactant modified clay aqueous suspension [76].
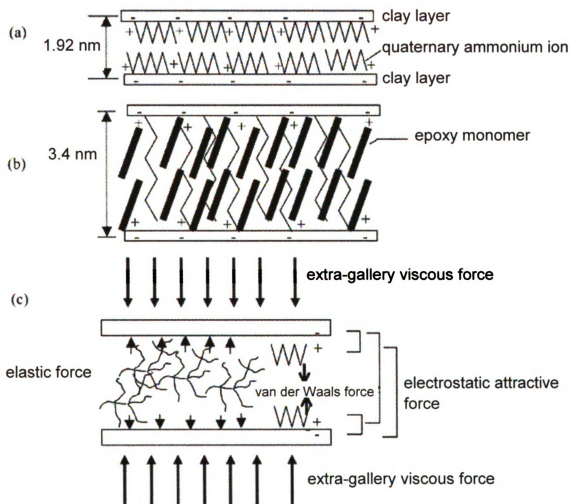
Figure 1.5 Schematic illustration of the intercalated state of the exfoliation process showing the forces acting on a pair of clay layers: (a) organically modified clay; (b) epoxy-intercalated state; (c) forces acting on a two-particle clay tactoids [73].

More recently, He and co-workers developed a so-called 'slurry compounding' process to prepare exfoliated epoxy-clay nanocomposites [44, 45]. The exfoliated morphology of the clay in aqueous suspension can be transferred to the epoxy matrix. The mechanism of exfoliation was believed to involve the silylation of hydroxyl groups on the basal planes of the clay structure. However, since the hydroxyl groups are buried in the second and third planes of oxygen atoms and are inaccessible for reaction, the proposed mechanism is unlikely. Instead, silylation most likely occurred only at the edges of the clay platelets. This would be consistent with the observation that the method required only small amounts of silane as a surface modifier. Figure 1.6 shows TEM images of the exfoliated clay nanolayers in the epoxy matrix. The same group also reported preparing PP – clay nanocomposites by reactive compounding PP with an epoxy – clay master batch made via "slurry compounding" [77]. Because epoxy and PP are immiscible, maleic anhydride grafted PP was incorporated as both a compatiblizer and an epoxy curing agent. Most clay particles were exfoliated or dispersed into small stacks clay layers in the resulting nanocomposites. The slurry compounding approach for nanocomposite formation is deserving of verification and extension to other polymer – clay systems.
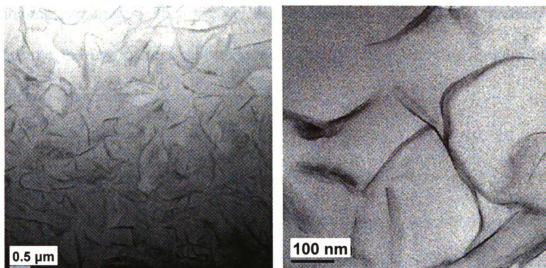
Figure 1.6 TEM images of an epoxy nanocomposite (2.5 wt% clay) prepared by slurry compounding [45].

Supercritical carbon dioxide fluid, as an environmentally friendly, inexpensive, low-viscosity and nonflammable liquid, has been used to replace conventional solvents in the preparation of PCN compositions based PS, Poly(ethylene oxide) and poly(methyl methacrylate) matrices [78-80]. Manke and coworkers patented a unique technique using supercritical fluid to delaminate clay [81]. A catastrophic depressurization of a supercritical – clay system and the associated catastrophic volume change of the fluid caused the clay layers to exfoliate, as judged by XRD patterns of the solids. The inventors claimed that the treated silicate particles were ready for polymer reinforcement purposes. More recently, Gulari and coworkers patented a technique to exfoliate contacted particles and reduce reaggregation of the structures by supercritical fluid diffused

with coating agents, such as polydimethylsiloxane [82]. These techniques eliminate the use of any clay surface modifiers. However, they require high-pressure environments.

1.4 Characterization of Clay Nanolayer Dispersion

PCN studies rely on accurate characterization of the nanometer-scaled clay morphology in polymer matrices. The most commonly used methods are wide-angel X-ray diffraction (WAXD) and transmission electron microscopy (TEM). WAXD has been used to measure the position, shape and intensity of the basal reflection of both initial clay particles and clay layers dispersed in polymers (Figure 1.7a). An increase in interlayer spacing due to the intercalation of polymer results in a lower-angle shift of the 001 peak, compared with the basal reflection of the initial clay particles. The peak also broadens when the layer orientation is disordered. The disappearance of the 001 reflection indicates the formation of some form of an exfoliated morphology. Small angle X-ray scattering (SAXS) technique can be used to detect interlayer spacings of 200 Å and beyond. SAXS has also been used to determine three-dimensional clay layer orientation in PCNs [83]. Although WAXD has been a convenient method to determine the d-spacing, the X-ray line broadening is directed relative to the crystal size and number of diffracting layers. Therefore, the d-spacing of only a few stacked layers or a relatively disordered intercalated structure may not

20

be detected using WAXD. Additionally, WAXD does not provide information on structure homogeneities throughout the composites.
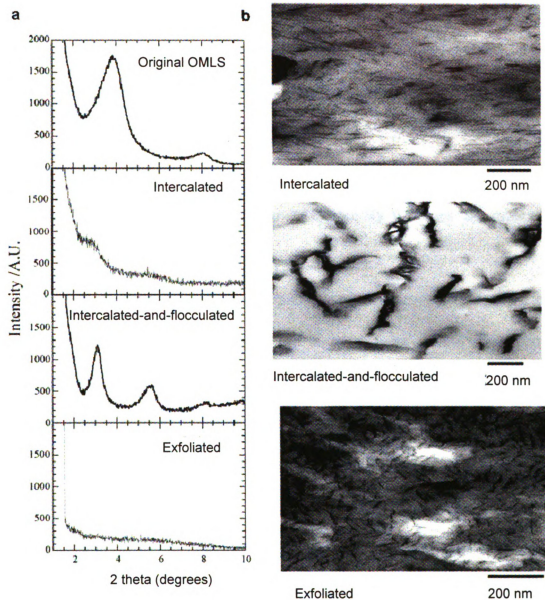
Figure 1.7 (a) WAXD patterns and (b) TEM images of three different types of PCNs [4].

High magnification and high resolution TEM has been a powerful technique for PCN characterization. The edge of individual clay layer can be directly imaged (Figure 1.7b). However, the sample preparation of TEM requires ultrathin-sectioning of the composite into 70-nm thick slices, which is a delicate and time-consuming process. To determine the overall homogeneity, a large number of TEM images must be taken from different regions of the composite sample. Quantitative analysis of a large number of images can be carried out by enumerating the interlayer spacing and layer aspect ratios of the platelets [84, 85]. The combination of WAXD and TEM usually provides an reasonable representation of PCN morphologies.

Optical microscopy and scanning electron microscopy (SEM) have been used to investigate clay dispersion on a micrometer scale, and can be complementary methods to WAXD and TEM. SEM is also a useful tool to investigate the fracture surfaces of the composites [44].

Vanderhart and coworkers first used ^{13}C solid state NMR to determine clay dispersion in polymers [86]. The spin-exchange interaction between the unpaired electrons of paramagnetic Fe atoms in clay particles shortens the longitudinal relaxation time (T_1^H) of protons within 1 nm of clay surfaces, and, further, contributes to the T_1^H of bulk composite by spin diffusion. Better clay dispersion leads to greater average paramagnetic contribution to T_1^H. The success of this method depends on two factors: the paramagnetic components of

22

the clay, such as Fe^{3+} in MMT, and an efficient spin diffusion processes. NMR has been an effective quantitative method to characterize polymer – MMT nanocomposites based on PS [87], nylon [86, 88, 89], styrene-acrylonitrile copolymer [90] and poly(ε-caprolactone) [91]. However, in rubbery polymers, where the dipolar interactions are too weak, NMR cannot be applied [90].

Atomic Force Microscopy (AFM) has also been used to investigate clay dispersion in PCNs. After chemical etching, the silicate particles were detectable on the composite surfaces. AFM can also be applied directly to the composite thin-sections [92-94]. Figure 1.8 shows a phase contrast AFM image of an epoxy – fluromica nanocomposite, where the intercalated morphology can be clearly seen. AFM has been found to be especially useful in mapping the heterogeneity of polymer blends [95-97]. Karger-Kocsis and coworkers studied polyamide-6 – PP – organo-clay nanocomposites by AFM and found that organoclay was located only in the PA-6 phase of the uncompatibilized blends [97]. When maleic anhydride grafted PP (MAH-g-PP) was added as a compatiblizer, the clay became embedded in the PA6-g-PP phase only.

Lo´pez-Manchado and coworkers introduced a novel PCN characterization method by measuring the freezing-point depression of a solvent encapsulated the swollen composite [99]. It has been found that vulcanizates containing highly dispersed clay particles exhibited a larger freezing point depression for the encapsulated solvent than the pristine rubber matrix. The

23

difference in freezing point depressions was attributed to a tighter network and smaller solvent cages for the composite. However, the change in the freezing point depression was comparatively small, and this method cannot reliably provide quantitative information on the degree of clay particle dispersion.
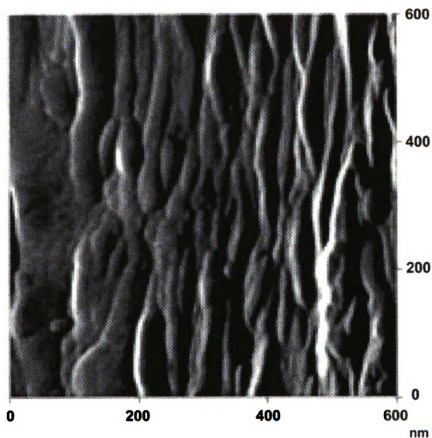
Figure 1.8 A phase contrast AFM image of an epoxy - synthetic fluoromica nanocomposite [92].

Researchers at Elementis Specialties, Inc. recently developed a technique to use FTIR to characterize the exfoliation and alignment of clay layers in

polymer matrices (W. Ijdo, personal communication). The bandwidth of the silicate vibrations of an organo-hectorite was found to narrow significantly upon layer delamination (Figure 1.9 a). It was possible to construct a calibration curve relating the bandwidth for the in-plane Si-O vibration vs. the fraction of nanolayer dispersion. A solvent containing different amounts of a chemical activator, such as propylene carbonate, was used to control the level of clay delamination (Figure 1.9 b). When other clays were used to reinforce polymers, the dispersion could be determined by measuring the in-plane Si-O bandwidth in comparison to the hectorite calibration curve. The same researchers also have used polarized FTIR to evaluate clay alignment in PNC films. Since the polarized FTIR absorbance changes with the electron density in the polarized direction, tilting a PNC film sample containing oriented clay particles in the path of a z-axis polarized IR beam will cause a decrease in the intensity of the in-plane Si-O absorbance and an increase in the out-plane Si-O absorbance (Figure 1.10). This phenomena was not observed in composite films with randomly orientated clay layers.

Figure 1.9 (a) FTIR spectrum of hectorite powder and delaminated hectorite in water; (b) a calibration curve of clay in-plane Si-O bandwidth vs. percent activator added and percent dispersion. (Figures provided by W. Ijdo, Elementis Specialties, Inc.)

(a) FT-IR spectra of Hectorite clay powder and delaminated Hectorite clay in water, with a band at 28.9 cm⁻¹. Wavenumber axis ranges from 1150 to 900 cm⁻¹.

(b) In-plane Si-O bandwidth (FWHM) [cm⁻¹] versus Percent activator added and Percent nanodispersion.
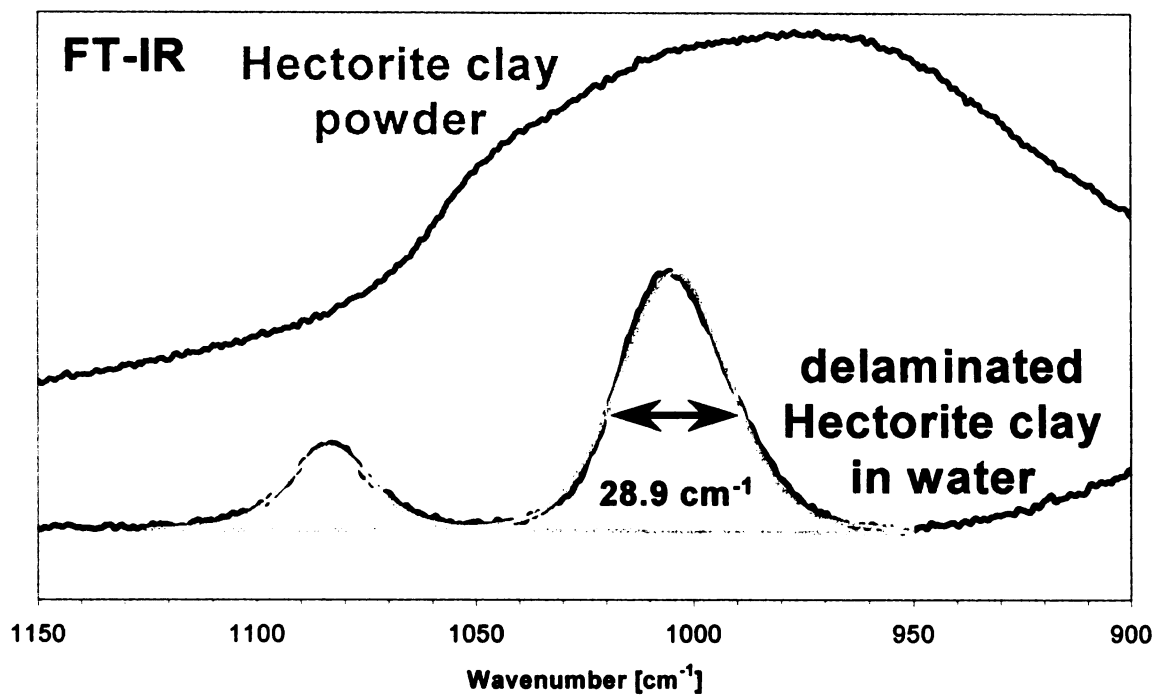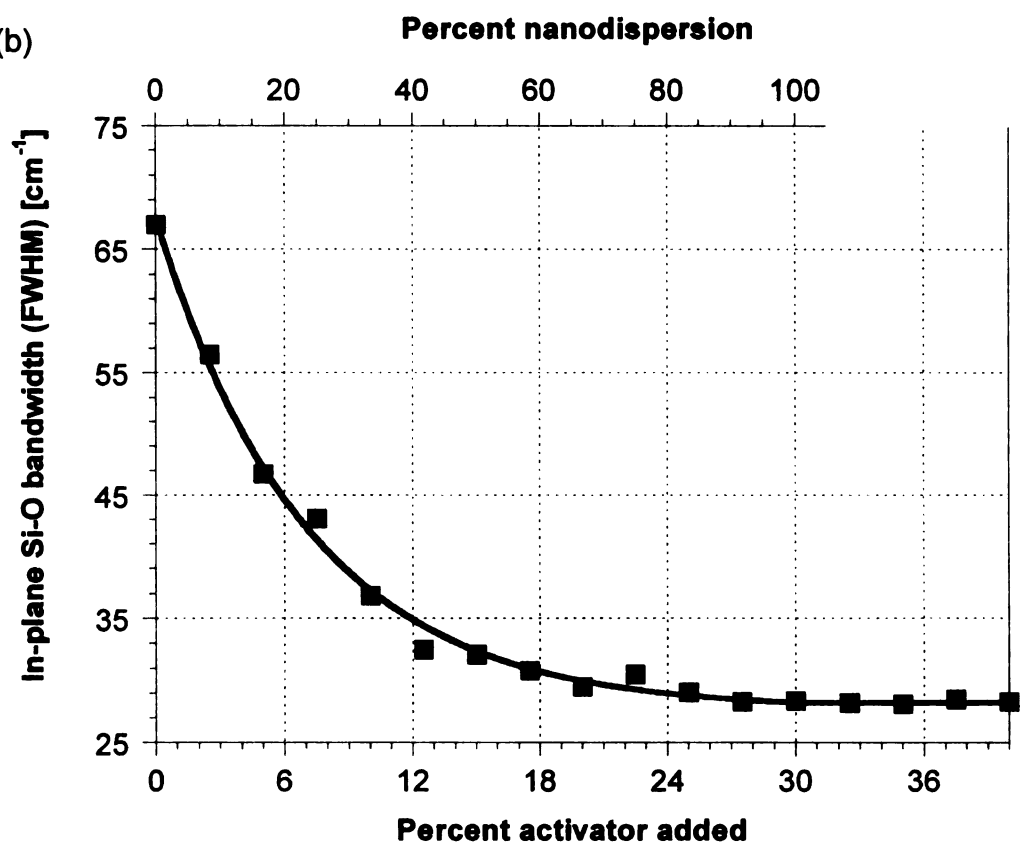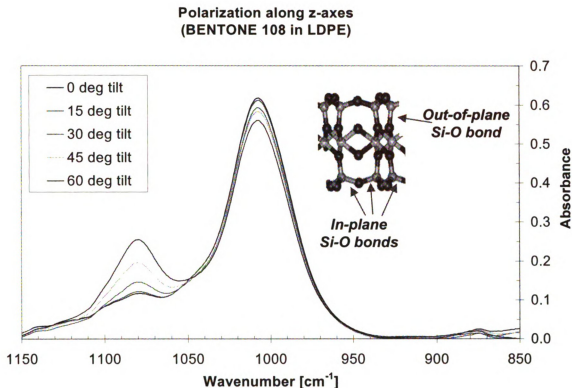
Figure 1.10 z-axis polarized FTIR spectra of a LDPE film containing oriented BentoneTM clay layers, with different tilt angle. Inset: schematic representation of clay in-plane and out-of-pane Si-O bonds. (Figure provided by W. Ijdo, Elementis Specialties, Inc.)

1.5 Nanolayer Orientation

To achieve control on the orientation of anisotropic fillers has been a challenge in nanocomposite studies. Conventional techniques, such as fiber weaving, obviously are not feasible for clay nanoparticles. Theoretical modeling studies of PCN composition have shown that substantial improvements in mechanical and barrier properties are possible for a composite reinforced by

aligned clay layers, compared with those containing random clay dispersions [100-103]. It has also been predicted that the enhanced mechanical properties observed for PCNs based on elastomers are due to the ability of realignment of clay layers under stress [61]. Relatively fewer experimental studies have been carried out on achieving good alignment of clay layers in PCNs. Vaia and coworkers applied AC electric field during the curing of epoxy-organo-clay nanocomposites [104]. The in-situ SAXS showed that the clay layers reoriented parallel to the electric field, and that, upon thermal curing, the complete development of alignment occurred before the onset of chemical crosslinking (~80 °C). At the same time, the clay layers swelled toward an exfoliated morphology (Figure 1.11). The driving force for clay particle alignment was possibly the induced dipole of the 'mobile' exchangeable organic cations on clay surfaces. Compared with epoxy – clay nanocomposite with random clay morphology, those with aligned morphology exhibited lower coefficient of thermal expansion, higher modulus and better optical clarity. More recently, Vaia and coworkers reported using a magnetic field > 1 T to align clay in an epoxy matrix before curing [105]. Clays, particularly MMT that contains antiferro- or ferrimagnetic impurities, were able to align parallel or perpendicular to the magnetic field respectively, indicating that the composition of the clay has great impact on the alignment, presaging the design of triaxial nanoparticle reinforcement on the basis of magnetic properties.
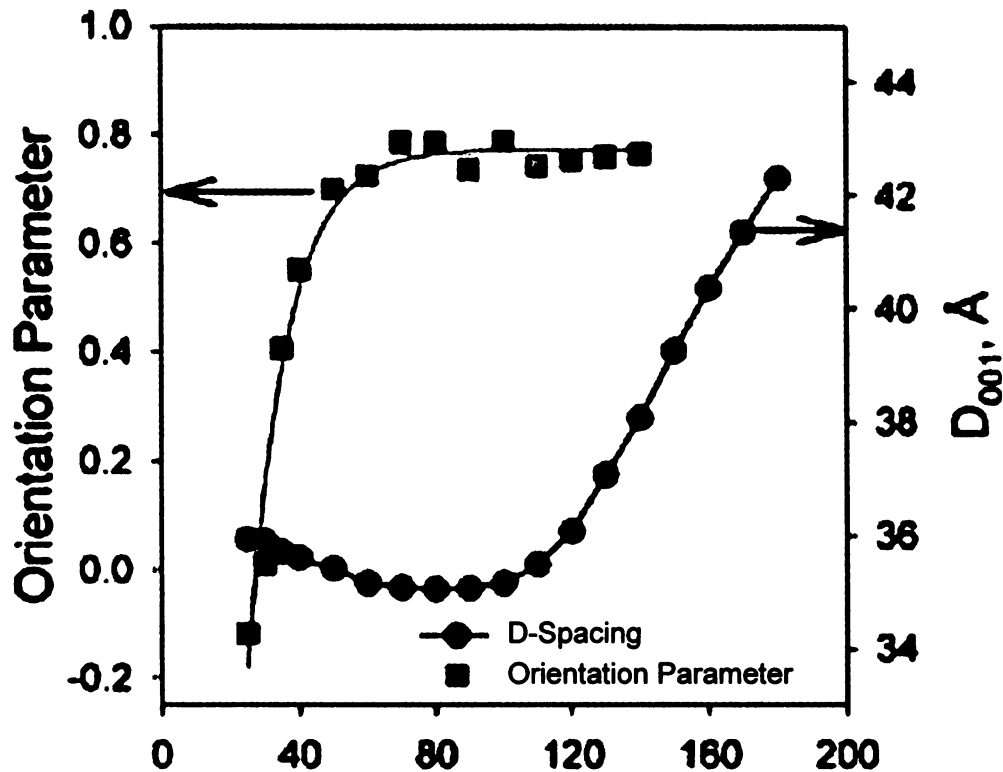
Figure 1.11 Hermans orientation parameter, Sd (squares), and layer spacing (circles) determined from in-situ scattering (3 °C/min). Note that the intensity of the basal reflection (d001=36Å) rapidly decreases above 120 °C, effectively disappearing by 180 °C. Orientation parameter above 120 °C was estimated from the featureless scattering around the beam stop [104].

1.6 Synthetic Materials for Polymer Reinforcement

Although naturally occurring clays are inexpensive and readily available, they have certain disadvantages for PCN applications, including the difficulty of purification and the need for organic modification. Researchers have been

looking for alternative synthetic clay-like materials for polymer reinforcing purposes. Clay materials can be synthesized under various laboratory conditions, ranging from ambient pressure and temperature to extreme hydrothermal conditions [106]. The products usually exhibit high purity and uniform particle morphology and charge distribution. More importantly, a well designed synthesis strategy raises the possibilities of tailoring clay properties to meet certain research requirements.
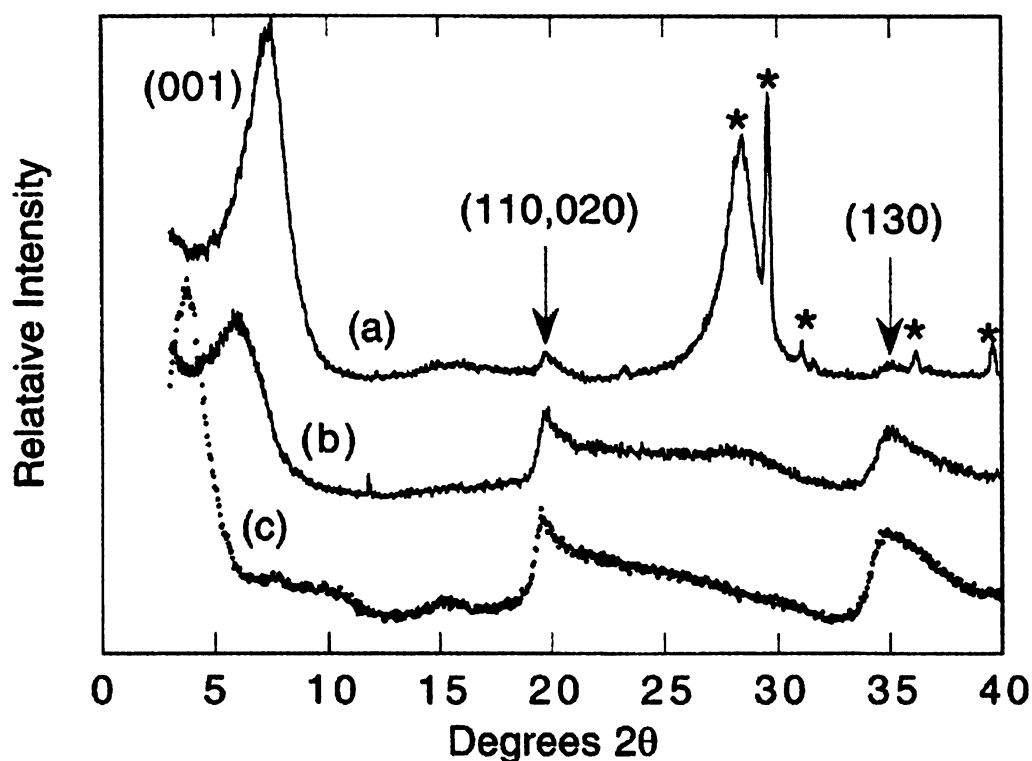
Figure 1.12 XRD patterns of (a) natural Na-hectorite, herein the peaks labeled by * are due to (Mg, Fe)SiO$_3$ and CaCO$_3$ impurities; (b) synthetic Li-hectorite, and (c) synthetic PVP-hectorite. Typical clay hkl reflections are identified [107].

Carrado and coworkers have developed a general technique to synthesize hectorite-like clay materials by refluxing a freshly precipitated brucite in solutions containing LiF and silica precursors [107]. A series of water-soluble, cationic or electrically neutral organics, varying from small molecules like tetramethyl ammonium to large polymer molecules like polyvinylpyrrolidone (PVP) can be present in the course of hectorite synthesis. When cationic organics were present, they ended up as the interlayer cations. The presence of neutral organic molecules during synthesis required larger amounts of LiF for successful hectorite synthesis, and both the neutral organic and Li^+ were incorporated into the interlayer spaces [107]. Figure 1.12 shows the XRD patterns of a natural Na^+-hectorite, synthetic Li^+-hectorite and a PVP-hectorite, showing the characteristic XRD diffraction peaks and higher level of purity of the synthetic hectorites. PVP-hectorite composites exhibited an increase in basal spacing with polymer uptake from 16.5 to 23.5 Å. The authors proposed two potential applications for synthetic-hectorite [107]. One was for the preparation of porous materials for potential use as catalysts or catalyst supports upon the removal of the organic polymer phase by combustion. A correlation was observed between catalyst mesoporous size and the size and concentration of a polymer used in the synthesis. The other potential application was for the preparation of organic-inorganic composites through a one-step process by allowing more polymer intercalation during the hectorite synthesis. The highest organic loadings, up to

86%, were observed for the polyaniline-hectorite composites. These composites had a so-called semi-exfoliated structure, in which small clay crystallites were intercalated by polymer and well-dispersed within a continuous polymer matrix. Carrado and coworkers also reported a one-step synthesis strategy of organo-smectite clays with organics grafted on the interlayer surfaces by using organotrialkylsilane as the silica sources [108]. These synthetic clay may be an interesting substitute for conventional organo-clay prepared from ion-exchange of natural clay.

Chastek, Stein and coworkers synthesized hexadecyl-functionalized lamellar silicates C16-LMS, aluminosilicates C16-LMAS and C16-SiO$_2$-LMAS by sol-gel synthesis, whose structures are shown in Figure 1.13 [109]. C16-LMS consisted of single or double layers of tetrahedral silicates. C16-LMAS had a pyrophyllite-type structure with an octahedral aluminum layer sandwiched between two tetrahedral silicate layers. C16-SiO$_2$-LMAS had additional silicate groups in the structure, compared with C16-LMAS and, thus, had a larger inorganic layer thickness and greater structural disorder. Hexadecyl groups were covalently attached to the inorganic layers in all three synthetic silicates, as verified via ^{29}Si-NMR. In a subsequent report, Stein and his coworkers investigated the dispersion of C16-LMS, C16-LMAS and C16-SiO$_2$-LMAS in different organic solvents and in polystyrene [110]. The solvent study showed that the synthetic clays formed stronger gels with aromatic solvents, such as

toluene, than with linear, branched or cyclic alkyl solvents, indicating that the synthetic clays were more suited for dispersion in polystyrene, which has a similar structure as the aromatic solvents. The clay – toluene gel strength increased with increasing clay concentration, although SAXS showed no intercalation of toluene in clay galleries. These three synthetic clays and Cloisite 20A (an organo-MMT) were compared in polystyrene – clay nanocomposites prepared from melt-blending process. The rheology study showed that, at the same inorganic content, composites made from C16-LMAS and C16-SiO$_2$-LMAS had higher elastic moduli (G') than from C16-LMS, due to the higher aspect ratio and better dispersion of the former two clays in polystyrene. However, SAXS showed that no polymer intercalation occurred in the composites. The flocculation of clay caused by the interactions of hydroxyl groups on clay surfaces, and the strong interactions between the interlayer covalently bonded alkyl groups made the polymer intercalation more difficult. Polystyrene-Cloisite 20A exhibited highest G', attributed to the better dispersion and possibly higher layer stiffness of Cloisite 20A (Figure 1.14).
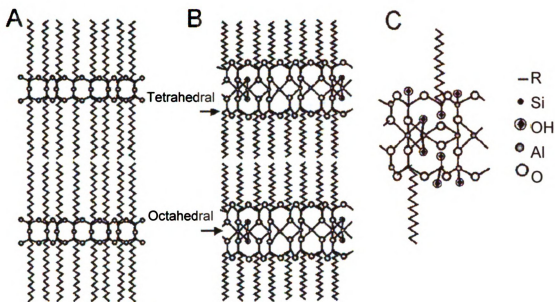
Figure 1.13 Proposed schematic structures of the functionalized clays. Two possible structures for C16-LMS include a single layer structure and a double layer structure which is shown in (A). The proposed structure of C16-LMAS (b) with both tetrahedral and octahedral Al present in the octahedral layer. In C16-SiO$_2$-LMAS (C) additional silicate groups without alkyl chains are present and tetrahedral Al is likely to occupy some of the sites in tetrahedral layer [109].
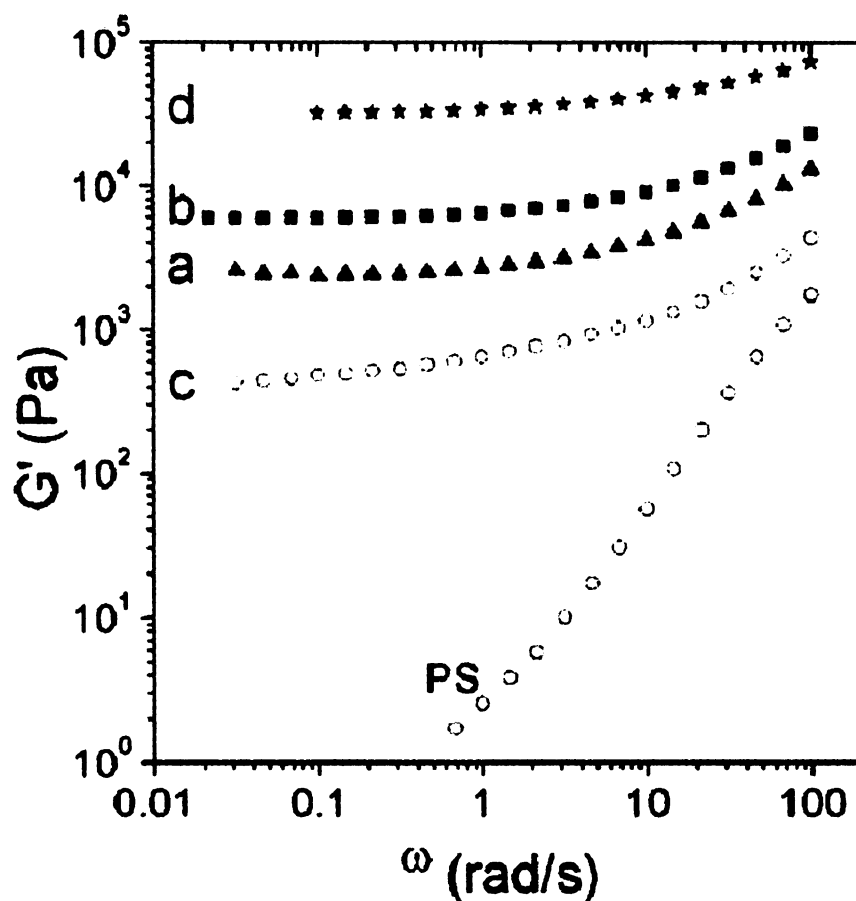
Figure 1.14 Elastic moduli of PS - clay nanocomposites using (a) C16-SiO₂-LMAS, (b) C16-LMAS, (c) C16-LMS, and (d) Cloisite 20A from melt rheology data obtained at $T=150$ °C, and 6.3 wt% inorganic material [110].

Clearfield and coworkers have used synthetic α-zirconium phosphate (α-ZrP) to make epoxy nanocomposites [111, 112]. The α-ZrP had a higher ion exchange capacity and narrower particle size distribution than MMT. The size and aspect ratio of α-ZrP can be controlled by varying the reaction time and reactant concentrations. A monoamine modified α-ZrP (M-α-ZrP) has been readily exfoliated in epoxy, while α-ZrP remained unswelled. A 1.9 vol% M-α-ZrP

loaded epoxy nanocomposite showed 50% increase in tensile modulus and 10% increase in yield strength. However, the ductility was dramatically reduced. α-ZrP has also been used to study the fracture behavior of epoxy nanocomposites [113].
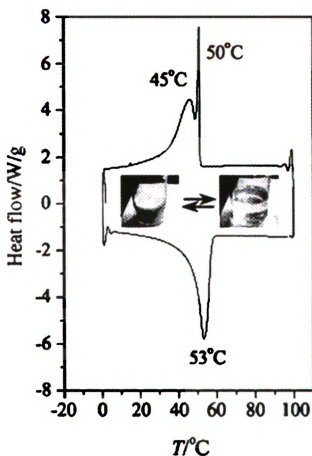
Figure 1.15 DSC traces of the organosilicate. Inset shows the phase transition from solid to liquid upon heating [114].

Giannelis and coworkers have reported surface-functionalized nanoparticles with liquid-like behavior [115]. For instance,

$[(CH_3O)_3Si(CH_2)_3N^+(CH_3)(C_{10}H_{21})_2]Cl^-$ functionalized silica nanoparticle with sulfonate anion $R(OCH_2CH_2)_7O(CH_2)_3SO_3^-$ as counterion appeared as a clear liquid at room temperature. This concept has been extended to various nanoparticles, including magnetic iron oxide nanoparticles, layer-like organosilicate, polyoxometalate cluster, anatase nanoparticles, and DNA oligonucleotide [116]. Layered organosilicate nanoparticles have been synthesized by refluxing octadecyltrichlorosilane in toluene with the presence of a small amount of water [114]. The solid product can be readily dispersed in various organo solvent, and exhibit reversible solid-liquid transition upon heating (Figure 1.15). These solvent-free, zero-vapor pressure, liquid-like nanostructures circumvent toxic solvents, possess unique conducting, magnetic or electrorheological properties, and exhibit low dimension restrictions, bringing new scientific and technological opportunities.

Meso-structured silica with large mesopore size has been a promising reinforcing agent for polymer materials. Improvement in mechanical properties have been reported based on nylon-6,6 [117], poly(vinyl acetate) [118], poly((3-trimethoxysilyl)propyl methacrylate) [119] etc. Very recently, Pinnavaia and coworkers reported epoxy – silica mesocomposites with enhanced tensile properties and oxygen permeability [120]. The mesoporous silica, denoted MSU-J, was synthesized using a α,ω-diamine polypropylene oxide (Jeffamine D2000). It had a wormhole framework structure with a pore diameter of 5.3 nm, a pore

volume 1.41 cm^3/g and a surface area 974 m^2/g. Both as-made MSU-J and calcined MSU-J, where the Jeffamine D2000 was removed in the latter case, dispersed uniformly in a rubbery epoxy matrix. Compared with epoxy – organo-clay nanocomposites, epoxy – silica mesocomposites exhibited comparable improvement in mechanical properties and thermal stability (Figure 1.16). The tensile modulus, strength, toughness, and elongation-at-break for the mesocomposites were systematically reinforced by up to 4.8, 5.7, 1.6, and 8.5 times, respectively, in comparison to the pure epoxy polymer. Additionally, no organic modification was needed for MSU-J, and the composites were prepared with a simple mix and cure method. Another remarkable property of the epoxy – as-made MSU-J mesocomposites is that the oxygen permeability increased dramatically at loadings ≥5 wt% due to the partitioning of curing agent between the as-made mesostructure and the liquid prepolymer, and, consequently, reduced chain cross-linking in the vicinity of the silica particles. Such phenomenon was not observed in epoxy – calcined MSU-J mesocomposites since the curing agent partitioning was not allowed (Figure 1.16). Balkus and coworkers have also reported improved gas permeability in polysulfone – MCM-41 membranes prepared by a solvent-blending method. A 30 wt% MSM-41 loaded polysulfone membrane had the oxygen, nitrogen, carbon dioxide, methane permeability increased by 2.5, 2.9, 2.7, and 2.6 times respectively [121].
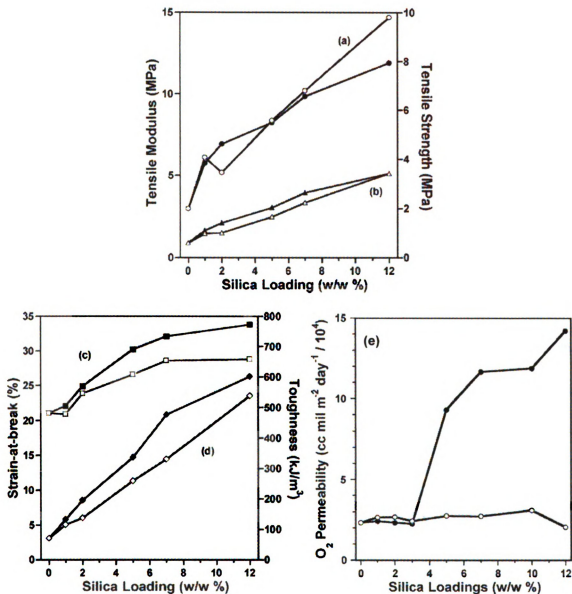
Figure 1.16 (a) Tensile modulus, (b) tensile strength, (c)strain-at-break, (d) toughness, and (e) oxygen permeabilities epoxy composites containing different loadings of as-made MSU-J (solid circles), and calcined MSU-J (open circles) mesostructured silica [120].

1.7 Conclusion

This chapter has reviewed certain aspects of PCN chemistry, particularly clay nanolayer modification, PCN preparation and characterization, nanolayer alignment and alternatives to natural clays as polymer reinforcement agents. Conventional techniques, such as onium-ion exchange, WAXD, TEM, have been and will continue to be effective for PNC study. New techniques and concepts are rising everyday, and holding additional promise for routine use in future PCN studies.

Despite all the efforts, it is still a great challenge to establish the morphology – processing – structure – property relationships of polymer - clay nanocomposites. To reach this goal, it is important to understand and evaluate the necessity of clay organic modification, considering the advantages of the modifiers as surface compatibilizers and their disadvantages in causing plasticizer effects and low thermal stability. It is also important to further develop polyolefin nanocomposites, since polyolefins have a wide range of commercial applications. Current techniques in forming polyolefin – clay nanocomposites requires extensive organic modifications and has not yet given satisfactory results on commercial scales. This thesis aims at developing organic-modifier-free preparation pathways for the formation of polymer – metal oxide nanocomposites to prove the feasibility of the proposed study, to discover novel

inorganic metal oxides for polymer reinforcement purposes and to attract more research interest in this area.

In the following chapters, both thermoset polymer epoxy and thermoplastic polyolefins are chosen as polymer matrices. Three different metal oxides with unique morphology and surface properties are studied: synthetic saponite, palygorskite, and mesoporous silicas. Specific research interests include:

- Synthesis of clay-like silicate materials in order to control the morphology and composition of the products by choice of synthesis conditions.

- Develop strategies for using inorganic metal oxides as polymer reinforcing agents. The inorganic metal oxides include synthetic saponite, palygorskite, and mesoporous silicas. The polymer matrices include epoxy and polyethylene.

- Compare the properties of nanocomposites reinforced by inorganic metal oxides with those of nanocomposites formed from organo-clay.

References

(1) Liu, J.; Boo, W. J.; Clearfield, A.; Sue, H. J. *Mater. Manuf. Processes* **2006**, *21*, 143.

(2) Becker, O.; Simon, G. P. *Adv. Polym. Sci.* **2005**, *179*, 29.

(3) Usuki, A.; Hasegawa, N.; Kato, M. *Adv. Polym. Sci.* **2005**, *179*, 135.

(4) Ray, S. S.; Okamoto, M. *Prog. Polym. Sci.* **2003**, *28*, 1539.

(5) LeBaron, P. C.; Wang, Z.; Pinnavaia, T. J. *Appl. Clay Sci.* **1999**, *15*, 11.

(6) Okamoto, M. *Encyclopedia of Nanoscience and Nanotechnology* **2004**, *8*, 791.

(7) D'Souza, N. A. *Encyclopedia of Nanoscience and Nanotechnology* **2004**, *3*, 253.

(8) Usuki, A.; Kojima, Y.; Kawasumi, M.; Okada, A.; Fukushima, Y.; Kurauchi, T.; Kamigaito, O. *J. Mater. Res.* **1993**, *8*, 1179.

(9) Kojima, Y.; Usuki, A.; Kawasumi, M.; Okada, A.; Fukushima, Y.; Kurauchi, T.; Kamigaito, O. *J. Mater. Res.* **1993**, *8*, 1185.

(10) Wang, Z.; Massam, J.; Pinnavaia, T. J. In *Polymer-clay nanocomposites*; Pinnavaia, T. J., Beall, G.W. Eds.; John Wiley & Sons: Chichester, 2000, pp 127.

(11) Okada, A.; Usuki, A. *Macromol. Mater. Eng.* **2006**, *291*, 1449.

(12) Mark, J. E. *Acc. Chem. Res.* **2006**, *39*, 881.

(13) Morgan, A.B. *Polym. Adv. Technol.* **2006**, *17*, 206.

(14) Zanetti, M.; Lomakin, S.; Camino, G. *Macromol. Mater. Eng.* **2000**, *279*, 1.

(15) Lee, H. S.; Fasulo, P. D.; Rodgers, W. R.; Paul, D. R. *Polymer* **2005**, *46*, 11673.

(16) Hotta, S.; Paul, D. R. *Polymer* **2004**, *45*, 7639.

(17) Lew, C. Y.; Murphy, W. R.; McNally, G. M. *Polym. Eng. Sci.* **2004**, *44*, 1027.

(18) Arroyo, M.; Suarez, R. V.; Herrero, B.; Lopez-Manchado, M. A. *J. Mater. Chem.* **2003**, *13*, 2915.

(19) Vaia, R. A. In *Polymer-clay nanocomposites*; Pinnavaia, T. J., Beall, G. W. Eds.; John Wiley & Sons: Chichester, 2000, pp 229.

(20) Lagaly, G. *Solid State Ionics* **1986**, *22*, 43.

(21) Park, J.; Jana, S. C. *Macromolecules* **2003**, *36,* 8391.

(22) Triantafillidis, C. S.; LeBaron, P. C.; Pinnavaia, T. J. *Chem. Mater.* **2002**, *14*, 4088.

(23) Zanetti, M.; Camino, G.; Reichert, P.; Mulhaupt, R. *Macromol. Rapid Commun.* **2001**, *22*, 176.

(24) Xie, W.; Gao, Z. M.; Pan, W. P.; Hunter, D.; Singh, A.; Vaia, R. *Chem. Mater.* **2001**, *13*, 2979.

(25) Vaia, R. A.; Giannelis, E. P. *Macromolecules* **1997**, *30*, 7990.

(26) Maiti, P.; Yamada, K.; Okamoto, M.; Ueda, K.; Okamoto, K. *Chem. Mater.* **2002**, *14*, 4654.

(27) Bottino, F. A.; Fabbri, E.; Fragala, I. L.; Malandrino, G.; Orestano, A.; Pilati, F.; Pollicino, A. *Macromol. Rapid Commun.* **2003**, *24*, 1079.

(28) Chu, L.-L.; Anderson, S. K.; Harris, J. D.; Beach, M. W.; Morgan, A. B. *Polymer* **2004**, *45*, 4051.

(29) He, A.; Hu, H.; Huang, Y.; Dong, J.-Y.; Han, C. C. *Macromol. Rapid Commun.* **2004**, *25*, 2008.

(30) Morgan, A. B.; Harris, J. D. *Polymer* **2004**, *45*, 8695.

(31) Zhao, J.; Morgan, A. B.; Harris, J. D. *Polymer* **2005**, *46*, 8641.

(32) Wu, T. M.; Hsu, S. F.; Wu, J. Y. *J. Polym. Sci., Part B* **2003**, *41*, 560.

(33) Davis, C. H.; Mathias, L. J.; Gilman, J. W.; Schiraldi, D. A.; Shields, J. R.; Trulove, P.; Sutto, T. E.; Delong, H. C. *J. Polym. Sci., Part B* **2002**, *40*, 2661.

(34) Gilman, J. W.; Awad, W. H.; Davis, R. D.; Shields, J.; Harris, R. H.; Davis, C.; Morgan, A. B.; Sutto, T. E.; Callahan, J.; Trulove, P. C.; DeLong, H. C. *Chem. Mater.* **2002**, *14*, 3776.

(35) Xie, W.; Xie, R. C.; Pan, W. P.; Hunter, D.; Koene, B.; Tan, L. S.; Vaia, R. *Chem. Mater.* **2002**, *14*, 4837.

(36) Awad, W. H.; Gilman, J. W.; Nyden, M.; Harris, R. H.; Sutto, T. E.; Callahan, J.; Trulove, P. C.; DeLong, H. C.; Fox, D. M. *Thermochim. Acta* **2004**, *409*, 3.

(37) Fox, D. M.; Bellayer, S.; Awad, W. H.; Gilman, J. W.; Davis, R. D.; Maupin, P. H.; De Long, H. C.; Trulove, P. C. *Polym. Prepr. (Am. Chem. Soc., Div. Polym. Chem.)* **2004**, *45*, 311.

(38) Malhotra, S. V.; Kim, N. H.; Xanthos, M. Abstracts of Papers, *231st A CS National Meeting*, Atlanta, GA, United States, March 26-30, 2006 .

(39) Pesek, J. J.; Matyska, M. T.; Yu, R. J. *J. Chromatogr., A* **2002**, *947*, 195.

(40) Isoda, K.; Kuroda, K.; Ogawa, M. *Chem. Mater.* **2000**, *12*, 1702.

(41) Chen, G.-X.; Kim, E.-S.; Yoon, J.-S. *J. Appl. Polym. Sci.* **2005**, *98*, 1727.

(42) Herrera, N. N.; Letoffe, J.-M.; Putaux, J.-L.; David, L.; Bourgeat-Lami, E. *Langmuir* **2004**, *20*, 1564.

(43) Lee, S.-S.; Kim, J. *J. Polym. Sci., Part B* **2004**, *42*, 2367.

(44) Wang, K.; Chen, L.; Wu, J.; Toh, M. L.; He, C.; Yee, A. F. *Macromolecules* **2005**, *38*, 788.

(45) Wang, K.; Wang, L.; Wu, J.; Chen, L.; He, C. *Langmuir* **2005**, *21*, 3613.

(46) Haraguchi, K.; Ebato, M.; Takehisa, T. *Adv. Mater.* **2006**, *18*, 2250.

(47) Liff, S. M.; Kumar, N.; McKinley, G. H. *Nature Mater.* **2007**, *6*, 76.

(48) Xue, S.; Pinnavaia, T. J. *Microporous Mesoporous Mater.* **2007**, doi: 10.1016/j.micromeso.2007.02.042.

(49) Moad, G.; Dean, K.; Edmond, L.; Kukaleva, N.; Li, G. X.; Mayadunne, R. T. A.; Pfaendner, R.; Schneider, A.; Simon, G. P.; Wermter, H. *Macromol. Mater. Eng.* **2006**, *291*, 37.

(50) Reinholdt, M. X.; Kirkpatrick, R. J.; Pinnavaia, T. J. *J. Phys. Chem. B* **2005**, *109*, 16296.

(51) Chaiko, D. J. *Chem. Mater.* **2003**, *15*, 1105.

(52) Kuppa, V.; Manias, E. *J. Chem. Phys.* **2003**, *118*, 3421.

(53) Jacob, M. M. E.; Hackett, E.; Giannelis, E. P. *J. Mater. Chem.* **2003**, *13*, 1.

(54) Kwiatkowski, J.; Whittaker, A. K. *J. Polym. Sci., Part B* **2001**, *39*, 1678.

(55) Aranda, P.; Ruizhitzky, E. *Chem. Mater.* **1992**, *4*, 1395.

(56) Ghosh, A. K.; Woo, E. M. *Polymer* **2004**, *45*, 4749.

(57) Wang, H. W.; Chang, K. C.; Yeh, J. M.; Liou, S. J. *J. Appl. Polym. Sci.* **2004**, *91*, 1368.

(58) Yang, F.; Zhang, X. Q.; Zhao, H. C.; Chen, B.; Huang, B. T.; Feng, Z. L. *J. Appl. Polym. Sci.* **2003**, *89*, 3680.

(59) Alexandre, M.; Dubois, P.; Sun, T.; Garces, J. M.; Jerome, R. *Polymer* **2002**, *43*, 2123.

(60) Bergman, J. S.; Chen, H.; Giannelis, E. P.; Thomas, M. G.; Coates, G. W. *Chem. Commun.* **1999**, *21*, 2179.

(61) Lan, T.; Pinnavaia, T. J. *Chem. Mater.* **1994**, *6*, 2216.

(62) Bruzaud, S.; Grohens, Y.; Ilinca, S.; Carpentier, J.-F. *Macromol. Mater. Eng.* **2005**, *290*, 1106.

(63) Sun, Q.; Deng, Y.; Wang, Z. L. *Macromol. Mater. Eng.* **2004**, *289*, 288.

(64) Vaia, R. A.; Ishii, H.; Giannelis, E. P. *Chem. Mater.* **1993**, *5*, 1694.

(65) Zhang, J.; Jiang, D. D.; Wang, D.; Wilkie, C. A. *Polym. Adv. Technol.* **2006**, *16*, 800.

(66) Bhiwankar, N. N.; Weiss, R. A. *Polymer* **2005**, *46*, 7246.

(67) Tanoue, S.; Utracki, L. A.; Garcia-Rejon, A.; Sammut, P.; Ton-That, M.-T.; Pesneau, I.; Kamal, M. R.; Lyngaae-Jorgensen, *J. Polym. Eng. Sci.* **2004**, *44*, 1061.

(68) Tanoue, S.; Utracki, L. A.; Garcia-Rejon, A.; Tatibouet, J.; Cole, K. C.; Kamal, M. R. *Polym. Eng. Sci.* **2004**, *44*, 1046.

(69) Lee, J. A.; Kontopoulou, M.; Parent, J. S. *Polymer* **2004**, *45*, 6595.

(70) Bicerano, J.; Balijepalli, S.; Doufas, A.; Ginzburg, V.; Moore, J.; Somasi, M.; Somasi, S.; Storer, J.; Verbrugge, T. *Polym. Rev.* **2004**, *44*, 53.

(71) Lan, T.; Kaviratna, P. D.; Pinnavaia, T. J. *Chem. Mater.* **1995**, *7*, 2144.

(72) Chen, J. S.; Poliks, M. D.; Ober, C. K.; Zhang, Y. M.; Wiesner, U.; Giannelis, E. *Polymer* **2002**, *43*, 4895.

(73) Park, J. H.; Jana, S. C. *Macromolecules* **2003**, *36*, 2758.

(74) Brown, J. M.; Curliss, D.; Vaia, R. A. *Chem. Mater.* **2000**, *12*, 3376.

(75) Hasegawa, N.; Okamoto, H.; Kato, M.; Usuki, A.; Sato, N. *Polymer* **2003**, *44*, 2933.

(76) Ma, J.; Yu, Z.-Z.; Kuan, H.-C.; Dasari, A.; Mai, Y.-W. *Macromol. Rapid Commun.* **2005**, *26*, 830.

(77) Chen, L.; Wang, K.; Toh, M. L.; He, C. *Macromol. Mater. Eng.* **2005**, *290*, 1029.

(78) Li, J. B.; Xu, Q.; Peng, Q.; Pang, M. Z.; He, S. Q.; Zhu, C. S. *J. Appl. Polym. Sci.* **2006**, *100*, 671.

(79) Zhao, Q.; Samulski, E. T. *Macromolecules* **2003**, *36*, 6967.

(80) Zerda, A. S.; Caskey, T. C.; Lesser, A. J. *Macromolecules* **2003**, *36*, 1603.

(81) Manke, C. W.; Gulari, E.; Mielewski, D. F.; Lee, E. C.-C. In *US Patent 6469073*; (Ford Global Technologies, Inc., USA; Wayne State University). Application: US. US, 2002.

(82) Gulari, E.; Serhatkulu, G. K.; Rangaramanujam, K. In *US Patent A1 20050825*; (Wayne State University). Application: US. US, 2005.

(83) Bafna, A.; Beaucage, G.; Mirabella, F.; Mehta, S. *Polymer* **2003**, *44*, 1103.

(84) Manias, E.; Touny, A.; Wu, L.; Strawhecker, K.; Lu, B.; Chung, T. C. *Chem. Mater.* **2001**, *13*, 3516.

(85) Vermogen, A.; Masenelli-Varlot, K.; Seguela, R.; Duchet-Rumeau, J.; Boucard, S.; Prele, P. *Macromolecules* **2005**, *38*, 9661.

(86) VanderHart, D. L.; Asano, A.; Gilman, J. W. *Macromolecules* **2001**, *34*, 3819.

(87) Bourbigot, S.; Vanderhart, D. L.; Gilman, J. W.; Awad, W. H.; Davis, R. D.; Morgan, A. B.; Wilkie, C. A. *J. Polym. Sci., Part B* **2003**, *41*, 3188.

(88) VanderHart, D. L.; Asano, A.; Gilman, J. W. *Chem. Mater.* **2001**, *13*, 3781.

(89) Vanderhart, D. L.; Asano, A.; Gilman, J. W. *Chem. Mater.* **2001**, *13*, 3796.

(90) Bourbigot, S.; Vanderhart, D. L.; Gilman, J. W.; Bellayer, S.; Stretz, H.; Paul, D. R. *Polymer* **2004**, *45*, 7627.

(91) Calberg, C.; Jerome, R.; Grandjean, J. *Langmuir* **2004**, *20*, 2039.

(92) Zilg, C.; Mulhaupt, R.; Finter, J. *Macromol. Chem. Phys.* **1999**, *200*, 661.

(93) Becker, O.; Varley, R.; Simon, G. *Polymer* **2002**, *43*, 4365.

(94) Reichert, P.; Nitz, H.; Klinke, S.; Brandsch, R.; Thomann, R.; Mulhaupt, R. *Macromol. Mater. Eng.* **2000**, *275*, 8.

(95) Anandhan, S.; De, P. P.; De, S. K.; Bandyopadhyay, S.; Bhowmick, A. K. *J. Mater. Sci.* **2003**, *38*, 2793.

(96) Raghavan, D.; Gu, X.; Nguyen, T.; VanLandingham, M.; Karim, A. *Macromolecules* **2000**, *33*, 2573.

(97) Tanem, B. S.; Kamfjord, T.; Augestad, M.; Lovgren, T. B.; Lundquist, M. *Polymer* **2003**, *44*, 4283.

(98) Chow, W. S.; Ishak, Z. A. M.; Karger-Kocsis, J. *J. Polym. Sci., Part B* **2005**, *43*, 1198.

(99) Lopez-Manchado, M. A.; Valentin, J. L.; Herrero, B.; Arroyo, M. *Macromol. Rapid Commun.* **2004**, *25*, 1309.

(100) Sheng, N.; Boyce, M. C.; Parks, D. M.; Rutledge, G. C.; Abes, J. I.; Cohen, R. E. *Polymer* **2004**, *45*, 487.

(101) Liu, T.; Kumar, S. *Nano Lett.* **2003**, *3*, 647.

(102) Buxton, G. A.; Balazs, A. C. *J. Chem. Phys.* **2002**, *117*, 7649.

(103) Gusev, A. A.; Lusti, H. R. *Adv. Mater.* **2001**, *13*, 1641.

(104) Koerner, H.; Jacobs, D.; Tomlin, D. W.; Busbee, J. D.; Vaia, R. D. *Adv. Mater.* **2004**, *16*, 297.

(105) Koerner, H.; Hampton, E.; Dean, D.; Turgut, Z.; Drummy, L.; Mirau, P.; Vaia, R. *Chem. Mater.* **2005**, *17*, 1990.

(106) Kloprogge, J. T.; Komarneni, S.; Amonette, J. E. *Clays Clay Miner.* **1999**, *47*, 529.

(107) Carrado, K. A. *Appl. Clay Sci.* **2000**, *17*, 1.

(108) Carrado, K. A.; Xu, L. Q.; Csencsits, R.; Muntean, J. V. *Chem. Mater.* **2001**, *13*, 3766.

(109) Chastek, T. T.; Que, E. L.; Shore, J. S.; Lowy, R. J.; Macosko, C.; Stein, A. *Polymer* **2005**, *46*, 4421.

(110) Chastek, T. T.; Stein, A.; Macosko, C. *Polymer* **2005**, *46*, 4431.

(111) Sun, Y.; Boo, W. J.; Browning, R. L.; Sue, H. J.; Clearfield, A. *Chem. Mater.* **2005**, *17*, 5606.

(112) Sue, H. J.; Gam, K. T.; Bestaoui, N.; Spurr, N.; Clearfield, A. *Chem. Mater.* **2004**, *16*, 242.

(113) Sue, H. J.; Gam, K. T.; Bestaoui, N.; Clearfield, A.; Miyamoto, M.; Miyatake, N. *Acta. Mater.* **2004**, *52*, 2239.

(114) Bourlinos, A. B.; Chowdhury, S. R.; Jiang, D. D.; An, Y. U.; Zhang, Q.; Archer, L. A.; Giannelis, E. R. *Small* **2005**, *1*, 80.

(115) Bourlinos, A. B.; Herrera, R.; Chalkias, N.; Jiang, D. D.; Zhang, Q.; Archer, L. A.; Giannelis, E. P. *Adv. Mater.* **2005**, *17*, 234.

(116) Bourlinos, A. B.; Chowdhury, S. R.; Herrera, R.; Jiang, D. D.; Zhang, Q.; Archer, L. A.; Giannelis, E. P. *Adv. Funct. Mater.* **2005**, *15*, 1285.

(117) Kojima, Y.; Matsuoka, T.; Takahashi, H. *J. Appl. Polym. Sci.* **1999**, *74*, 3254.

(118) He, J.; Shen, Y.; Yang, J.; Evans, D. G.; Duan, X. *Chem. Mater.* **2003**, *15*, 3894.

(119) Ji, X.; Hampsey, J. E.; Hu, Q.; He, J.; Yang, Z.; Lu, Y. *Chem. Mater.* **2003**, *15*, 3656.

(120) Park, I.; Peng, H.-G.; Gidley, D. W.; Xue, S.; Pinnavaia, T. J. *Chem. Mater.* **2006**, *18*, 650.

(121) Reid, B. D.; Ruiz-Trevino, F. A.; Musselman, I. H.; Balkus, K. J., Jr.; Ferraris, J. P. *Chem. Mater.* **2001**, *13*, 2366.

CHAPTER 2

SYNTHESIS OF SAPONITE-LIKE PLATEY SILICATES AND THEIR ORGANO HYBRID DERIVATIVES

2.1 Introduction

The term "clay" is usually used to describe particles of mineral sediments that are smaller than 0.2 μm in size [1]. Clay minerals are some of the most important industrial minerals, and find applications in process industries, agriculture, environmental remediation, construction. pigments, coatings, ceramics, catalysts and polymer materials [2]. The major structural building blocks of clay minerals are tetrahedral SiO_4 units and octahedral MO_6 units, where is M = Al, Mg, Fe, Zn and the like. Saponite, the clay of interest in the present study, belongs to the smectite clay family. Natural saponite has a stacked layered morphology wherein the layers are made of a 2:1 ratio of tetrahedral silica sheets and magnesia sheets, and a unit cell formula of $(M^+_{x-y}nH_2O)[Mg_{6-y}Al_y](Si_{8-x}Al_x)O_{20}(OH)_4$, where M^+ is the exchangeable gallery cations. Isomorphous substitution by Al takes place in both tetrahedrals and octahedrals and generates negative layer charges that are balanced by exchangeable alkali or alkaline earth cations located inside the galleries.

Natural clay minerals are abundant and inexpensive resources. However, they usually contain impurities and their purification is a time-consuming process. The nanolayer compositions and corresponding surface charges are usually heterogeneous, even in the same clay sample, making it difficult to obtain reliable results in systems where the clay surface properties play important roles. Natural layered clays usually exhibit a well-stacked layered morphology, and their low accessible surface area limits some of their potential applications, such as catalysts. On the other hand, synthetic clays are promising substitutes to natural clays. Smectic clays can be synthesized through sol-gel methods under conditions varying from mild room-temperature conditions to extreme hydrothermal conditions [3-8]. Synthetic clays exhibit reproducible high purity, uniform composition and surface properties. These properties are controllable through mediation of synthesis conditions.

Natural smectic clay minerals are hydrophilic inorganic materials. Their organic modification can be achieved by either organo-cation exchange or silylation of the edge hydroxyl groups. Previously, attempts have been made to synthesize organo-clay derivatives via one-pot sol-gel synthesis using organosiloxanes of the type $RSi(OR')_3$ as the silicon source for clay formation [9-12]. The products contain gallery alkyl groups, which are covalently bonded to the basal silicon centers. Consequently, the products exhibit a stacked morphology and hydrophobic surface properties. However, since the alkyl

groups of the organosiloxane cannot serve as bridging groups for neighboring silica tetrahedra, the products have significant structural distortion, in comparison to a well-ordered clay structure [10]. It is also possible that inversion of silica tetrahedral may occur, so that the apical alkyl group points to the clay gallery, while the oxygen atoms are bridged to adjacent silicon center of the tetrahedral sheet.

Bissiloxanes of the type $(R'O)_3Si-R-Si(OR')_3$ have been used for the synthesis of hybrid zeolites and periodic mesoporous organosilicates (PMOs) [13, 14], which have 3-D structures made exclusively of tetrahedral SiO_4 and AlO_4 centers. When bis(triethoxylsilyl)methane (BTESM) is used as the silicon source for clay synthesis, the bridging methylene group might substitute in part for the bridging oxygen atoms in the basal plane of the clay structure, as illustrated in Figure 2.1. The organically modified clay layers differ from organo-cation-exchanged clays or silylated clays in that the organic groups are incorporated directly into the clay lattice structure. These novel hybrid clay materials may have promising application as absorbances, polymer reinforcing agents, etc.

In the present study, inorganic saponite-like layered silicates also were synthesized through modification of literature methods [3, 4]. Depending on the choice of reagents and synthesis temperature, the products exhibited different layer stacking order that varied between irregularly stacked layers to a well-stacked layered morphology. The structure and surface properties of the

53

synthetic saponites were characterized using XRD, NMR, TEM and N_2 adsorption-desorption isotherms. The organic hybrid derivatives were prepared using bissiloxanes as the Si sources, specifically bis(triethoxylsilyl)methane (BTESM) and bis(triethoxylsilyl)ethane (BTESE). The former siloxane afforded a hybrid clay-like structure with methylene groups incorporated in clay lattice structure in place of bridging oxygen atoms, while the latter could not direct the formation of clay structure due to the bulky size of the ethylene groups.
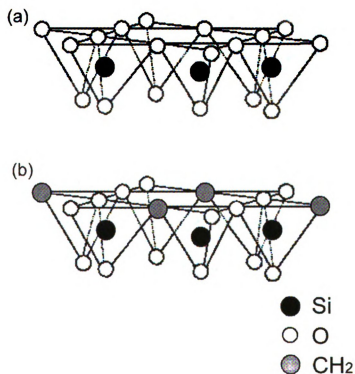
Figure 2.1 Schemes illustrating the difference in tetrahedral sheet structure for (a) an inorganic clay and (b) an organo hybrid clay made from BTESM.

2.2 Experimental

2.2.1 Materials

BTESM and BTESE were purchased from Gelest and used without purification. All other chemicals were purchased from Aldrich and used without purification.

2.2.2 Inorganic saponite synthesis

A synthetic saponite, denoted Mg-SAP, was prepared at 90 °C by modification of previously described methods [3] using water glass solution (27 wt% silica, 14 wt% NaOH), $Al(NO_3)_3 \cdot 9H_2O$, $Mg(NO_3)_2 \cdot 6H_2O$, NaOH and urea in the molar ratio 3.6 : 0.40 : 3.0 : 3.0 : 10 per 400 moles of water. In a typical synthesis, 38.48 g of the sodium silicate solution (0.173 mol silica) and 7.218 g (0.019 mol) $Al(NO_3)_3 \cdot 9H_2O$ were mixed in 346 g deionized water at room temperature for 1.5 h. Then 28.8 g (0.48 mol) urea was introduced to the white suspension, followed by another 1.5 h of stirring at room temperature. The mixture was then brought to 90 °C and heated under stirred consitions for 30 min, followed by the introduction of 37.0 g (0.144 mol) of $Mg(NO_3)_2 \cdot 6H_2O$ as a solid. The mixture was refluxed under stirring conditions at 90 °C for 24 h in a 1 L flask. Then 70 mL of hot NaOH aqueous solution containing 5.64 g (0.141 mol) NaOH was added to the synthesis mixture. The mixture was allowed to age for another 15 h. Finally, the product (denoted Mg-SAP) was centrifuged, triple washed with

deionized water, and dried at 50 °C under N_2 flow. Around 20 g Mg-SAP can be obtained, indicating the yield to be close to 100%.

A synthetic saponite, denoted Zn-SAP, with Zn as the dominant octahedral species was synthesized using the same method as the Mg-SAP synthesis [3], except that $Zn(NO_3)_2·6H_2O$ was used instead of $Mg(NO_3)_2·6H_2O$.

A well-crystallized saponite, denoted SAP-200, was obtained under hydrothermal conditions [4]. In a typical synthesis, 0.35 g of 28wt% NH_4OH solution (2.8 mmol NH_4OH), 0.61 g (3.0 mmol) $Al(OC_3H_7)_3$, 1.6 g (27 mmol) fumed silica, and 4.77 g $Mg(CH_3CO_2)_2$ (22 mmol) were introduced into 40 g deionized water one by one, and the mixture was stirred for 10 minutes after the addition of each reagent. The mixture was then stirred at room temperature for 24 h before being introduced into an autoclave vessel. The crystallization was carried out at 200 °C for 6 days. The product (denoted SAP-200) was centrifuged, washed with water, and dried at 50 °C under N_2 flow. A 2.2 g quantity of SAP-200 can be obtained, indicating the yield to be 80%.

2.2.3 Ion exchange of Mg-SAP

Prior to the exchange reaction, 120 mL 5 wt% aqueous suspension of Mg-SAP was stirred under ambient conditions for 24 h. The Cs^+ exchange reaction was carried out by adding 3.37 g (20 mmol) CsCl to 40 mL of the 5 wt% Mg-SAP aqueous suspension, followed by stirring for 8 h and centrifugation once to separate the solid from the liquid. The supernatant liquid was discarded, and the

solid was again suspended in 40 mL water. The reaction was repeated for 3 times to ensure a complete ion exchange. The product (denoted Cs-[Mg-SAP]) was washed with water four times before drying at 50 °C. K^+- and Ca^{2+}- forms of exchanged Mg-SAP were prepared in the same way, using KCl and $CaCl_2 \cdot 2H_2O$ as the exchange salts, respectively. The latter products were denoted K-[Mg-SAP] and Ca-[Mg-SAP].

2.2.4 Hybrid organo-saponite synthesis

The hybrid organo-saponite was synthesized using a method analogous to the method for the preparation of Mg-SAP, except that hydrolyzed bissiloxane were used exclusively as the Si source. Two types of bissiloxane were used: bis(triethoxylsilyl)methane (BTESM) and bis(triethoxylsilyl)ethane (BTESE), and the products were denoted C1-SAP and C2-SAP respectively. In a typical synthesis, 1.236 g (3.6 mmol) of BTESM was prehydrolyzed in 20 mL of 0.3 M NaOH aqueous solution at 90 °C overnight. After cooling the solution to room temperature, 0.300 g (0.8 mmol) $Al(NO_3)_3 \cdot 9H_2O$ was mixed with the hydrolyzed BTESM solution and stirred for 3 h, followed by the introduction of 1.200 g (20 mmol) urea and another 1.5 h of stirring. The suspension was then brought to 90 °C and heated for 1 hour before the addition of 1.538 g (6 mmol) $Mg(NO_3)_2 \cdot 6H_2O$. The reaction mixture was allowed to age at 90 °C for 24 h with stirring. The product (denoted C1-SAP) was filtered, washed with water and dried at 50 °C.

The C2-SAP was prepared in the same way, expect that 1.276 g (3.6 mmol) BTESE was used in place of BTESM.

2.2.5 Characterization

X-ray diffraction (XRD) patterns were obtained on a Rigaku rotaflex 200B diffractometer equipped with Cu Kα X-ray radiation and a curved crystal graphite monochromator, operating at 45 kV and 100 mA. Powder samples were pressed onto a glass X-ray sample holder.

N_2 adsorption-desorption isotherms were recorded at -196 $^{\circ}$C on a Micrometritcs ASAP 2010 sorptometer. Prior to analysis samples were outgassed at 150 $^{\circ}$C and 10^{-6} Torr for a minimum of 12 h. BET surface areas were calculated from the linear part of the BET plot and BJH pore sizes were obtained from adsorption isotherms.

Transmission electron microscopy (TEM) images were obtained on a JEOL 2200FS field emission microscope with a ZrO/W Schottky electron gun and an accelerating voltage of 200 kV. The powdered samples were sonified in ethanol, and the resulting suspension was dripped onto 300 mesh copper grids.

Scanning electron microscope energy dispersive X-ray microanalysis (SEM EDS) was performed on a JEOL 6400V microscope with LaB$_6$ emitter, and the EDS detector was an INCA x-sight. The powder samples were mounted on aluminum stubs and coated with carbon before the analysis. The quantitative

analysis was performed using an INCA suite version 4.07 (Oxford Instruments) analysis program.

^{29}Si and ^{27}Al MAS NMR spectra were obtained at 79 MHz on a Varian VXR-400S solid-state NMR spectrometer equipped with a magic angle-spinning probe. The samples were spun at 4 kHz for each measurement. The pulse delay for ^{29}Si MAS NMR was 400 s. Talc was used as a chemical shift reference (-98.1 ppm). The pulse delay for ^{27}Al MAS NMR was 0.50 s. A 0.10 M aqueous Al(NO$_3$)$_3$ solution was used as the chemical shift reference (0.0 ppm).

FTIR spectra of samples dispersed in KBr disks were recorded at ambient temperature on a Mattson Galaxy 3000 FTIR spectrometer over the range 400 to 4000 cm^{-1}.

2.3 Results

2.3.1 Inorganic saponite derivatives

The XRD patterns of the synthetic saponite clays Mg-SAP, Zn-SAP and SAP-200 are compared in Figure 2.2. Characteristic smectite clay in-plane diffraction peaks are observed in all three cases. Mg-SAP did not possess a well-stacked morphology, as verified by the absence of a 001 peak in the XRD pattern (Figure 2.2b). However, once the powder was pressed in a hydraulic presser at 10,000 psi for 1 min to form a pellet and subject to XRD analysis, a weak 001 peak appeared (Figure 2.2a), indicating that the as-made Mg-SAP had

an irregularly stacked platy morphology. In contrast, Zn-SAP and SAP-200 exhibited a sharp 001 peak, indicating a well-stacked morphology. Zn-SAP and SAP-200 had better crystallinity compared with Mg-SAP, as revealed by the narrower line widths of the clay in-plane diffraction peaks.
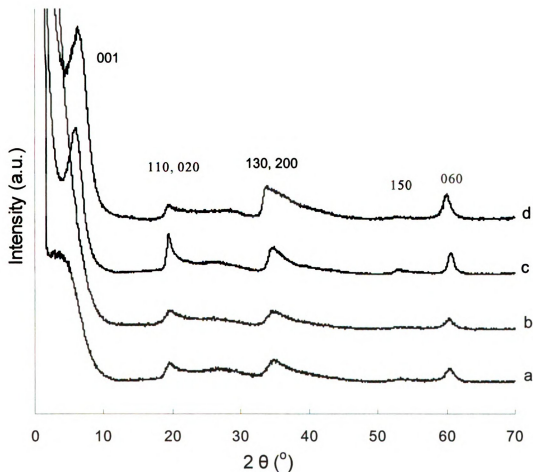
Figure 2.2 Wide angle *hkl* X-ray diffractions of (a) pressed Mg-SAP, (b) as-made Mg-SAP, (c) Zn-SAP and (d) SAP-200.

The platy morphologies of the synthetic saponites are clearly shown in TEM images (Figure 2.3). The dark thin lines in the images represent clay

platelets with edge-on orientations to the electron beam. The length of such edges increases dramatically in the order of Mg-SAP < Zn-SAP < SAP-200, indicating an increase in lateral dimension and layer stacking. Also, the number of the edges appearing in the TEM images decreases in the reverse order. The in-plane dimensions of the Mg-SAP platelets were of the order of 50 nm, whereas Zn-SAP had in-plane platelet dimensions of several hundred nanometers, and SAP-200 had an even larger lateral dimensions. Layer stacking was evident for both Zn-SAP and SAP-200. Although the layer stacking was absent in Mg-SAP, the clay platelets were highly aggregated and interacted with each other through edge-face interactions.

Table 2.1 The BET surface areas and pore volumes of Mg-SAP, Zn-SAP, and SAP-200 and the Ca^{2+}-, Cs^+-, and K^+- exchanged forms of Mg-SAP.

	BET surface area (m^2/g)	Total pore volume (cm^3/g)	BJH adsorption pore size (nm)
Mg-SAP	920	1.98	3
Zn-SAP	310	0.70	-
SAP-200	270	0.10	-
K-[Mg-SAP]	820	1.16	-
Cs-[Mg-SAP]	700	0.98	-
Ca-[Mg-SAP]	690	1.02	2

The relative standard deviations of the BET surface areas are less than 0.5%.
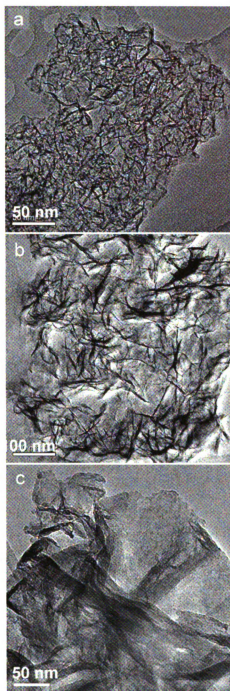
Figure 2.3 TEM images of the synthetic saponites: (a) Mg-SAP; (b) Zn-SAP and (c) SAP-200.

Figure 2.4 (a) Nitrogen adsorption-desorption curves and (b) BJH adsorption

pore size distributions (off set by 0.1 for clarification) of as-made Mg-SAP and its

Ca^{2+}-, Cs^+-, and K^+- exchanged derivatives.
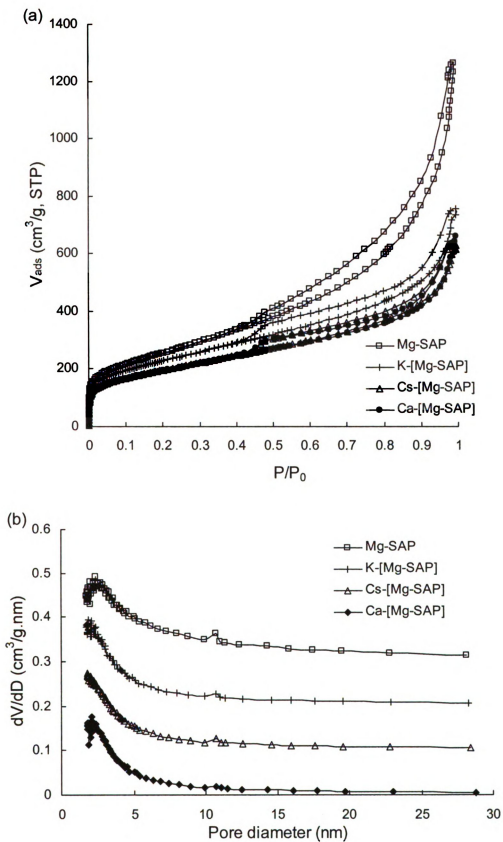
The textural properties of Mg-SAP, Zn-SAP and SAP-200 were determined from the nitrogen adsorption-desorption isotherms. The results are summarized in Table 2.1. Mg-SAP exhibited a large BET surface area (920 m^2/g), a uniform BJH adsorption pore size (3.0 nm) and a large pore volume (1.98 cm^3/g). The abrupt nitrogen uptake at low pressure indicates the presence of micropores. (Figure 2.4) The well-stacked Zn-SAP and SAP-200 derivatives had lower surface areas and pore volumes. The sodium exchange form of naturally occurring sodium montmorillonite exhibited a surface area < 10 m^2/g and virtually no pore volume. Clearly, the exceptionally high surface area and porosity of SAP is a manifestation of the relatively small platelet size and the aggregation of the platelets in poorly stacked form. We have shown that this unique porous morphology makes Mg-SAP a good reinforcing agent for epoxy polymers [15].

Vibration modes typical of a 2:1 layered silicate structure were observed in the FTIR spectrum of Mg-SAP (Figure 2.5). The broad adsorption band 3000-3600 cm^{-1} is a mixture of the stretching vibrations of OH from structural hydroxyl groups, symmetric and asymmetric OH stretching frequencies from surface water molecules, and gallery NH_4^+. The adsorption bands at 1646 and 1400 cm^{-1} are assigned to the bending vibrations of OH from surface water and gallery NH_4+, respectively. The strong adsorption band at 1050 cm^{-1} is assigned to Si-O stretching. The band at 476 cm^{-1} is assigned to Si-O-Si bending [16].
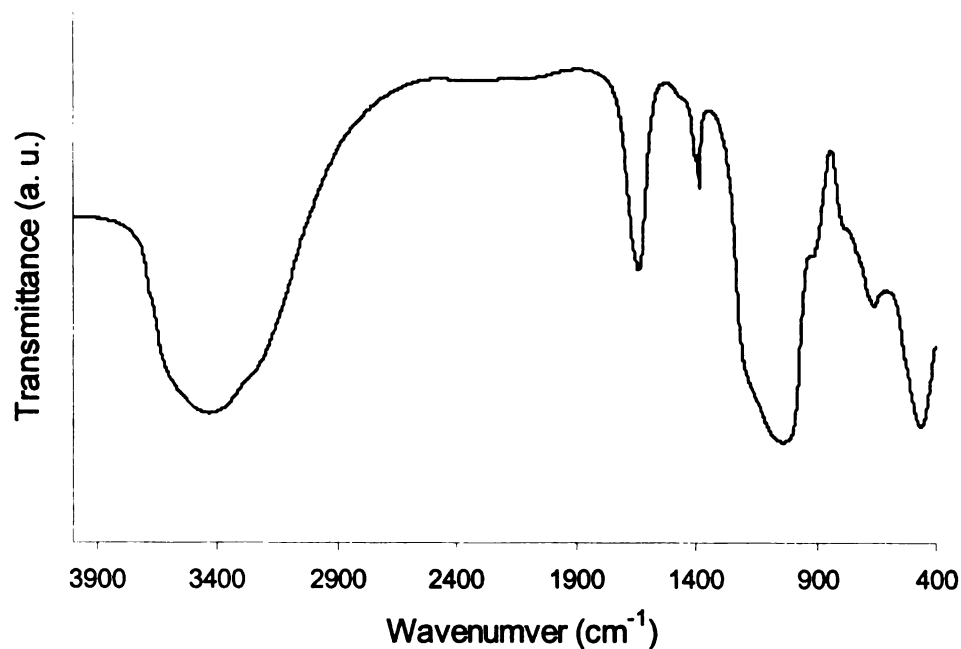
Figure 2.5 The FTIR spectrum of Mg-SAP.

The 2:1 lattice structure of Mg-SAP was further characterized using solid state NMR. The ^{29}Si MAS NMR spectrum (Figure 2.6a) showed the presence of two Q^3 signals at chemical shifts of -87.3 and –95.2 ppm. In accord with previous assignments [17], the -87.3 ppm line is assigned to Si centers linked through bridging oxygen atoms to one tetrahedral Al site and two tetrahedral Si sites. The -95.2 ppm resonance is attributed to Si linked to three adjacent tetrahedral sites that are exclusively occupied by Si. In addition, a weak resonance near -110 ppm is present which may be indicative of the presence of a small amount of amorphous silica.

The ^{27}Al MAS NMR spectrum (Figure 2.6b) of Mg-SAP contains two signals at chemical shifts of 62.8 ppm and 6.5 ppm, indicating that Al substitution occurred in both the tetrahedral and octahedral sheets of the 2:1 layered silicate structure. Deconvolution analysis of the overlapping ^{27}Al NMR lines at 62.8 ppm and 6.5 ppm revealed the ratio of tetrahedral to octahedral aluminum to be 0.83 : 0.17. Due to potential differences in the electric field gradient at the quadrupolar ^{27}Al nucleus in tetrahedral and octahedral environments, the relative intensities of the resonances may not be proportional to the aluminum populations in these sites. Nevertheless, the presence of octahedral and tetrahedral was clearly indicated by the ^{27}Al NMR spectrum. Similar ^{29}Si NMR and ^{27}Al NMR spectra were observed for Zn-SAP and SAP-200, indicating both had a saponite-like structure.

An SEM EDS analysis of Mg-SAP showed that the molar ratio of Si : Mg : Al equals to 17 : 13 : 2, corresponding to a saponite unit cell formula of $(Na^{+},$ $NH_4^{+})_{0.5}(Si_{7.3}Al_{0.7})[Mg_{5.8}Al_{0.2}]O_{20}(OH)_4$. The atomic ratio of Si : Zn : Al was 19 : 15 : 2 in Zn-SAP, as revealed by SEM-EDS, corresponding to a unit cell formula of Zn-SAP was $(Na^{+}, NH_4^{+})_{0.4}(Si_{7.4}Al_{0.6})[Zn_{5.8}Al_{0.2}]O_{20}(OH)_4$. The atomic ratio of Si : Mg : Al was 18 : 14 : 3 for SAP-200, and corresponding unit cell formula was $(NH_4^{+})_{0.4}(Si_{7.2}Si_{0.8})[Mg_{5.6}Al_{0.4}]O_{20}(OH)_4$.
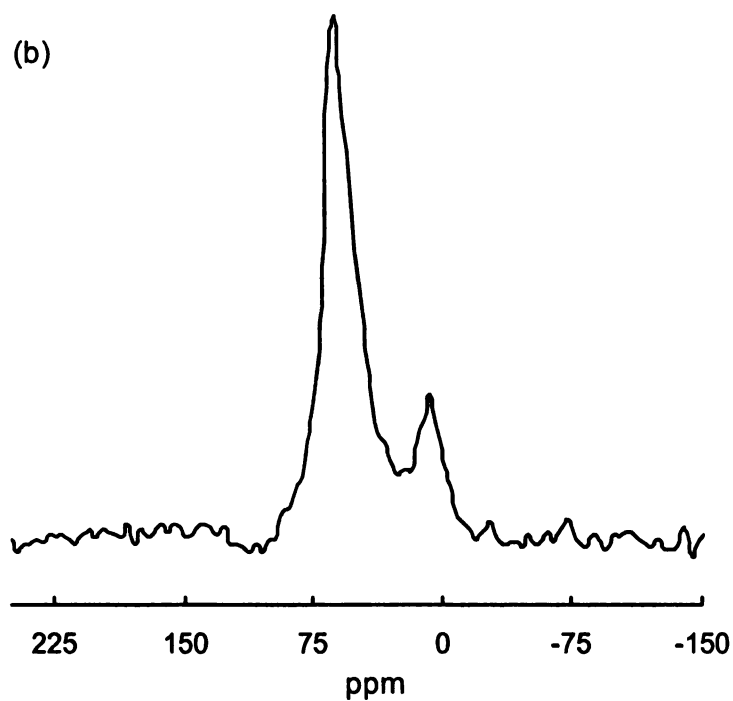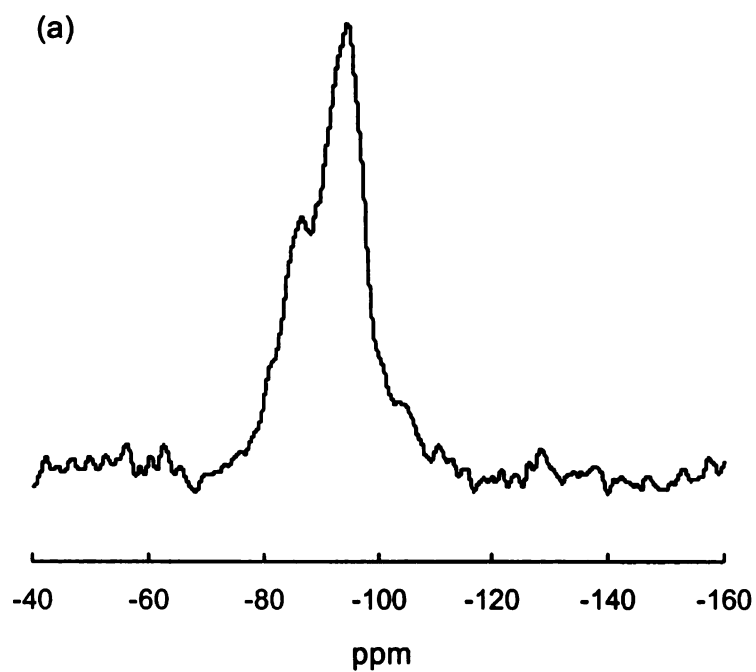
Figure 2.6 (a) ^{29}Si MAS NMR and (b) ^{27}Al MAS NMR spectra for Mg-SAP.

As-made Mg-SAP contains mixed exchange cations of Na^+ and NH_4^+. These gallery cations can be exchanged by various other cations. The Ca^{2+}, Cs^+ and K^+ exchanged derivatives of Mg-SAP were obtained by mixing Mg-SAP and excessive corresponding metal chloride salts in water. The exchanged products were denoted Ca-[Mg-SAP], Cs-[Mg-SAP] and K-[Mg-SAP] respectively. The irregularly stacked morphology of Mg-SAP was maintained after the exchange reaction, as the exchanged saponites showed XRD patterns equivalent to Mg-SAP. (Figure 2.7) However, the 110 diffraction peak of Cs-[Mg-SAP] was weakened. These suggest that the Cs^+ cation may be bound tightly to the hexagonal cavities in the clay basal plane, leading to an X-ray phase shift which weakens the 110 diffraction peak. The other exchange cations could be more heavily hydrated, and not tightly bound to hexagonal cavities. Therefore, these cations do not affect the intensity of the 110 peak.

Nitrogen adsorption-desorption isotherms and BJH adsorption pore size distribution curves of the saponites are shown in Figure 2.4. The exchanged Mg-SAP clays had lower BET surface areas and total pore volumes compared with Mg-SAP (Table 2.1).
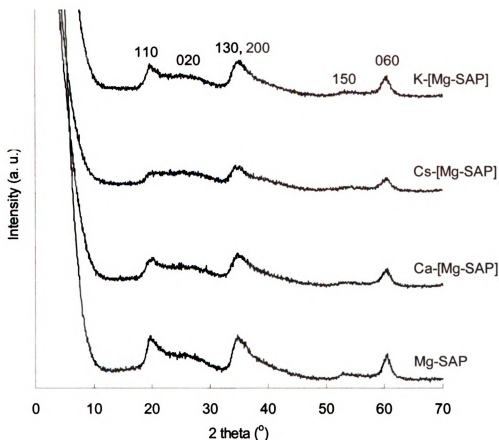
Figure 2.7 Wide angle *hkl* X-ray diffractions of the Ca^{2+}-, Cs$^+$-, and K$^+$-exchanged Mg-SAPs, compared with that of as-made Mg-SAP.

The ion exchange of Ca^{2+}, Cs$^+$, or K$^+$ was verified using SEM-EDS analysis. The atomic ratios of Si : Mg : Al of the exchanged saponites were consistent within experimental error with the unexchanged Mg-SAP, while the gallery Na$^+$ cations of Mg-SAP were replaced by Ca^{2+}, Cs$^+$, and K$^+$, respectively in the exchanged forms (Table 2.2). A lower Si ratio was observed in Cs-[Mg-SAP], due perhaps to leeching, consistent with the XRD results. The concentrations of the metal cations were the same in Ca-[Mg-SAP], Cs-[Mg-SAP]

and K-[Mg-SAP]. Mg-SAP exhibited a lower exchange cation concentration since NH_4^+, as the other part of the Mg-SAP surface cations, cannot be detected accurately using SEM-EDS.

Table 2.2 Elemental atomic ratios for Mg-SAP and its exchanged derivatives obtained from quantitative SEM-EDS analysis.

	Si [*]	Mg [*]	Al [*]	M [*]
Mg-SAP	19.0	14.7	2.0	$0.5\ Na^+$
Ca-[Mg-SAP]	19.6	14.6	2.0	$1.1\ Ca[(OH)]^+$
Cs-[Mg-SAP]	18.1	15.0	2.0	$1.0\ Cs^+$
K-[Mg-SAP]	19.0	15.5	2.0	$1.1\ K^+$

[*] Each value is the average of three measurements performed on different regions of the sample.

2.3.2 Hybrid organo-saponite derivatives

We used a method analogous to that for Mg-SAP synthesis to prepare an inorganic-organic hybrid saponite. Prehydrolyzed BTESM and BTESE containing two triethoxylsilyl groups bridged by a methane and ethylene group, respectively, were used as the Si sources for hybrid clay synthesis. The XRD patterns of C1-SAP (made from BTESM) and C2-SAP (made from BTESE) are shown in Figure 2.8, compared with Mg-SAP. The organo saponite synthesis was successful with BTESM, as verified by the characteristic clay in-plane diffraction peaks in the XRD pattern of C1-SAP. The 110 peak was not well resolved, indicating the possibility of structural distortion in the basal plane.

Although a weak 060 diffraction peak is present in the XRD pattern of C2-SAP, the principal product is a mixture of clay and hydroxides of magnesium and aluminum, indicating that BTESE was not completely converted to a clay structure due to the unsuitable bulky size of the ethylene bridging group.

C1-SAP had a BET surface area of 656 m^2/g. The presence of micropores on C1-SAP surfaces was verified by the uptake of nitrogen at low pressure in the nitrogen adsorption-desorption isotherm curve (Figure 2.9), similar as in the isotherm curve of the inorganic Mg-SAP. However, the mesoporous region (0.1 ~ 1 P/P$_0$) of C1-SAP was dramatically reduced, resulting in a lower total pore volume of 0.54 cm^3/g, compared with 1.98 cm^3/g for Mg-SAP.
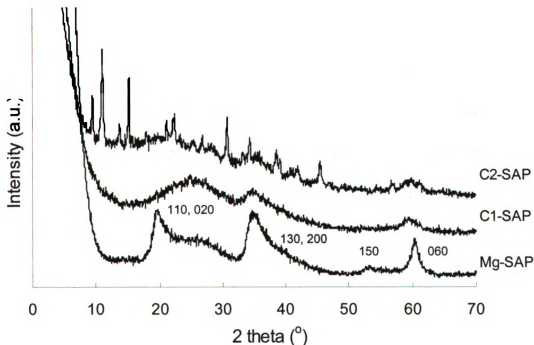
Figure 2.8 XRD patterns of Mg-SAP, C1-SAP and C2-SAP reaction products.
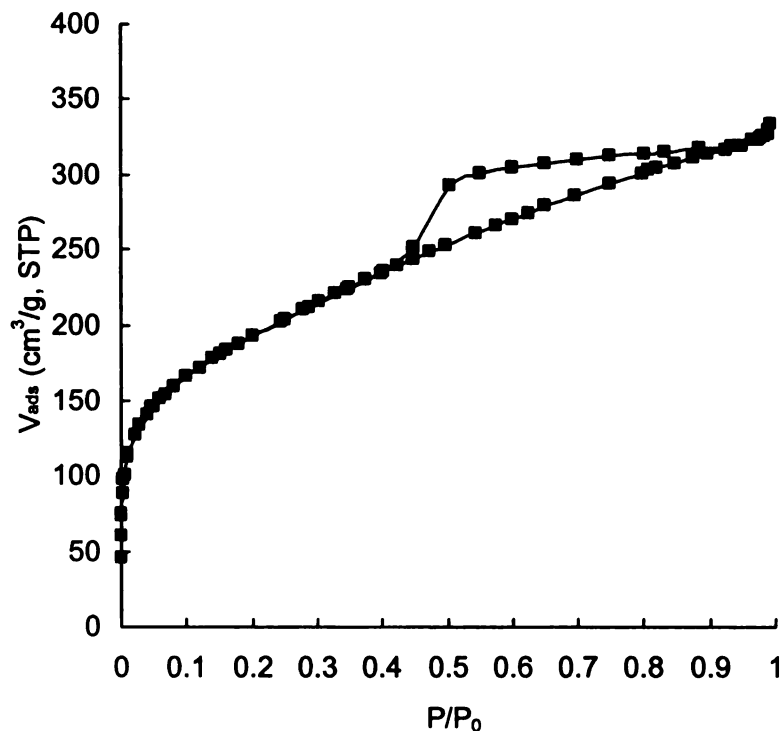
Figure 2.9 The nitrogen adsorption-desorption isotherms for C1-SAP.

The incorporation of methylene group in the structure of C1-SAP was verified using ^{29}Si, ^{13}C, and ^{27}Al MAS NMR (Figure 2.10) and FTIR. In the ^{29}Si NMR spectrum, two chemical shifts at -55 ppm and -90 ppm were observed, and were assigned to T^2 and Q^2 silicon species respectively. The presence of methylene group and C-Si bonds in C1-SAP was verified by the T bands in the ^{29}Si NMR spectrum, as well as by the chemical shift at -3 ppm in the ^{13}C NMR spectrum. The presence of Q^2 silicon species in the C1-SAP structure was possibly due to the cleavage of C-Si bonds during BTESM hydrolysis. Details will be discussed in the Discussion part. Isomorphous substitution by Al in both

the tetrahedral and octahedral centers of the C1-SAP structure was verified by the presence of tetrahedral and octahedral Al resonances at 55 and 4 ppm, respectively, in the ^{27}Al NMR spectrum (Figure 2.10c).

The FTIR spectrum of C1-SAP exhibited characteristic clay in-plane lattice vibration modes that were comparable with those of Mg-SAP (Figure 2.11). The new bands at 2980 and 1275 cm^{-1} in the spectrum of C1-SAP are assigned to C-H and Si-C stretching bands, respectively. C1-SAP has a platy morphology with lateral dimensions in the range of 20 ~ 50 nm, as shown in its TEM image (Figure 2.12). Unlike Mg-SAP, C1-SAP did not exhibit an aggregated nanolayer morphology. CHN elemental analysis revealed that C1-SAP contained around 4.7 wt% carbon.

Figure 2.10 The (a) ^{29}Si MAS NMR, (b) ^{13}C MAS NMR and (c) ^{27}Al MAS NMR

spectra of C1-SAP.

(a)
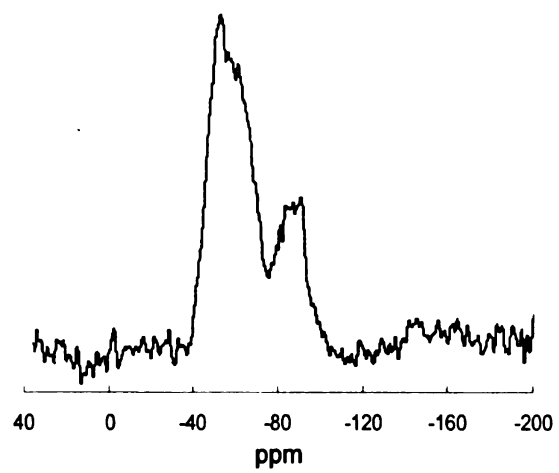
(b)
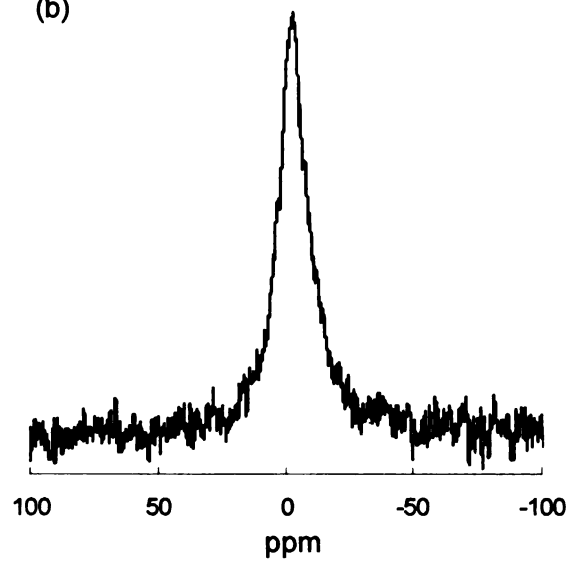
(c)
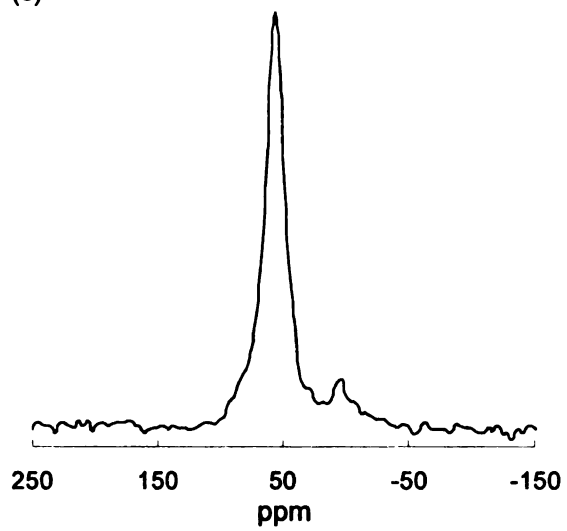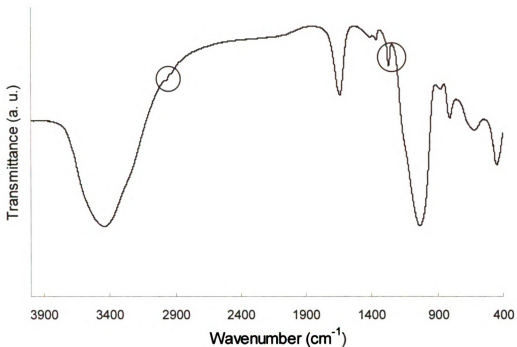
Figure 2.11 FTIR spectrum of C1-SAP. The circled regions in the spectrum of

C1-SAP indicate the incorporation of methylene groups in C1-SAP structure.
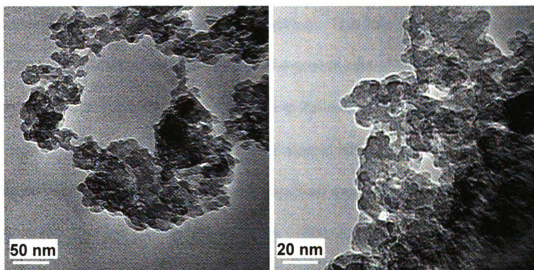
Figure 2.12 TEM images of C1-SAP showing its platy morphology.

2.4 Discussion

2.4.1 Inorganic saponite derivatives

The physical properties of the synthetic inorganic clay products are directly determined by synthesis conditions, particularly the synthesis temperature and the composition of the octahedral sheet. Comparing Mg-SAP made at 90 °C and SAP-200 made at 200 °C, the higher synthesis temperature and a longer crystallization time for SAP-200 resulted in ordered layer stacking and larger in-plane platelet dimensions. Consequently, SAP-200 exhibited a well stacked layered morphology, while the stacking was not ordered for Mg-SAP. The octahedral species also plays important role in determining clay particle morphology determination. With Zn as the primary octahedral species, Zn-SAP had a faster platelets octahedral sheet growth rate, which afforded larger clay platelets dimensions and better layer stacking. This fact also indicates that the clay stacking formation is dependent on the growth rate of the octahedral sheet..

Synthetic saponites can be subject to ion-exchange reaction. Although K^+, Cs^+, Ca^{2+}, Na^+ and NH_4^+ have different atomic diameters and could result in different gallery spacings, the irregularly stacked morphology of Mg-SAP was not affected by the ion exchange reactions. The exchanged Mg-SAP exhibited surface porosities, mainly micropores, as verified by the abrupt nitrogen uptake in the low partial pressure region of the N_2 adsorption-desorption isotherms. (Figure 2.4) The mesoporous volumes forthe exchanged Mg-SAPs were lower than the

pore volume of as-made Mg-SAP, as judged by the lower nitrogen uptake in the range of $0.1 \sim 1.0$ P/P_0. The BJH pore size distribution curves also revealed that exchanged forms of Mg-SAP had smaller pore sizes than Mg-SAP. The decrease in surface areas and pore volumes of the exchanged saponites might be due to the collapse of the aggregated clay layers upon replacement of mixtures of Na^+ and NH_4^+ cations by Ca^{2+}, Cs^+ or K^+.

2.4.2 Hybrid organo-saponite derivatives

The clay-like structure has been verified for C1-SAP based on the characteristic smectic clay diffraction peaks in the XRD pattern. The incorporation of methylene group as groups between silica tetrahedra in the basal plane was verified by the ^{29}Si and ^{13}C MAS NMR and FTIR. The size of the organo bridging group in bissiloxane, as the starting reagent for clay synthesis, has to be suitable for the replacement of oxygen in the Kagome network. Bulky groups, such as the ethylene group in BTESE, can not substitute for oxygen and cannot lead to the formation of the hybrid clay structure. However, the methylene group is isoelectronic with oxygen and well suited as a replacement for bridging oxygen.

The surface porosity was much reduced in C1-SAP, compared with inorganic Mg-SAP. The surface porosity of Mg-SAP arises from the formation of an irregularly aggregated layer morphology. However, the possible presence of organo groups on the edges of C1-SAP platelets weakened the edge-face

interactions. Therefore, the platelets correlated with each other without leaving inter-platelet pores. Some layer stacking was observed in the TEM image (Figure 2.11). However, a stacking peak was not resolved in the XRD pattern of C1-SAP due to the low stacking order and small domain sizes of the platelets.

Despite the incorporation of methylene groups in C1-SAP basal plane, some structural distortions occurred, compared with an ideal smectic clay structure, as evidenced by the Q^2 silicon species in the ^{29}Si NMR and the absence of a 110 diffraction peak in the XRD pattern. There are two main causes for the structural distortions. First, since BTESM was used exclusively as the Si source to prepare C1-SAP, there was a high possibility that one of the siloxanes is in the clay basal plane while the other is inverted and oriented out of the basal plane. Using a mixture of an inorganic Si source, such as a sodium silicate solution, and BTESM for clay synthesis may solve this problem, although the products would have a lower methylene loading. Second, BTESM was susceptible to nucleophilic substitution under basic conditions, and would yield inorganic Si-$(OH)_4$ species and intermediate Si-CH_2^- species [13]. The hydrolysis reaction introduces Q^2 Si species and methyl terminal groups into the Kagome network. Although the prehydrolysis of bissiloxane has been used in the preparation of hybrid zeolite materials, the hydrolysis conditions, such as pH and reaction temperature, have to be adjusted for hybrid clay synthesis to avoid the C-Si bond cleavage and to minimize clay structural distortion. It is expected that,

by using a mixture of sodium silicate solution and BTESM as the Si source, the prehydrolysis step of BTESM can be removed, and the hydrolysis of BTESM will take place in the basic sodium silicate solution even at room temperature.

2.5 Conclusion

Synthetic saponites have been prepared at 90 °C and under hydrothermal conditions. The products shared a similar smectic clay structure, while their layer stacking order, surface porosity varied according to the synthesis conditions and octahedral composition. A higher synthesis temperature and rapid octahedral sheet formation leads to better crystallinity and layer stacking in the products. An analogous synthesis method was used to make organo clay hybrids using exclusively BTESM as the Si source so that the hybrid product would have methylene group bridging silica tetrahedra in the clay basal plane. Although some structural distortions still occurred, this strategy provides a novel approach to achieve organic decoration of a clay structure from a one-pot sol-gel synthesis while preserving the basic clay lattice structure. Potential applications of the synthetic hybrid clay include polymer reinforcement, catalysts, absorbance etc.

References

(1) Brindley, G. W.; Brown, G. *Crystal Structures of Clay Minerals and Their X-ray Identification;* Mineralogical Society: London, **1980**.

(2) Murray, H. H. *Clay Miner.* **1999**, *34*, 39.

(3) Vogels, R. J. M. J.; Kerkhoffs, M. J. H. V.; Geus, J. W. *Stud. Surf. Sci. Catal.* **1995**, *91*, 1153.

(4) Kloprogge, J. T.; Breukelaar, J.; Jansen, J. B. H.; Geus, J. W. *Clays Clay Miner.* **1993**, *41*, 103.

(5) Kloprogge, J. T.; Komarneni, S.; Amonette, J. E. *Clays Clay Miner.* **1999**, *47*, 529.

(6) Reinholdt, M.; Miehe-Brendle, J.; Delmotte, L.; Tuilier, M.-H.; le Dred, R.; Cortes, R.; Flank, A.-M. *Eur. J. Inorg. Chem.* **2001**, *11*, 2831.

(7) Carrado, K. A. *Appl. Clay Sci.* **2000**, *17*, 1.

(8) Prihod'ko, R.; Sychev, M.; Hensen, E. J. M.; van Veen, J. A. R.; van Santen, R. A. *Stud. Surf. Sci. Catal.* **2002**, *142*, 271.

(9) Chastek, T. T.; Que, E. L.; Shore, J. S.; Lowy, R. J.; Macosko, C.; Stein, A. *Polymer* **2005**, *46*, 4421.

(10) Chastek, T. T.; Stein, A.; Macosko, C. *Polymer* **2005**, *46*, 4431.

(11) Whilton, N. T.; Burkett, S. L.; Mann, S. *J. Mater. Chem.* **1998**, *8*, 1927.

(12) Burkett, S. L.; Press, A.; Mann, S. *Chem. Mater.* **1997**, *9*, 1071.

(13) Yamamoto, K.; Sakata, Y.; Nohara, Y.; Takahashi, Y.; Tatsumi, T. *Science* **2003**, *300*, 470.

(14) Hatton, B.; Landskron, K.; Whitnall, W.; Perovic, D.; Ozin, G. A. *Acc. Chem. Res.* **2005**, *38*, 305.

(15) Xue, S.; Pinnavaia, T. J. Microporous Mesoporous Mater. 2007, doi: 10.1016/j.micromeso. 2007.02.042.

(16) Madejova, J.; Komadel, P. *Clays Clay Miner.* **2001**, *49*, 410.

(17) Lipsicas, M.; Raythatha, R. H.; Pinnavaia, T. J.; Johnson, I. D.; Giese Jr, R. F.; Costanzo, P. M.; Robert, J.-L. *Nature*, **1984**, *309*, 604.

CHAPTER 3

Porous Synthetic Smectic Clay for the Reinforcement of Epoxy Polymers

3.1 Introduction

Polymer – smectic clay nanocomposites, first demonstrated for a Nylon-6 polymer [1], have attracted much research interest over the past decade. When the clay nanolayers are fully dispersed in the polymer matrix, significant improvements in mechanical strength, thermal stability, barrier properties, and other properties can be realized [2-5] at low clay loadings (< 10 wt%). Naturally occurring smectite clays have poor wetting properties when combined with polymer or polymer precursor due to incompatible surface polarity. Thus, when unmodified clays are combined with a polymer, the nanolayers retain a stacked structure, resulting in the formation of a conventional composite containing clay tactoids in micrometer size. In order to achieve exfoliation of the clay nanolayers in the polymer matrix, it is almost always necessary to replace the inorganic exchange cations on the clay basal surfaces with alkylammonium or other organic cations. The organocations enlarged the galley space between stacked nanolayers, lower the polarity of the surface and allow for the intercalation of polymer between nanolayers. Under appropriate though often stringent [6]

84

processing conditions, complete exfoliation of the nanolayers into the polymer matrix can be achieved.

Although natural smectic clay minerals are abundant and inexpensive, they require extensive purification for nanocomposite applications. On the other hand, they also can be synthesized through sol-gel methods under hydrothermal conditions [7-12]. Organosilicates with lamellar structures analogous to smectic clays also have been prepared using one-pot sol-gel methods [11, 13, 14]. In addition, the composition and surface polarity of synthetic clays can be easily modified through a judicious choice of cations in the tetrahedral and octahedral interstacies of the layers.

In the present work we investigate the properties of a synthetic smectic clay (saponite) for the reinforcement epoxy polymers. The obtained clay forms a 2D micrometric network of irregularly stacked nanolayers approximately 50 nm in diameter. Sonification reduces the domain size of the aggregated platelet network and facilitates the dispersion of clay particles in the polymer. Moreover, the dispersion of clay aggregates is achieved without the need for organo-modification of the clay surfaces through ion exchange with alkylammonium ions. Thus, it is possible to achieve polymer reinforcement while avoiding the plasticizing effects of the alkylammonium ions [15, 16] and the complications caused by Hoffman degradation of such ions at temperatures above 200 °C [17, 18]. Although epoxy – clay nanocomposites have been extensively studied [6,

15, 19-24], improving the mechanical strength of glassy epoxy derivatives remains a challenge. We show that the synthetic clay of the present study substantially improves the tensile properties of both rubbery and glassy epoxy matrices.

3.2 Experimental

3.2.1 Materials

The diglycidyl ethers of bisphenol A (DGEBA), more specifically, Shell EPON resin 826 and 828, and polyoxypropylene diamines of the type $NH_2CH(CH_3)CH_2[OCH_2CH(CH_3)]_xNH_2$ (Huntsman Chemicals Jeffamine D230 with x=2.6 and D2000 with x=33) were used to form glassy and rubbery epoxy matrices. PGV Na^+-montmorillonite (NaMMT) was provided by Nanocor Inc. All other chemicals were purchased from Aldrich Chemical Co. and used without further purification.

3.2.2 Saponite synthesis

Synthetic saponite was prepared at 90 °C according to previously described methods [9] using water glass solution (27 wt. % silica, 14 wt. % NaOH), $Al(NO_3)_3 \cdot 9H_2O$, $Mg(NO_3)_2 \cdot 6H_2O$ and urea as the source of base in the molar ratio 3.6 : 0.40 : 3.0 : 10 per 400 moles of water. After a crystallization period of 24 h the as-made NH^{4+}, Na^+ mixed ion form of the clay was converted to the sodium ion form by ion exchange and denoted SAP. An organic ion

derivative, denoted C16-SAP, was prepared by ion exchange reaction of SAP with cetyltrimethylammonium bromide (CTAB).

3.2.3 Composite preparation

SAP was used to reinforce both glassy and rubbery epoxies, prepared from stoichiometric amounts of EPON 826 - Jeffamine D230 (weight ratio 76 : 24) and EPON 828 - Jeffamine D2000 (weight ratio 27.5 : 72.5), respectively. For comparison purposes, sodium montmorillonite (NaMMT) and C16-SAP clays were also used to make glassy epoxy composites.

Glassy epoxy composites were obtained by first suspending the clay in ethylacetate and subjecting the suspension to ultrasonification for 10 min using a Branson 102C digital laboratory sonifier. The EPON resin was added to the sonified clay suspension and the mixture was stirred in a fume hood overnight and then heated at 50 °C for 4 h under vacuum to complete the evaporation of solvent. Then the curing agent was added to the epoxy-clay mixture and the mixture was stirred at 75 °C for 10 min, outgassed at room temperature for 20 min, and then poured into silicone molds to obtain tensile testing specimens. The composites were partially cured at 75 °C for 3 h and then fully cured at 125 °C for 3 h.

Rubbery composites were prepared in the same manner as the glassy composites except that the clay, epoxy resin, and curing agent were directly mixed without the aid of ethylacetate or ultra-sonication.

3.2.4 Characterization

X-ray diffraction (XRD) patterns were obtained on a Rigaku rotaflex 200B diffractometer equipped with Cu Kα X-ray radiation and a curved crystal graphite monochromator, operating at 45 kV and 100 mA. Powder samples were pressed onto a glass X-ray sample holder. Rectangular flat specimens of cross-linked composites were mounted onto an aluminum holder for XRD examination.

Transmission electron microscopy (TEM) images were obtained on a JEOL 2200FS field emission microscope with a ZrO/W Schottky electron gun and an accelerating voltage of 200 kV. The powdered samples were sonified in ethanol, and dripped onto 300 mesh copper grids. For composites, thin sections (~100 nm thick) of the composites were put on naked copper grids.

Tensile mechanical properties of dog-bone shaped specimens were tested according to ASTM procedure D3039 using an SFM-20 United Testing System equipped with a laser extensometer. The measurements were conducted at room temperature with a crosshead speed of 0.5 mm/min for glassy specimens, and 12.5 mm/min for rubbery specimens. The reported tensile values are the averages for 4-5 specimens with dog-bone shapes. The standard deviation for the modulus and strength was +/- 3%. The standard deviation for the toughness values, obtained by integrating the area under the stress – strain curves, was +/- 35%.

Dynamic mechanical analysis (DMA) was performed on a DMA 2980 dynamic mechanic analyzer (TA Instruments) operated in three-point bending mode at a frequency of 1Hz and amplitude of 40 µm, from 25 to 140 °C at a heating rate of 4.0 °C/min. The specimens were rectangular bars with dimensions 60 X 13 X 3 mm.

3.3 Results

3.3.1 Epoxy – saponite nanocomposites

The synthetic SAP has an irregularly stacked platy morphology. Consequently, it exhibited a large BET surface area (920 m^2/g) and a average BJH pore size of 5.0 nm and a pore volume of 1.98 cm^3/g. Detailed characterization of SAP is described in Chapter 2.

Both SAP and NaMMT were tested for the reinforcement of epoxy polymers, particularly in the glassy state, without the use of organic surface modifier. Rapid settling-out of clay particles was observed for suspensions of NaMMT in the epoxy resin, curing agent, and stoichiometric mixtures of the resin and curing agent, making it impossible to form uniform composites. However, little or no particle settling occurred for SAP clay suspensions, as judged by the depth profiling of the XRD intensity of the clay 060 reflection for cured composites (Figure 3.1).
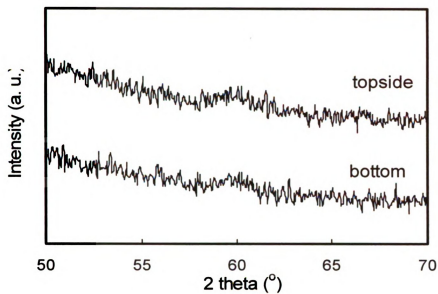
Figure 3.1 The XRD patterns of the topside and bottom of an epoxy – SAP 5.4% composite, both showing 060 clay diffraction peak of similar intensity.
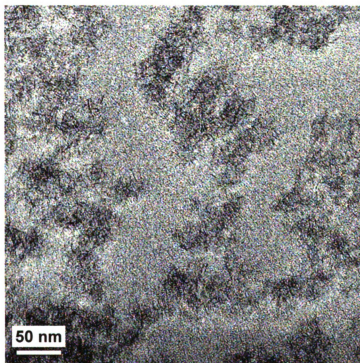
Figure 3.2 A TEM image of thin-sections of a glassy epoxy – SAP 5.4 wt% composite.

TEM images of thin-sections of a 5.4 wt% epoxy – SAP composite showed a uniform dispersion of aggregated SAP particles (Figure 3.2). The edges of randomly oriented clay platelets with lateral dimensions ~ 50 nm are clearly observed in the aggregates. Clay platelets lying flat in the sections are visible as lighter regions of the image due to the low contrast. The particle aggregates are comprised of face-face stacks of nanolayers and edge-face interactions between the stacks. There is little evidence for the presence of single, delaminated platelets within the aggregates. Thus, the absence of a well-resolved 001 stacking reflection in the XRD pattern of SAP and SAP-epoxy composites is the result of irregular stacking of nanolayers and not the result of nanolayer exfoliation. Although bent clay nanolayers are sometimes observed for polymer – clay nanocomposites [25, 26], little or no layer bending is observed for epoxy – SAP nanocomposites due primarily to the small lateral dimensions of the nanolayers.

3.3.2 Composite Properties

The tensile properties of glassy epoxy - SAP and - NaMMT composites are provided in Table 3.1. The improvement in the tensile properties of the SAP composites is correlated with the exceptional dispersion of these particles in the polymer matrix. On the other hand, NaMMT exhibited poor dispersion in the epoxy matrix, and the corresponding composites exhibit mechanical properties typical of conventional composites. Although the modulus is improved with the

addition of NaMMT, the tensile strength and elongation-at-break decreased dramatically with increasing clay loading. In contrast, the SAP composites showed improved tensile strength and elongation-at-break, in addition to improved modulus. The increase in the elongation-at-break substantially improves toughness. For example, a 45% increase in toughness was achieved at a 9.4 wt% SAP loading.

Table 3.1 Tensile properties of glassy epoxy composites reinforced by SAP and NaMMT clay nanoparticles.

Clay	Clay Loading[a] (wt%)	Tensile strength (MPa)	Tensile modulus (GPa)	Elongation-at-break (%)	Toughness (MJ/m^3)
Pristine	0.0	66.1	2.9	4.3	2.1
SAP	2.1	67.8	3.1	5.7	3.0
	5.4	70.2	3.1	8.9	4.9
	9.4	72.5	3.8	5.4	3.1
NaMMT	7.2	34.8	5.1	0.8	0.2
	12.4	29.4	5.2	0.6	0.1

[a] The clay loading is on a silicate basis; The standard deviations for all values is ~ 3%, except for the values of elongation-at-break and toughness for the SAP composites in which case the standard deviation is ~30%.

Representative strain-stress curves for epoxy – SAP nanocomposites are provided in Figure 3.3. The pristine epoxy showed a typical failure behavior for a brittle material. The stress increased with increasing loading to a maximum value, after which the specimen ruptured with little yield. Similar behavior was observed for the nanocomposites, except that the initial slopes were larger due to

the increased modulus and the stress maximum was increased due to increased strength. Also, the composites exhibited substantial yield and an increase in elongation-at-break, resulting in increased toughness. Although the standard deviations for the modulus and strength was less than 3%, the magnitude of the break at elongation was much larger (> 30%) and most likely dependent on local defects in the composites.
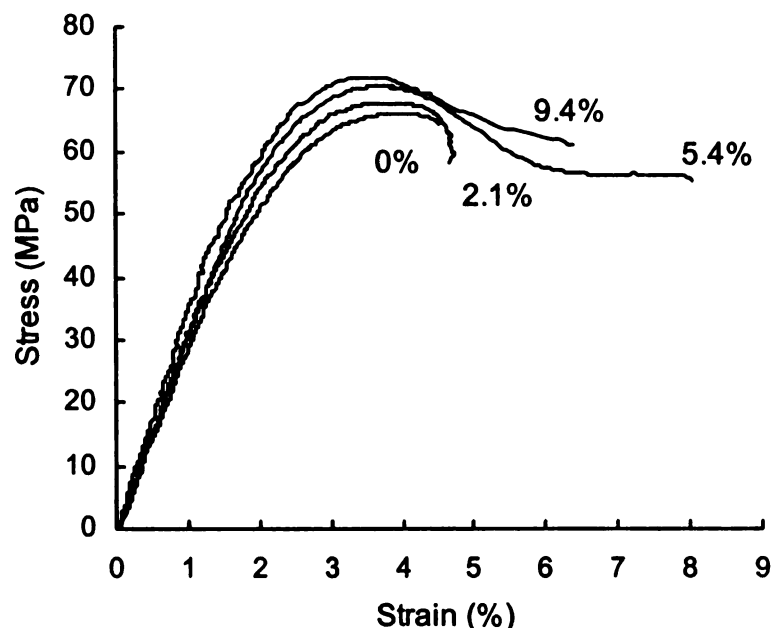
Figure 3.3 Representative stress - strain curves for glassy epoxy – SAP clay nanocomposites at the wt % clay loadings indicated.

DMA also showed improved storage modulus for the glassy epoxy – SAP nanocomposites, compared with pristine epoxy (Table 3.2). Additionally, the

glass transition temperatures of the composites are comparable to the pristine epoxy. However, the onium ion modified clay formed by ion exchange with cetyltrimethylammonium cations, denoted C16-SAP, which contains about 20 wt% organic components as determined from elemental analysis, causes the glass transition temperature of the polymer to decrease due to the plasticizing effect of the modifiers.

Table 3.2 Dynamic mechanical analysis (40 °C) of glassy epoxy composites filled with SAP and C16-SAP clay.

Clay	Loading[a] (wt%)	T_g[b] (°C)	Storage Modulus (GPa)
Pristine	0.0	87.2	2.7
SAP	5.2	86.9	3.0
	10.3	87.6	3.3
C16-SAP	4.1	84.2	2.9
	8.6	84.0	3.2

[a] Clay loading is on a silicate basis. [b] Estimated from tan δ_{max}.

As expected for the dispersion of rigid inorganic particles in a soft polymer matrix, far greater improvements in tensile strength, modulus and elongation-at-break were observed for rubbery epoxy - SAP nanocomposites (Table 3.3). A 730% increase in strength, 360% increase in modulus, and 86% increase in elongation-at-break was observed at a loading of 15.0 wt% SAP.

Table 3.3 Tensile properties of rubbery epoxy composites reinforced by SAP clay nanoparticles.

Clay Loading[a] (wt%)	Tensile strength (MPa)	Tensile modulus (MPa)	Elongation-at-break (%)
0	0.6	2.8	24.9
2.1	1.2	3.8	38.7
5.5	1.8	5.6	38.0
10.9	2.7	7.7	39.2
15.0	5.0	12.9	46.4

[a] Clay loading is on a silicate basis. The standard deviations for the values of strength, modulus, and elongation-at-break are <5 %.
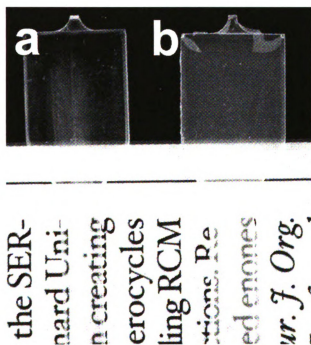
Figure 3.4 Pictures of (a) a pristine glassy epoxy polymer and (b) the corresponding epoxy - SAP nanocomposite containing 5.4 wt% clay.

Another advantage of synthetic SAP clay as a reinforcement agent is the optical transparency of the resulting composites (Figure 3.4). In contrast, the iron impurities in naturally occurring Na-MMT clay imparts an off-white color to the composites, along with reduced transparency [27].

3.4 Discussion

The irregular platelet stacking and associated high surface area of SAP allows for the reinforcement of both rubbery and glassy epoxy matrices without the need for organic modification of the basal surfaces (Tables 3.1 and 3.3). On the other hand, NaMMT provide improvements in modulus, but suffer from a severe loss of strength due to the non-uniform dispersion of aggregates in the polymer matrix. Although organic modification of the SAP basal surfaces by ion exchange with cetylammonium cations facilitates platelet dispersion and provides reinforcement, the glass transition temperature of the polymer is compromised due to the plastisizing effect of the modifier (Table 3.2). This is only one of several reasons why eliminating the use of an organic modifier in the formation of polymer nanocomposites can be advantageous.

The dispersion of SAP nanoparticles into glassy and rubbery epoxy matrices occurs with the retention of nanolayer aggregated in the form of tactoids (Figure 3.2). That is, the presence of single nanolayers in the polymer matrix is virtually non-existent. However, the tactoids are uniformly dispersed throughout

the polymer matrix. It has been previously observed that aggregated clay tactoids in glassy epoxy matrices typically improve modulus, but sacrifice strength and toughness, especially at high clay loadings [21, 24, 26]. The fracture mechanism in this case was attributed to the weak interaction between the stacked nanolayers and the development of microcracks between the stacked nanolayers. However, for the SAP-epoxy composites obtained in the present work, the clay nanolayers are not regularly stacked and the disordering of the aggregated nanolayers allows the polymer to fill at least some of the pores between nanolayers, thereby reducing the tendency toward microcrack formation. Thus, epoxy - SAP nanocomposites can approach the tensile properties of composites containing fully delaminated organoclay nanolayers [22].

The ability of exfoliated clay nanolayers to improve the strength and toughness of a rubbery epoxy matrix has been attributed in part to the ability of the single nanolayers to align under applied strain. It also has been suggested [28] that for the rubbery domain above T_g, the clay layers have better mobility than below T_g, leading to improvements in strength, as well as modulus. On the basis of the present work it can now be said that disordered clay tactoids provide strength and toughness analogous to exfoliated organoclay nanolayers. Moreover, the reinforcement is extended for the first time to glassy, as well as rubbery epoxy matrices. In fact, the present glassy system is the only reported example for which the modulus, strength and toughness all are improved without

sacrificing the glass transition temperature. Thus, disordered SAP clay tactoids are made even more appealing as reinforcing agents for epoxy matrices, not only because they avoid the undesirable plasticizing effects of an organic modifier, but also because they benefit both rubbery and glassy matrices and minimize costs by eliminating the need for an organic modifier. Still further, these benefits can be realized with relatively little loss in optical transparency (Figure 3.4).

3.5 Conclusion

A porous synthetic saponite-like material (denoted SAP) was used to reinforce rubbery and glassy epoxy polymers. Remarkably, reinforcement properties superior to those of organo-montmorillonite can be achieved without the need for a surface organic modifier, as evidenced by the improvements in tensile strength, modulus and toughness at temperature above and below the glass transition temperature of the polymer. The disordered stacking of clay platelets ~50 nm in lateral dimension gives rise to aggregated tactoids with a BET surface area of 920 m^2/g, an average BJH pore size of 5.0 nm, and a pore volume of 1.98 cm^3/g. These unique textural properties facilitate the dispersion of the tactoids into the polymer matrix and allow reinforcement of the polymer matrix in the absence of an organic modifier.

References

(1) Usuki, A.; Kojima, Y.; Kawasumi, M.; Okada, A.; Fukushima, Y.; Kurauchi, T.; Kamigaito, O. *J. Mater. Res.* **1993**, *8*, 1179.

(2) Ray, S. S.; Okamoto, M. *Prog. Polym. Sci.* **2003**, *28*, 1539.

(3) LeBaron, P. C.; Wang, Z.; Pinnavaia, T. J. *Appl. Clay Sci.* **1999**, *15*, 11.

(4) Becker, O.; Simon, G. P. *Adv. Polym. Sci.* **2005**, *179*, 29.

(5) Lloyd, S. M.; Lave, L. B. *Environ. Sci. Technol.* **2003**, *37*, 3458.

(6) Kornmann, X.; Lindberg, H.; Berglund, L. A. *Polymer* **2001**, *42*, 1303.

(7) Kloprogge, J. T.; Breukelaar, J.; Jansen, J. B. H.; Geus, J. W. *Clays Clay Miner.* **1993**, *41*, 103.

(8) Kloprogge, J. T.; Komarneni, S.; Amonette, J. E. *Clays Clay Miner.* **1999**, *47*, 529.

(9) Vogels, R. J. M. J.; Kerkhoffs, M. J. H. V.; Geus, J. W. *Stud. Surf. Sci. Catal.* **1995**, *91*, 1153.

(10) Reinholdt, M.; Miehe-Brendle, J.; Delmotte, L.; Tuilier, M.-H.; le Dred, R.; Cortes, R.; Flank, A.-M. *Eur. J. Inorg. Chem.* **2001**, *11*, 2831.

(11) Carrado, K. A. *Appl. Clay Sci.* **2000**, *17*, 1.

(12) Prihod'ko, R.; Sychev, M.; Hensen, E. J. M.; van Veen, J. A. R.; van Santen, R. A. *Stud. Surf. Sci. Catal.* **2002**, *142*, 271.

(13) Chastek, T. T.; Que, E. L.; Shore, J. S.; Lowy, R. J.; Macosko, C.; Stein, A. *Polymer* **2005**, *46*, 4421.

(14) Chastek, T. T.; Stein, A.; Macosko, C. *Polymer*, **2005**, *46*, 4431.

(15) Triantafillidis, C. S.; LeBaron, P. C.; Pinnavaia, T. J. *Chem. Mater.* **2002**, *14*, 4088.

(16) Park, J.; Jana, S. C. *Macromolecules* **2003**, *36*, 8391.

(17) Zanetti, M.; Camino, G.; Reichert, P.; Mulhaupt, R. *Macromol. Rapid Commun.* **2001**, *22*, 176.

(18) Xie, W.; Gao, Z. M.; Pan, W. P.; Hunter, D.; Singh, A.; Vaia, R. *Chem. Mater.* **2001**, *13*, 2979.

(19) Wang, K.; Chen, L.; Wu, J.; Toh, M. L.; He, C.; Yee, A. F. *Macromolecules* **2005**, *38*, 788.

(20) Triantafillidis, C. S.; LeBaron, P. C.; Pinnavaia, T. J. *J. Solid State Chem.* **2002**, *167*, 354.

(21) Miyagawa, H.; Foo, K. H.; Daniel, I. M.; Drzal, L. T. *J. Appl. Polym. Sci.* **2005**, *96*, 281.

(22) Lan, T.; Pinnavaia, T. J. *Chem. Mater.* **1994**, *6*, 2216.

(23) Lan, T.; Kaviratna, P. D.; Pinnavaia, T. J. *Chem. Mater.* **1995**, *7*, 2144.

(24) Park, J. H.; Jana, S. C. *Macromolecules* **2003**, *36*, 2758.

(25) Zilg, C.; Mulhaupt, R.; Finter, J. *Macromol. Chem. Phys.* **1999**, *200*, 661.

(26) Wang, K.; Wang, L.; Wu, J.; Chen, L.; He, C. *Langmuir* **2005**, *21*, 3613.

(27) Park, I.; Peng, H.-G.; Gidley, D. W.; Xue, S.; Pinnavaia, T. J. *Chem. Mater.* **2006**, *18*, 650.

(28) Shah, D.; Maiti, P.; Jiang, D. D.; Batt, C. A.; Giannelis, E. P. *Adv. Mater.* **2005**, *17*, 525.

CHAPTER 4

PALYGORSKITE AS AN EPOXY POLYMER REINFORCING AGENT

4.1 Introduction

Montmorillonite and other members of the smectite family of clay minerals have been extensively studied as polymer reinforcement agents [1-4]. In order to make these intrinsically hydrophilic clay compatible with polymer matrices, onium-ion exchange reactions normally are used to mediate the surface polarity. When the organoclay derivatives are dispersed as individual 1-nm thick sheets in a polymer matrix, resulting nanocomposites usually exhibit excellent mechanical properties, thermo-stability, barrier property, fire retardant, and other material properties.

Palygorskite and sepiolite have structures related to the 2:1 layered structure of smectite clays, except that the layers are pleated to form cross-linked ribbons [5,6]. This cross-linking feature precludes the possibility of exfoliating the structure into 1-nm thick nanoparticles. Nevertheless, owing to the relatively high surface area and lath morphology of these minerals, particularly in the case of palygorskite, they have found use as absorbents, pigments, catalysts, and rheological control agents [5, 7-10]. However, palygorskite has received relatively little attention as a polymer reinforcement agent with only a few studies

101

being devoted to composites of polyolefins, polyurethane, polyimide and polyamide [11-19].

In the present work we investigate the properties of pristine and silylated palygorskite for the reinforcement of rubbery and glassy epoxy polymers. Silylation has been used previously to modify the surface polarity of palygorskite [20], as well as other mineral [21-23] and synthetic silicates [24] with potential polymer reinforcement properties. Silylation also is used in the present work to enhance the hydrophobic character of palygorskite and to improve its dispersion in an epoxy matrix.

4.2 Experimental

4.2.1 Materials

The commercially available diglycidyl ethers of bisphenol A (DGEBA) with the structure shown in Scheme 4-1 were provided by the Shell company under the trade names Epon 828 [n=0 (88%), 1 (10%), 2 (2%)] and Epon 826 [n=0 (99%), n=1 (1%)]:

$$(4-1)$$
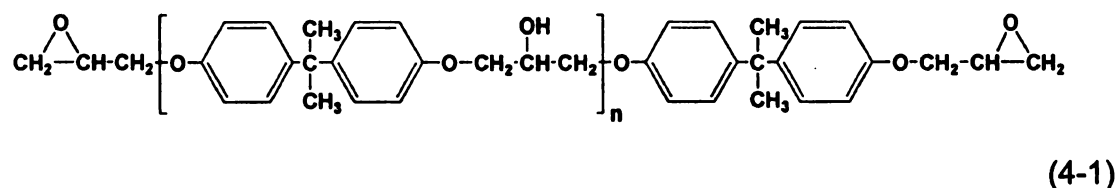
The curing agents, shown in Scheme 4-2, were α,ω-polyoxypropylene diamines provided by Huntsman Chemicals under the trade names Jeffamine

D2000 [x=33.2, MW~2000] and Jeffamine D230 [x=2.6, MW~230] or the glassy

system respectively (Scheme 4-2).

$$H_2N-\underset{\underset{CH_3}{|}}{CH}-CH_2\left[O-CH_2-\underset{\underset{CH_3}{|}}{CH}\right]_x NH_2$$
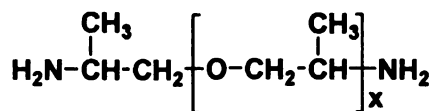
(4-2)

Palygorskite was provided by the Active Minerals Company LLC under the

trade name Acti-Gel 208. Other chemicals were purchased from Aldrich

Chemical Co. and were used as received.

4.2.2 Palygorskite purification

The as-received palygorskite was found to contain small amounts of

mineral impurities. A purification process was carried out by preparing a 10 wt%

aqueous suspension of the mineral and allowing the more dense impurities

(quartz and carbonates) to sediment out. After a certain sedimentation time, the

supernatant suspension was decanted off and the sedimentation process

continued. X-ray diffraction analysis of each sediment fraction provided an

indication of the purity of the mineral remaining in suspension. The purification

was repeated until there was no evidence by X-ray diffraction for the presence of

quartz or carbonate minerals in the sediment. The purified mineral remaining in

suspension then was collected and used to form nanocomposites for comparison

with composites made from as-received palygorskite. Survey experiments

revealed no difference in the mechanical properties of epoxy composites

prepared from the purified and as-received palygorskite. Accordingly, for use in all subsequent experiments, the as-received palygorskite was dispersed in acetone and subjected to sonification for 30 min. The suspension was evaporated in air to collect the mineral.

4.2.3 Palygorskite silylation

The silylation of palygorskite was carried out in a mixture of the clay and the silylation reagent in toluene under reflux conditions. A 1- to 2-g amount of palygorskite and a stoichiometric amount of silylation agent were added to 50 mL of toluene. The amounts of silylation agent used were determined by assuming there were 4 silanol sites per nm^2 of clay surface area. The mixture was submitted to ultrasonication for 30 min and then the suspension was heated under reflux for 4 h. The resulting silylated product was air-dried, ground in a mortar and pestle, and used for nanocomposite formation. The silylation reagents used were γ-aminopropyltrimethoxysilane (APTMS), N-dodecyltriethoxysilane (DTES), and 1,1,1,3,3,3-hexamethyldisilazane (HMSZ). The corresponding silylated palygorskite (PLG) clays were denoted APTMS-PLG, DTES-PLG, and HMSZ-PLG, respectively.

4.2.4 Composites Preparation.

Both as-received and silylated palygorskite materials were used to make rubbery or glassy epoxy composites. Equivalent amounts of epoxy monomer and curing agent were mixed at 75 °C for 10 min, out-gassed at room

104

temperature for 20 min, and transferred into a dog-bone shaped aluminum mold for curing. The composites were partially cured at 75°C for 3 h and then fully cured at 125°C for 3 h under nitrogen flow.

4.2.5 Characterization Methods

X-ray diffraction (XRD) patterns were obtained on a Rigaku rotaflex 200B diffractometer equipped with Cu Kα X-ray radiation and a curved crystal graphite monochromator, operating at 45 KV and 100 mA. Clay films for X-ray diffraction analysis were prepared by dripping droplets of aqueous clay suspension onto a glass slide and allowing the suspensions to dry. The diffraction patterns were recorded from 1 to 70 ° 2θ with a step scan of 0.02 °/point and a scan rate of 0.5 °/min. Cured composite samples were prepared by fitting rectangular flat specimens into the windows of aluminium holders. The patterns were recorded from 1 to 40 ° 2θ with a step interval of 0.05 °/point and a scan rate of 2 °/min.

TEM images were obtained on a JEOL 2010F 200kV field emission TEM with an acceleration voltage of 200 kV. The clay samples for TEM imaging were prepared by evaporating clay-ethanol suspensions on a holy carbon coated copper grid. Composites samples for TEM imaging are in the form of 80~100 nm thick thin sections supported on a copper grid.

The tensile measurements on dog-bone shaped samples were carried out at room temperature according to ASTM procedure D3039 using an SFM-20 United Testing System equipped with a laser extensometer. The measurements

were conducted with a crosshead speed of 25 mm/min for rubbery samples and 0.5 mm/min for glassy samples. The reported tensile parameters are values averaged over four independent specimens.

FTIR spectra of samples dispersed in KBr disks were recorded at ambient temperature on a Mattson Galaxy 3000 FTIR spectrometer over the range 400 to 4000 cm^{-1}. ^{29}Si MAS NMR spectra were obtained at 79.4 MHz on a Varian VXR-400S solid state NMR spectrometer equipped with a magic angle spinning probe. For each measurement the sample was spun at 4 kHz. The pulse delay was 400 s, and chemical shifts were referenced to talc. Thermogravimetric analyses (TGA) were carried out on a Cahn TG System 121 Analyser. The powdered clay samples were heated to 800 °C at a rate of 5 °C/min.

4.3 Results

4.3.1 Characterization and Purification of Palygorskite

Palygorskite, with an idealized unit cell formula of $M^{2+}_{(x-y+2z)/2} \cdot nH_2O$ [$Mg_{5-y-z}R_y\square_z$]$(Si_{8-x}R_x)O_{20}(OH)_2(H_2O)_4$, where R is Al(III) or Fe(III), $\square$ is an interstitial vacancy, and M^{2+} is an exchangeable cation, adopts the pleated layered structure shown in Figure 4.1 [6, 25]. The linked ribbons represent a 2:1 layer that is continuous along the a-axis, but of limited lateral extend along the b-axis. Rectangular channels, formed through the pleating of sheets, contain exchangeable Ca^{2+} and Mg^{2+} cations, zeolitic water, and water molecules bound

to coordinatively unsaturated metal ion centers at the edges of the ribbons. Small polar molecules, such as ammonia, and acetone, can access the tunnels by displacing the zeolitic water molecules upon partial dehydration of the clay materials. Further dehydration enables the formation of bonds between terninal Mg (II) and the small molecules to afford hybrid materials [26, 27].
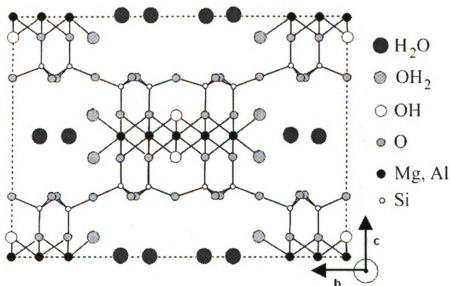
Figure 4.1 A schematic [100] projection of palygorskite structure [6].

Sedimentation of a 10% (w/w) aqueous suspension of the mineral was used to separate the clay from quartz and carbonate impurity phases [8]. Figure 4.2 shows the X-ray patterns of the sedimented fractions collected after different settling times. The impurity phases were almost completely removed from the suspension after an aging time of 14 days. Owing to the low concentrations of
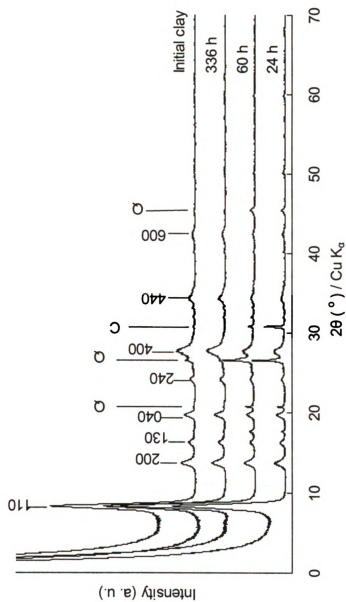
Figure 4.2 The hkl X-ray reflections of as-received palygorskite and of the sedimented fractions obtained upon aging a 10% (w/w) aqueous slurry of the mineral. Q and C mark diffraction peaks indicative of quartz and carbonate mineral impurities, respectively.

the impurity phases, composites made from the as-received and purified versions of the mineral showed no difference in mechanical properties. Thus, the as-received mineral was used in all nanocomposite experiments.

Nitrogen adsorption measurements indicated the BET surface area of the as-recived palygorskite to be 182 m^2/g, which is substantially larger than the surface area for pristine montmorillonite (~ 10 m^2/g). The TEM images provided in Figure 4.3 clearly show the presence of bundled lath-like crystals of palygorskite ~ 5- 20 nm in width and several µm in length. Thermal gravimetric analysis showed the loss of water over three temperature regions corresponding to the loss of 7.5 % (w/w) surface and zeolitic water at 25–130 °C, 3 % coordinated water (130–270 °C), and 6.5 % water due to dehydroxylation of the 2:1 layered structure (>270 °C) [10]. The ^{29}Si MAS NMR spectrum of the as-received palygorskite (not shown) contains two Q^3 peaks at –98 ppm and –92 ppm, corresponding to SiO_4 units at the central and edge positions of the ribbons, respectively [9]. The absence of a resonance characteristic of SiOH groups (~ -84 ppm), indicates that the fraction of silicon centers at the external surfaces of the laths is very small (<2 %).
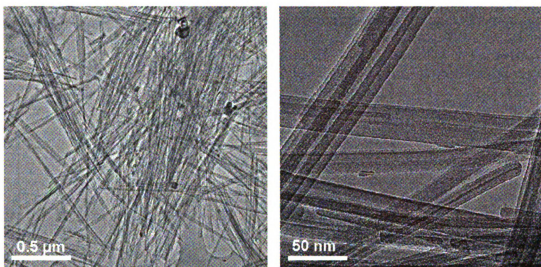
Figure 4.3 TEM images of as-received palygorskite.

4.3.2 Silylated Paygorskite

The silylation reactions of palygorskite with γ-aminopropyltrimethoxysilane (APTMS), N-dodecyltriethoxysilane (DTES), and 1,1,1,3,3,3-hexamethyldisilazane (HMSZ) resulted in no changes in the XRD pattern or the ^{29}Si MAS NMR spectrum of palygorskite. The N_2 adsorption-desorption isotherms show that the BET surface area of the HMSZ silylation product, denoted HMSZ-PLG, was reduced slightly to 122 m^2/g. The FTIR spectra of the as-received palygorskite and the HMSZ-PLG silylation product are compared in Figure 4.4. The appearance of weak C-H stretching vibrations near 2900 cm^{-1} are observed for HMSZ-PLG, indicating that trimethylsilyl groups have been coupled to the external surfaces of the mineral. Analogous FTIR bands were observed for the APTMS- and DTES- PLG reaction products. Additional evidence in favor

of silylation was provided by the inability of the silylation products to disperse in water.
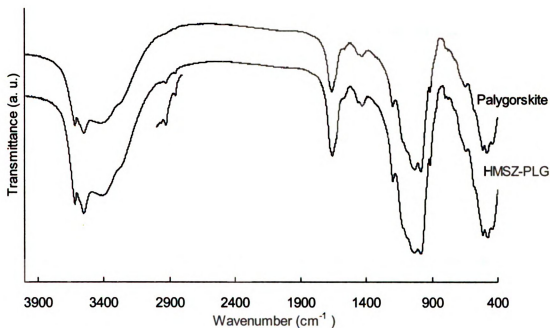
Figure 4.4 FTIR spectra (KBr) of as-received palygorskite and the HMSZ silylation product. The inset shows an expansion of the C-H stretching region between 2800-3000 cm^{-1} for HMSZ-palygorskite.

4.3.3 Epoxy Nanocomposites

Rubbery and glassy epoxy nanocomposites were prepared by dispersing as-received and silylated forms of palygorskite in degassed equivalent amounts of epoxy monomer and curing agent and then curing the mixtures under nitrogen. The dispersion of the mineral was qualitatively judged by examining the relative
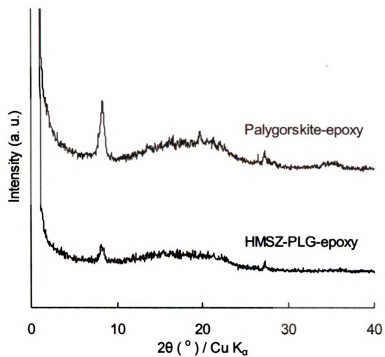
Figure 4.5 XRD patterns of the bottom sides of epoxy nanocomposite specimens

prepared from as-received and silylated palygorskite.
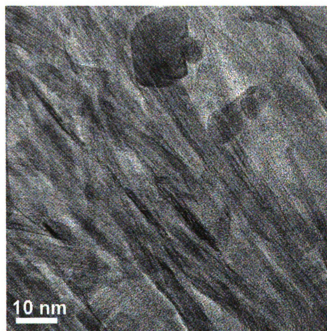
Figure 4.6 TEM image of a thin section of a glassy epoxy nanocomposite

containing 5% (w/w) of HMSZ-PLG

intensities of palygorskite diffraction peaks obtained from the bottom and top surfaces of the composite specimens. As seen by the comparison of 110 and 400 reflections in Figure 4.5, much more palygorskite settles to the bottom of the composite made from as-received palygorskite in comparison to the silylated palygorskite composite. The top surfaces of both specimens show no palygorskite reflections, indicating that there is a graded distribution of palygorskite from top to bottom in both cases. But the particle gradient is substantially less for the composite made from silylated palygorskite than for as-received palygorskite.

A TEM image of a thin-section of a glassy epoxy composite containing 5 % (w/w) HMSZ-PLG is shown in Figure 4.6. In comparison to the image for the pristine clay in Figure 4.3, the clay laths in the composite appear to be thinner, suggesting that the aggregation of clay laths is reduced in the composite.

Representative stress - strain curves for HMSZ-PLG reinforced rubbery epoxy composites are presented in Figure 4.7. The mechanical properties of rubbery and glassy epoxy composites containing 0 – 10 % (w/w) palygorskite are given in Table 4.1 and 4.2, respectively. Included in Table 1 for comparison are the tensile properties of a rubbery epoxy nanocomposite reinforced by an organo-montmorillonite [28]. The tensile properties of the rubbery composites are substantially improved in comparison to the pristine polymer, but less so for the glassy composites.
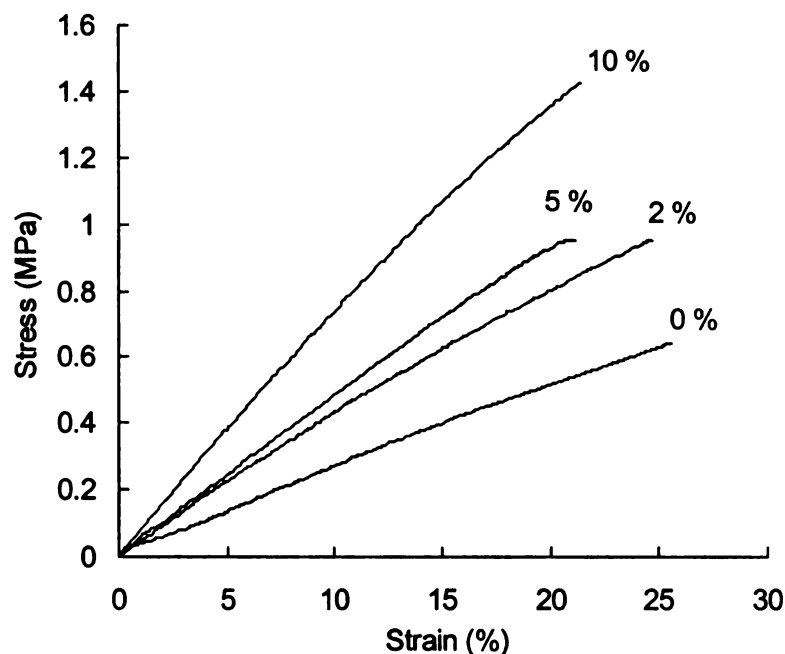
Figure 4.7 Representative strain-stress curves for rubbery epoxy composites containing different loadings of silylated palygorskite HMSZ-PLG.

4.4 Discussion

The commercial form of palygorskite used in this study contained detectable amounts of quartz and carbonate minerals (Figure 4.2). However, these impurity phases were present in such small amounts that their removal by sedimentation methods did not improve the nanocomposite performance properties of the mineral. The hydrophilic nature of pristine palygorskite arises from the presence of coordinated water at the edges of the pleated 2:1 layers and the filling of the

Table 4.1 The tensile properties of rubbery palygorskite-epoxy composites. Numbers in the parentheses are relative standard deviations.

Nanoparticle and Nanoparticle Loading		Tensile Strength (Mpa)	Tensile Modulus (Mpa)	Tensile Elongation (%)
None		0.62 (6.8%)	2.8 (5.0%)	25.0 (8.0%)
Palygorskite	2%	0.71 (8.2%)	4.4 (7.7%)	25.3 (9.2%)
	5%	0.74 (8.5%)	4.0 (6.9%)	20.7 (8.9%)
	10%	1.32 (7.3%)	5.0 (6.4%)	28.1 (9.0%)
APTMS-PLG	2%	0.81 (4.7%)	4.7 (7.0%)	24.0 (10.3%)
	5%	0.89 (5.5%)	3.5 (6.0%)	28.4 (8.8%)
	10%	1.03 (9.2%)	4.4 (7.3%)	21.8 (9.8%)
DTES-PLG	2%	1.18 (2.3%)	4.7 (5.2%)	30.9 (2.6%)
	5%	0.98 (4.2%)	3.5 (9.1%)	30.8 (5.5%)
	10%	1.47 (6.3%)	6.2 (8.4%)	26.0 (7.7%)
HMSZ-PLG	2%	0.97 (5.0%)	4.8 (3.8%)	24.3 (8.1%)
	5%	1.00 (7.2%)	5.4 (6.0%)	21.1 (6.0%)
	10%	1.35 (6.4%)	6.7 (9.5%)	21.2 (13.4%)
$CH_3(CH_2)_{17}NH_3^+$-montmorillonite-epoxy 28	0%	~0.5	~2.6	-
	2%	~0.8	~5.5	-
	5%	~1.5	~7.5	-
	10%	~3.3	~13	-

channels by zeolitic water (Figure 4.1). Thermal dehydration of the mineral removes the channel water, but dehydration is not expected to alter the hydrophilic nature of the laths, because terminal hydroxyl groups still decorate the external edge and base surfaces of the structure. Thus, pristine palygorskite was not effectively dispersed in the epoxy pre-polymer and tended to sediment out prior to polymer curing. However, silylation of the mineral substantially improved dispersion, even though a graded distribution of particles was evident based on the presence of observable XRD reflections from the bottom surfaces of a specimen containing 5 % (w/w) of the mineral (Figure 4.5).

The silylation of palygorskite was readily accomplished using γ-aminopropyltrimethoxysilane (APTMS), N-dodecyltriethoxysilane (DTES), and 1,1,1,3,3,3-hexamethyldisilazane (HMSZ) as silylating agents. The presence of silylated surfaces was verified by FTIR (Figure 4.4). Bands near 2900 cm^{-1} were assigned to C-H bond stretching modes of the grafted organosilane, in accord with previous assignments [22-24]. It is noteworthy that the broad bands at 3556 cm^{-1} due to coordinated water and at 3410 cm^{-1} and 3283 cm^{-1} due to zeolitic water [7] indicated the retention of the channel water after silylation in toluene under reflux conditions. The sharp band at 3620 cm^{-1} is assigned to the stretching mode of hydroxyl groups in the 2:1 ribbons. Thus, the silylation of the mineral was confined to hydroxyl groups at the external edge and basal surfaces. The hydrophobic nature of the silylated products was evidenced in part by the

inability to suspend the products in water.

Table 4.2 Tensile properties of glassy epoxy reinforced by silylated palygorskite

HMSZ-PLG.. Numbers in the parentheses are relative standard deviations.

Clay loading (wt%)	Tensile strength (MPa)	Tensile modulus (GPa)	Tensile elongation (%)
0%	66.1 (1.4%)	2.9 (7.0%)	3.9 (4.0%)
2%	67.1 (2.1%)	3.1 (8.7%)	3.6 (4.6%)
5%	66.0 (2.5%)	3.0 (3.2%)	3.9 (2.8%)
10%	68.9 (4.0%)	3.3 (5.3%)	3.5 (6.1%)

The comparison of tensile properties in Table 4.1 for a rubbery epoxy

matrix shows that as-received palygorskite provides some improvement in the

modulus, but little or no improvement in the tensile strength at loadings of 2 and

5 % (w/w). The abrupt increase in tensile strength at a loading of 10 % (w/w) is

associated with an increase in the viscosity of the pre-polymer – palygorskite

mixture. The increase in viscosity retards the settling-out of the as-received

mineral prior to curing and provides a more uniform dispersion of palygorskite

particles in the matrix. In comparison to the pristine mineral, the silylated mineral

improves the degree of dispersion at loadings of 2 and 5 % (w/w). Consequently,

improved tensile properties are observed at these lower loadings for the silylated

mineral. But at a loading level of 10 % (w/w), where the increased viscosity of

the pre-polymer facilitates the dispersion of the pristine mineral, there is little

difference in the tensile properties of the composites formed from as-received and silylated palygorskite.

It is remarkable that the pristine mineral in the absence of any organic modifiers provides approximately a two-fold increase in strength and modulus for the rubbery epoxy matrix at 10 % loading. Other pristine clay minerals (eg., montmorillonite) invariably weaken an engineering polymer, regardless of the level of loading. The low layer charge, lath-like morphology and high surface area (182 m^2/g) of palygorskite makes it much more suitable for polymer reinforcement in comparison to pristine smectite clays which retain their low surface area tactoidal form (<10 m^2/g) when dispersed in a polymer matrix.

In general, the as-received and silylated forms of palygorskite all provide a substantial benefit in tensile properties at a loading of 10 % (w/w), due in large part to the improved dispersion of the mineral laths in the matrix (cf., Table 4.1). However, as shown in Table 4.1 for $[CH_3(CH_2)_{17}NH_3]^+$ exchanged montmorillonite [28], this organoclay provides ~ 5 – 6-fold increases in tensile properties at 10 % (w/w) loading. In comparison, palygorskite at the same loading level provides only 2-3-fold improvements in tensile properties. Nevertheless, it also must be realized that the improvements achieved with palygorskite come at a level of organic modification that is < 0.2% of the levels needed to achieve the dispersion of montmorillonite in the polymer matrix. Thus, the benefit to cost ratio lies in favor of palygorskite.

Despite the reinforcement achieved for a rubbery epoxy matrix, little or no benefit is realized when silylated palygorskite is dispersed in a glassy matrix (cf., Table 4.2). In view of the pleated layer structure of palygorskite, the tensile properties of the mineral may be approaching those of the polymer matrix itself, thus precluding the possibility of reinforcement. Further studies are needed to explore this possibility.

Although palygorskite has been investigated as a reinforcement agent for several other polymer systems [11-19], the benefits seldom approach those observed in the present work. For instance, the tensile strength of polyethylene-palygorskite formed by in-situ polymerization was increased by a maximum of only 20 % in comparison to the pristine polymer [15, 16, 19]. For the related polypropylene-palygorskite composite system, the clay served as a good nucleating agent for isotactic polypropylene, and the relative crystallinity and crystallization temperature of the composite materials generally increased with filler content [17] An improvement of only 25% in mechanical properties was found for polyimide composites containing 5% palygorskite [13].

Among the best improvements previously reported for any palygorskite composite was the 220% boost in tensile strength found for polyurethane reinforced by 10% (w/w) of the mineral silylated by N-[3-(trimethoxysilyl)propyl]ethylenediamine [14]. As note above, comparable levels of reinforcement are obtained for the rubbery epoxy composites reported in the

present work, even without silylation of the mineral. Thus, the key to achieving polymer reinforcement benefits with palygorskite lies first in achieving optimal particulate dispersion, whether the dispersions are achieved through viscosity increases in the pre-polymer or through surface modification of the mineral itself.

4.5 Conclusion

Palygorskite, a silicate clay with a pleated 2:1 layered structure, has a lath-like particle morphology that makes the clay, in both pristine and silylated forms, an attractive candidate for the formation of polymer nanocomposites. Three silylation reagents were used for surface modification of the mineral, namely, aminopropyltrimethoxysilane (APTMS), N-dodecyltriethoxysilane (DTES), and 1,1,1,3,3,3-hexamethyldisilazane (HMSZ). The silylated palygorskite derivatives provided better dispersions in rubbery epoxy matrices than the pristine mineral, affording improvements in mechanical properties at low loadings levels of 2 and 5% (w/w). But at higher loadings where increases in the viscosity of the pre-polymer helps to stabilizes the mineral dispersion, little or no differences were observed for the reinforcement benefits provided by the pristine and silylated forms of palygorskite. Glassy epoxy nanocomposites formed from both pristine and silylated palygorskite exhibited marginal improvements in tensile properties regardless of the mineral loading level, suggesting that the tensile strength of the pleated sheet silicate may be approaching that of the

polymer matrix.

References

(1) Becker O.; Simon G. P. *Adv Polym. Sci.* **2005**, *179*, 29.

(2) D'Souza N. A. *Encyclopedia of Nanoscience and Nanotechnology* **2004**, *3*, 253.

(3) Okamoto M. *Encyclopedia of Nanoscience and Nanotechnology* **2004**, *8*, 791.

(4) Ray S. S.; Okamoto M. *Prog. Polym. Sci.* **2003**, *28*, 1539.

(5) Murray H. H. *Appl. Clay Sci.* **2000**, *17*, 207.

(6) U.S. Geological Survey Open-File Report 01-041: http://pubs.usgs.gov/of/of01-041/htmldocs/clays/seppaly.htm.

(7) Augsburger M. S.; Strasser E.; Perino E.; Mercader R. C.; Pedregosa J. C. *J Phys. Chem. Solids* **1998**, *59*, 175.

(8) Chipera S. J.; Bish D. L. *Clays Clay Miner.* **2001**, *49*, 398.

(9) D'Espinose de la Caillerie J-B, Fripiat J. J. *Clay Miner.* **1994**, *29*, 313-318.

(10) Guggenheim S.; van Groos A. F. K. *Clays Clay Miner.* **2001**, *49*, 433.

(11) Shen L.; Lin Y.; Du Q.; Zhong W.; Yang Y. *Polymer* **2005**, *46*, 5758.

(12) Wang L.; Sheng J.; *Polymer* **2005**, *46*, 6243.

(13) Lai S. Q.; Yue L.; Li T. S.; Liu X. J.; Lv R. G. *Macromol. Mater. Eng.* **2005**, *290*, 195.

(14) Ni P.; Li J.; Suo J.; Li S. *J. Mater. Sci.* **2004**, *39*, 4671.

(15) Du Z.; Rong J.; Zhang W.; Jing Z.; Li H. *J. Mater. Sci.* **2003**, *38*, 4863.

(16) Rong J.; Sheng M.; Li H.; Ruckenstein E. *Polym. Compos.* **2002**, *23*, 658.

(17) Medeiros E. S.; Tocchetto R. S.; Carvalho L. H.; Conceicao M. M.; Souza A. G. *J. Ther. Anal. Calorim.* **2002**, *67*, 279.

(18) Rong J.; Jing Z.; Li H.; Sheng M. *Macromol. Rapid Commun.* **2001**, *22*, 329.

(19) Rong J.; Li H.; Jing Z.; Hong X.; Sheng M. *J. Appl. Polym. Sci.* **2001**, *82*, 1829.

(20) Wang L.; Sheng J. *J. Macromol. Sci. Pure Appl. Chem. A40* **2003**, *11*, 1135.

(21) Grandjean J.; Bujdak J.; Komadel P. *Clay Miner.* **2003**, *38*, 367.

(22) Johnson L. M.; Pinnavaia T. J. *Langmuir* **1991**, *7*, 2636.

(23) Okutomo S.; Kuroda K.; Ogawa M. *Appl. Clay Sci.* **1999**, *15*, 253.

(24) He J.; Shen Y.; Yang J.; Evans D. G.; Duan X. *Chem. Mater.* **2003**, *15*, 3894.

(25) Fernandez M. E.; Ascencio J. A.; Mendoza-Anaya D.; Rodriguez Lugo V.; Jose-yacaman M. *J. Mater. Sci.* **1999**, *34*, 5243.

(26) Facey G. A.; Kuang W.; Detellier C. *J. Phys. Chem. B* **2005**, *109*, 22359.

(27) Kuang W.; Facey G. A.; Detellier C. *J. Mater. Chem.* **2006**, *16*, 179.

(28) Lan T.; Pinnavaia T. J. *Chem. Mater.* **1994**, *6*, 2216.

CHAPTER 5

MESOCELLULAR SILICA FOAM FOR POLYETHYLENE REINFORCEMENT

5.1 Introduction

Nanoparticle dispersion in polymer matrices provides an innovative pathway to combine the properties of polymers and filler materials (often inorganic particles). The enormous interacting surface area between polymer matrix and filler nanoparticles makes it possible to transfer the properties of the fillers, such as high strength, high thermal stability and low permeability, to the polymer even at low filler loadings [1]. More interestingly, when the nanoparticle fillers are capable of binding with the polymer matrix via chemical or physical bonding, such as hydrogen bonding, they may affect the crystallinity and phase behavior of polymers [2]. Nanocomposites can be divided into three categories depending on whether the filler has one, two, or three dimensions in the nanometer range. Clay minerals in exfoliated form are representative of the first type of nanoparticle filler, since the silicate sheets are 1-nm thickness, but up to several microns in diameter [3, 4]. Carbon nanotubes and metal nanoparticles are representative of the second and third types of nanoparticle fillers, respectively [5-7].

124

It is almost always necessary to modify inorganic filler particles for polymer reinforcement purposes. The use of organic modifiers, which usually have low molecular weight, may affect the properties of the composites via plasticizer effects [8, 9]. The organic modifiers also are susceptible to thermal degradation, and may initiate the restacking of clay layers or the decomposition of the polymer matrix [10, 11]. The complicated effects of modifier on nanocomposite formation make it difficult to correlate process-structure-property relationships to optimize nanocomposite reinforcement. Additionally, using organic modifiers increase the cost of composite processing.

Polyolefins are of critical significance in composite research, because they represent the most commonly used thermoplastic polymers. Conventional fillers, such as carbon fibers and glass fibers, are able to improve the mechanical properties of polyethylene at high filler loadings [12, 13]. However, the fibers have to be weaved to achieve uniform alignment, and, consequently, the composites are anisotropic and are reinforced only in the direction of the oriented fibers. More recently, clay minerals have been studied as polyolefin reinforcing agents [14, 15]. Since polyolefins are highly hydrophobic polymers, the preparation of polyolefin – clay nanocomposites requires modification to both clays and polymers to achieve compatibility. The former is usually via organic ion exchange reaction of the clay, and the latter is achieved by grafting maleic anhydride to the polymer.

The term "polymer mesocomposite" was used to distinguish composites reinforced by mesoporous silicas [16]. Mesoporous silicas can be synthesized using supermolecular assembly techniques. They exhibit controlled pores in the meso scale range (2-50 nm) and surface areas that are comparable to those of exfoliated clays [17]. Attempts have been made to intercalate polymer chains within the mesopores of silica particles using different techniques, such as in-situ monomer polymerization and employing high-pressure as a driving force for intercalation [18, 19, 20]. In a recent report, large pore wormhole mesostructured MSU-J silica, with and without the removal of the amine surfactant porogen, was used to reinforce epoxy polymers. Systematic improvements were achieved for the tensile strength, modulus, toughness, and elongation-at-break of the resulting composites. [16]

In the present study we investigated mesocellular foam-structured MSU-F silicas with different pore sizes for the preparation of polyolefin – silica mesocomposites. The MSU-F silicas have pore sizes greater than 20 nm and electrically neutral surfaces, making it possible to readily intercalate polymer even without surface modification of the silica or the polymer. We investigated both low density polyethylene (LDPE), and high density polyethylene (HDPE) as the polymer matrix. Both LDPE - and HDPE - silica mesocomposites exhibited improved tensile strength and modulus that are analogous to the best reported values for polyethylene - organo-clay nanocomposites.

5.2 Experimental

5.2.1 Materials

The LDPE pellets were Dow Polyethylene 6401 with a density of 0.922 g/cc, and the HDPE pellets were Dow Polyethylene 25455N with a density of 0.955 g/cc. Pluronic P123 Block Copolymer was purchased from BASF. All other chemicals were purchased from Aldrich, and used without further purification.

5.2.2 Mesoporous silica synthesis

Mesocellular foam silicas with large pore sizes, denoted MSU-F, were assembled using sodium silicate solution as the silica source and a triblock copolymer P123 as the structure-directing poregen. The MSU-F used in the present study was provided by Dr. Seong-Su Kim. Detailed preparation method was reported in a previous report [21]. When ethanol as a co-solvent substitutes in part for water at a concentration of 15 vol%, the product, denoted MSU-F2 exhibited further expanded pore size [22]. In a typical synthesis, 9.6 g (1.6 mmol) porogen P123 was dissolved in a mixed solution of 80 mL 1M acetic acid, 20 mL water and 60 mL ethanol in a shaking bath at room temperature for 1.5 h. After the introduction of 7.968 g (0.06 mol) tetramethylbezene, the solution was again mixed in a shaking bath at room temperature for 1 hour. A solution of sodium silicate (21.6 g containing 27% silica and 14% sodium hydroxide) was added to the porogen solution forming a milky suspension. The suspension was shaked at

35 °C for 20 h, and heated at 100 °C under static conditions for 20 h. The product was filtered, washed with water, dried in air and denoted MSU-F2. Both MSU-F and MSU-F2 were calcined at 600 °C for 4 hours to remove P123 and dried at 125 °C overnight prior to composite processing.

5.2.3 Mesocomposites preparation

Low density polyethylene (LDPE) and high density polyethylene (HDPE) were used as polymer matrices for the mesocomposites. The LDPE and HDPE pellets were dried at 75 °C under vacuum overnight beforehand. The composites were processed using a twin-screw extruder (DSM Research 15 cc Micro Extruder Injection molder), and the hot melt was transferred into a hot cylinder and injection molded. The processing conditions are listed in Table 5.1.

Table 5.1 The extrusion and injection molding conditions for pure polymers and their mesocomposites.

	Extrusion temperature (°C)	Extrusion duration (min)	Cylinder temperature (°C)	Mold temperature (°C)
LDPE	185	10	185	70
HDPE	195	10	195	70

5.2.4 Characterization

N_2 adsorption-desorption isotherms were recorded at −196 °C on a Micrometritcs ASAP 2010 sorptometer. Prior to analysis, samples were

outgassed at 150 $^{\circ}$C and 10^{-6} Torr for a minimum of 12 h. BET surface areas were calculated from the linear part of the BET plot and BJH pore sizes were obtained from adsorption isotherms.

Transmission electron microscopy (TEM) images were obtained on a JEOL 2200FS field emission microscope equipped with a ZrO/W Schottky electron gun and an accelerating voltage of 200 kV. The powdered samples were sonified in ethanol, and dripped onto 300 mesh copper grids. For composites, thin sections (~100 nm thick) of the composites were put on naked copper grids.

Tensile mechanical properties of dog-bone shaped specimens were tested according to ASTM procedure D3039 using an SFM-20 United Testing System equipped with a laser extensometer. The measurements were conducted at room temperature with a crosshead speed of 0.5 mm/min for LDPE and its composites and 1.5 mm/min for HDPE and its composites. The reported tensile values are the averages for 4 specimens with dog-bone shapes. The standard deviation for the modulus and strength was +/- 3%.

DSC measurements were conducted on a 2920 modulated DSC (TA Instruments). An 8 mg quantity of sample was heated to 185 $^{\circ}$C, and held at the same temperature for 10 min, before cooling down to room temperature. The heating and cooling rates were both 10 $^{\circ}$C/min.

The polarized light microscope images were obtained using a LSM 5 Pascal confocal microscopy (Carl Zeiss, Inc). A 1 mg quantity of polymer or composite specimen was melted between two glass slides to form a film for microscopy imaging.

5.3 Results and Discussion

The surface properties of MSU-F and MSU-F2 were analyzed using N_2 adsorption-desorption isotherms. The isotherm curves and pore size distributions are shown in Figure 5.1, and the surface properties are listed in Table 5.2. MSU-F has a BET surface area of 544 m^2/g, a cell size of 22 nm, and a window size of 11 nm. The cell size and window size were determined from the adsorption and desorption isotherms, respectively. MSU-F2 has a lower BET surface area, but larger pore sizes and pore volume, especially cell size, compared with MSU-F. The decrease in surface area of MSU-F2 might be due to the fact that it has a greater wall thickness. The foam mesostructure was clearly exhibited in the TEM images of both MSU-F and MSU-F2 (Figure 5.2). The cell size of MSU-F is centered around 20 nm, and the cell sizes of MSU-F2 is centered over a broad range around 50 nm, consistent with the N_2 isotherm results.

Figure 5.1 (a) The N_2 adsorption-desorption isotherms of MSU-F and MSU-F2. The curves were offset by 200 for clarity. (b) Cell size (solid lines) and window size (dash lines) distributions of MSU-F and MSU-F2 obtained from the adsorption and desorption isotherm curves, respectively. The distributions were determined by applying BJH model.

(a)

(b)
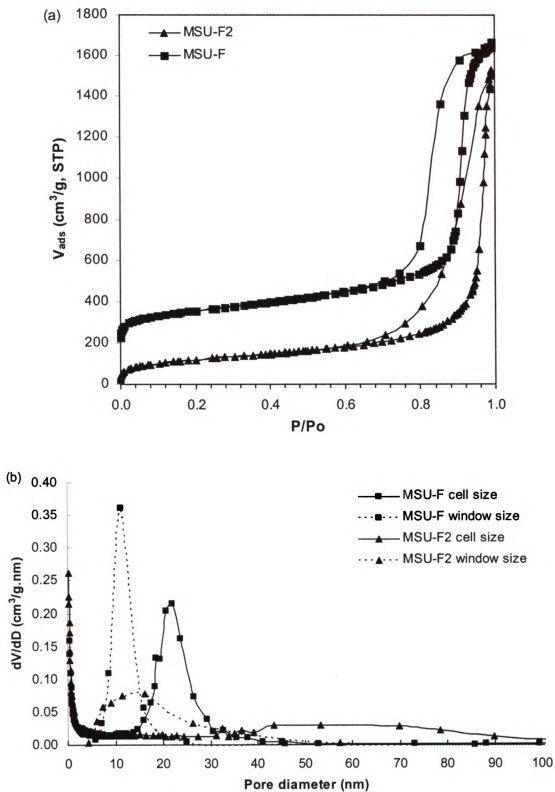
Table 5.2 The surface properties of MSU-F and MSU-F2

	BET S.A (m^2/g)	Cell size (nm)	Window size (nm)	Pore volume (cm^3/g)
MSU-F	544	22	11	2.24
MSU-F2	410	50~70	16	2.34

The relative standard deviations of the BET surface areas are less than 0.5%.
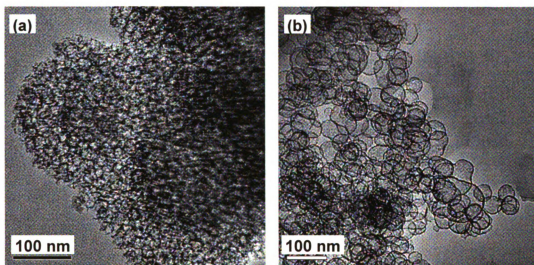
Figure 5.2 The TEM images of (a) MSU-F and (b) MSU-F2.

Both MSU-F and MSU-F2 were extruded with PE to make the mesocomposites. The optimum blending time was 10 min. Other attempts showed that too short an extrusion time (5 min) resulted in the presence of visible white particles in the products, while too much extrusion (15 min) lowered the mechanical performance of the composites. The TEM images of composite thin-sections (Figure 5.3) exhibit the presence of silica particles of semi-micron sizes and large blank polymer regions (not shown in the images). Despite of the non-

uniform silica dispersion, the polymer chains filled the pores of the silica particles, as revealed by the TEM EDS analysis showing the presence of C element in the silica porous region.
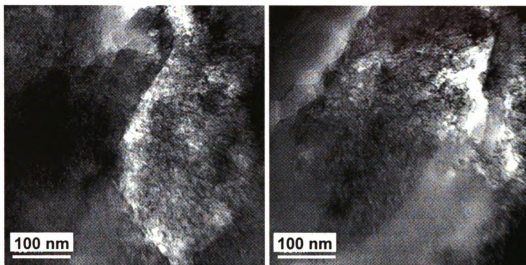
Figure 5.3 TEM images of thin-sections of a HDPE – MSU-F 4.2 wt% mesocomposites.

The crystallinity of the LDPE and its silica mesocomposites were studied using DSC (Table 5.3). The melting or crystallization temperatures of the composites are comparable with those of pure LDPE. However, the degree of crystallinity was slightly reduced with the addition of silica, especially at high loading of 7.4 wt%. Polarized light microscopy (PLM) is also a powerful tool to study polymer crystallinity, such as spherulite sizes and nucleation effects. The polarized light can only pass through the polymer crystal lamellas with a

matching chain orientation direction, and, consequently, gives bright spots. Polymer chains that are perpendicular to the polarize plane will appear as dark spots on the image. LDPE spherulites can be clearly seen in the PLM image (Figure 5.4). The diameters of the spherulites have a wide range from several microns to over 20 microns. In a LDPE mesocomposites containing 5.5 wt% MSU-F, the range of spherulite sizes is similar as in LDPE, despite the lose in contrast due to the scattering of light by the silica particles. HDPE has a higher crystallinity compared with LDPE, and, consequently, the addition of MSU-F had a greater effect in lowering the degree of crystallinity. A more than 10% decrease in degree of crystallinity was observed upon the addition of 8.6 wt% MSU-F. A decrease in crystallinity is commonly observed for polymer composites, especially those reinforced by nano- or sub-micron particles. The lose of crystallinity is related to the fast crystallization rate and the nucleation effects of the filler particles [23].

Due to the compatible surfaces and good dispersion of silica in the polymer matrix, the foam-structured mesoporous silicas provided substantial reinforcement in mechanical properties to both LDPE and HDPE. For LDPE, the addition of 8.3 wt% MSU-F improved the strength and modulus by 55% and 100%, respectively (Table 5.4). This improvement is comparable to that achieved in PE-organo-clay systems that require extensive modification of both polymer and clay [14, 15]. However, at low MSU-F loading (5.5 wt%), the

improvement in strength and modulus was less significant. The elongation at break decreased with the addition of MSU-F. The large pore sizes of MSU-F allow polymer intercalation inside the pores, and, consequently, provided reinforcement to the polymer. Similar improvement was achieved using MSU-F2, which had larger pore sizes than MSU-F, indicating that a further expansion of pore sizes of the silicas has negligible effects on the reinforcement.

Table 5.3 The crystallinity of LDPE and HDPE mesocomposites.

Polymer	Filler and loading (wt%)	Melting temp. (°C)	Crystallization temp. (°C)	ΔH_m [a] (J/g)	Degree of crystallinity [b] (%)
LDPE	Pristine	111.6	97.0	111.1	38.3
	MSU-F 5.5	111.6	96.9	112.8	38.9
	MSU-F 8.3	111.6	97.1	105.3	36.3
	MSU-F2 7.4	112.0	97.4	101.7	35.1
HDPE	Pristine	133.1	115.4	200.2	69.0
	MSU-F 4.2	133.1	116.0	187.0	67.3
	MSU-F 8.6	132.7	117.0	162.0	61.1

[a] The heat of fusion was obtained from the area under the melting curve from DSC scan.
[b] The degree of crystallinity was obtained by comparing the ΔH_m with the 290 J/g heat of fusion for a 100% crystalline polyethylene.

When HDPE was used as the polymer matrix, substantial improvement was also observed with the addition of MSU-F (Table 5.5). Specifically, the strength and modulus were improved by 40% and 60% respectively at 8.6 wt% MSU-F loading. Unlike the LDPE system, improvement was also achieved at a low loading 4.2%. Both tensile elongation and elongation at break were reduced

with the addition of MSU-F. However, they were not significantly weakened at the low loading (4.2 wt%).
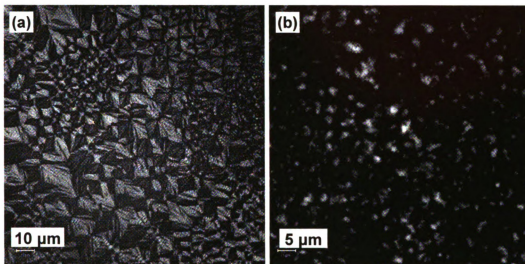
Figure 5.4 PLM images of (a) LDPE and (b) a LDPE – MSU-F 5.5 wt% loaded mesocomposite.

Compared with other commonly used inorganic filler materials for polyethylene reinforcement, there are advantages of large pore mesostructured silicas. Firstly, no surface modification is necessary for both the silica and the polymer; secondly, the reinforcement in mechanical properties far exceeds those of composites made from regular sphere silicas [24]; thirdly, due to the mesoporous structure of MSU-F, the reinforcement benefit is comparable to the best reported PE – organo-clay nanocomposites; fourthly, the isotropic nature of

the MSU-F pore system eliminates the issue of orientation, which is a common occurrence for fibrous fillers.

The oxygen permeability of LDPE was increased by 15.7% with the addition of 5.5 wt% MSU-F, and by 42.6% with the addition of 7.4 wt% MSU-F2 (Table 5.4). The reduction in crystallinity may contribute to the increased permeability of the mesocomposites. This phenomenon is consistent with the literature studies on composites membrane permeability and selectivity, which attributed the increase in permeability to increases in free volume between the polymer matrix and filler surfaces [25]. This result further indicates that even greater improvement in material properties can be expected once better compatibility of PE and silica surfaces is achieved.

Table 5.4 The mechanical properties and oxygen permeabilities of LDPE – silica mesocomposites.

	Loading (wt%)	Tensile strength (MPa)	Tensile modulus (MPa)	Elongation at break (%)	Oxygen permeability $(cc.mil/m^2d)$
none	-	14.1	119.7	104.0	5456.7
MSU-F	5.5	15.8	156.8	42.3	6311.0
	8.3	21.8	240.3	32.2	-
MSU-F2	3.0	13.7	164.6	49.5	-
	7.4	20.3	243.7	41.1	7779.5

The relative standard deviations are less than 3% for strength and modulus, and are less than 20% for the elongation.

Table 5.5 The mechanical properties of HDPE – silica mesocomposites.

	Loading (wt%)	Tensile strength (MPa)	Tensile modulus (MPa)	Tensile Elongation (%)	Breaking elongation (%)
pristine	-	21.9	733	11.7	830
MSU-F	4.2	26.8	891	9.5	670
MSU-F	8.6	31.1	1165	8.2	28

The relative standard deviations are less than 3% for strength and modulus, and are less than 20% for the elongation.

5.4 Conclusion

Mesoporous silica MSU-F with large pore sizes allow polyethylene intercalation inside the porous regions without the need for surface modifiers. LDPE- or HDPE- mesocomposites formed from MSU-F silica exhibited significantly improved strength and modulus, despite the in-homogeneous overall dispersion of the silica in the polyethylene matrix. However, the crystallinity of the mesocomposites was slightly reduced, as were the barrier properties, indicating some weakness in surface affinity between polyethylene and silica particles. Chemical modification might be able to further improve the dispersion of silica, and to enhance the compatibility between polymer and silica particles.

References

(1) Mark, J. E. *Acc. Chem. Res.* **2006**, *39*, 881.

(2) Usuki, A.; Hasegawa, N.; Kato, M. *Adv. Polym. Sci.* **2005**, *179*, 135.

(3) Ray, S. S.; Okamoto, M. *Prog. Polym. Sci.* **2003**, *28*, 1539.

(4) Okada, A.; Usuki, A. *Macromol. Mater. Eng.* **2006**, *291*, 1449.

(5) Moniruzzaman, M.; Winey, K. I. *Macromolecules* **2006**, *39*, 5194.

(6) Balazs, A. C.; Emrick, T.; Russell, T. P. *Science* **2006**, *314*, 1107.

(7) Glogowski, E.; Tangirala, R.; Russell, T. P.; Emrick, T. *J. Polym. Sci. Part A: Polym. Chem.* **2006**, *44*, 5076.

(8) Triantafillidis, C. S.; LeBaron, P. C.; Pinnavaia, T. J. *Chem. Mater.* **2002**, *14*, 4088.

(9) Park, J.; Jana, S. C. *Macromolecules* **2003**, *36*, 8391.

(10) Zanetti, M.; Camino, G.; Reichert, P.; Mulhaupt, R. *Macromol. Rapid Commun.* **2001**, *22*, 176.

(11) Xie, W.; Gao, Z. M.; Pan, W. P.; Hunter, D.; Singh, A.; Vaia, R. *Chem. Mater.* **2001**, *13*, 2979.

(12) Paesano, A.; Cohee, D.; Palmese G. R. *J. Thermoplast. Compos.* **2003**, *16*, 139.

(13) Van Dyke J. D.; Gnatowski, M.; Burczyk, A. *J. Appl. Polym. Sci.* **2002**, *83*, 2562.

(14) Zhang, M.; Sundararaj, U. *Macromol. Mater. Eng.* **2006**, *291*, 697.

(15) Hotta, S.; Paul, D. R. *Polymer* **2004**, *45*, 7639.

(16) Park, I.; Peng, H.-G.; Gidley, D. W.; Xue, S.; Pinnavaia, T. J. *Chem. Mater.* **2006**, *18*, 650.

(17) Corma, A. *Chem. Rev.* **1997**, *6*, 2373.

(18) He, J.; Shen, Y.; Yang, J.; Evans, D. G.; Duan, X. *Chem. Mater.* **2003**, *15*, 3894.

(19) Ji, X.; Hampsey, J. E.; Hu, Q.; He, J.; Yang, Z.; Lu, Y. *Chem. Mater.* **2003**, *15*, 3656.

(20) Reid, B. D.; Ruiz-Trevino, F. A.; Musselman, I. H.; Balkus, K. J., Jr.; Ferraris, J. P. *Chem. Mater.* **2001**, *13*, 2366.

(21) Kim, S. S.; Pauly, T. R.; Pinnavaia, T. J. *Chem. Comm.* **2000**, *17*, 1661.

(22) Kim, S. S.; Pinnavaia, T. J. unpublished results.

(23) Xie, Y.; Yu, D.; Kong, J.; Fan, X.; Qiao, W. *J. Appl. Polym. Sci.* **2006**, *100*, 4004.

(24) Zhang, M. Q.; Rong, M. Z.; Zhang, H. B.; Friedrich, K. *Polym. Eng. Sci.* **2003**, *43*, 490.

(25) Takahashi, S.; Paul, D. R. *Polymer* **2006**, *47*, 7535.

CHAPTER 6

CONCLUSIONS AND FUTURE DIRECTIONS

6.1 Comparison of Various Polymer Reinforcing Agents

In the proceeding chapters, three inorganic particles, namely, synthetic saponites, palygorskite, and mesocellular silica foam (MSU-F), have been studied as polymer reinforcing agents with little or no need for a surface organic modifier. The polymer matrices included thermoset epoxy and thermoplastic polyethylene. In this chapter, as a conclusion to the thesis, epoxy - synthetic saponite nanocomposites and polyethylene (PE) - MSU-F mesocomposites will be compared with literature reports on nanocomposites based on epoxy and PE made from different reinforcing particles to evaluate the advantages of synthetic saponite and MSU-F as polymer reinforcing agents.

6.1.1 Nanoparticles for Epoxy Reinforcement

Spherical alumina nanoparticles have been used for epoxy reinforcement in both untreated or silylation forms. At loadings in the range of 1 to 10 wt%, the inorganic alumina had negligible effects on the tensile strength and modulus of epoxy [1]. In a separate study, it has been shown that inorganic alumina improved the tensile modulus by 40% at a loading of 15%, but weakened the strength and elongation, while [3-(2-aminoethylamino)-propyl]-triethoxysilane

modified alumina could only manage to maintain the strength and modulus of pristine epoxy [2].

Silica nanoparticles in epoxy polymers can be formed in-situ by mixing alkoxysilane (TEOS) aqueous solution with epoxy monomer in organic solvent to form a homogenous mixture [3-5]. The gelation reaction of hydrolyzed TEOS occurs simultaneously with the evaporation of solvents, resulting in a colloidal dispersion of silica nanoparticles in the epoxy resin. In a representative report, epoxy - silica nanocomposites made through the in-situ sol-gel method exhibit a 15% increase in tensile modulus, a 40% increase in fracture toughness and same strength, compared with pristine epoxy, at a filler loading of 8 wt% [4]. Fumed silica can also be directly introduced to a mixture of epoxy monomer and curing agent to form nanocomposites upon epoxy curing. However, dramatic decreases in stress and elongation were observed [6].

Ever since Iijima first discovered carbon nanotubes in 1991, carbon nanotubes have been attractive polymer reinforcing agents due to the combination of their superb mechanical properties, electrical conductivities, and thermal stability and conductivity [7]. Molecular modeling approaches have predicted greater improvement in material properties [8]. Even after purification, carbon nanotubes still have a great tendency to form bundles through aggregations. Therefore, in order to achieve good dispersion in an epoxy matrix, carbon nanotubes need to be either surface modified or to be put into a

homogenous suspension in a solvent, followed by mixing with epoxy prepolymer. Plasma treatment and maleic anhydride grafting of the carbon nanotubes provided a 50% increase in tensile strength, a 100% increase in tensile modulus, as well as improvement in elongation and glass transition temperature at a loading of only 1 wt%[9]. However, such improvements were based on a rubbery epoxy system, which is relatively soft and easy to reinforce. The reinforcement of carbon nanotubes became less significant for rigid glassy epoxies. For example, in a study that utilized acetone to achieve carbon nanotube dispersion, the addition of 0.5 wt% carbon nanotubes improve the tensile strength by 100% for an soft epoxy (tensile strength was 5.4 MPa for pristine epoxy), but had no effects on a glassy epoxy with a tensile strength of 45.5 MPa. The reason for the latter results was attributed to poor interfacial interaction between the carbon nanotubes and the polymer [10].

Carbon nanofibers also have been used to reinforce epoxy. At a 2 wt% nanofiber loading, increase of 17% and 14% can be achieved in strength and modulus, respectively [11]. However, the strength tends to decrease with increase in carbon nanofiber loadings [11, 12].

Epoxy - organo-clay nanocomposites have been extensively studied. Great improvements were reported for rubbery epoxy matrices. More than a 10-fold increase in strength and modulus is realized by the addition of 15 wt% of the exfoliated organoclay [13]. However, for clays dispersed in glassy epoxies, the

strength of the nanocomposites was not significantly improved [14-16]. Even when uniform dispersion of exfoliated or intercalated clay nanolayer is achieved in epoxy, a 25% decrease in strength compared with pristine epoxy is observed with the addition of 5 wt% organoclay, although the modulus is improved by 40% [16]. It was proposed that the presence of intercalated clay nanolayers may initiate the rupture of the composites under stress and, consequently, lower the mechanical properties.

In chapter 3, a synthetic saponite was investigated for rigid glassy epoxy reinforcement. Compared with the other nanoparticles for glassy epoxy reinforcement, saponite is the only example that improves the tensile strength, modulus, elongation and toughness of the polymer. Additionally, facile dispersion of the saponite nanoparticles in the polymer matrix can be achieved without the need for an organic surface modifier.

6.1.2 Nanoparticles for Polyethylene Reinforcement

Polyethylene (PE) is one of the most extensively used thermoplastic polymers. Property enhancement of PE using various nanoparticles has been studied, and the representative results are summarized in Table 6.1. The results obtained for LDPE - MSU-F mesocomposites described in chapter 5 also are included for comparison.

Table 6.1 Comparison of various inorganic particles for PE reinforcement.

Composite system		Filler Loading	Tensile strength (MPa)	Tensile modulus (MPa)	Breaking elongation (%)
LDPE - MSU-F		-	14.08	119.7	104.0
		8.3 wt% (3.8 vol%)	21.80	240.3	32.2
HDPE - oriented carbon fiber [17]		-	30.5	1076	600
		50 vol%	317	$3.1*10^4$	-
LDPE - CNT [18]		-	10.7	235	380
		10 wt%	15.6	444	12
LLDPE - glass fiber [19]		-	10.4	74	34
		20 wt%	8.9	79	26
HDPE - [20]		-	29	870	440
	silica particle	0.75 vol%	30	900	440
	g-PBA silica	0.75 vol%	29	1100	330
LLDPE - [21]		-	11.8	190	>400
	organo-MMT	7 wt%	15.3	435	>400
	organo-MMT, g-MAH-PE	7 wt%	18.8	569	221

LLDPE, g-PBA, MMT, and g-MAH are abbreviations for linear LDPE, polybutyl acrylate-grafted, montmorillonite, maleic anhydride grafted, respectively.

Mesocellular silica foam MSU-F provides far better reinforcement for PE in comparison to glass fiber and spherical silica nanoparticles. The reason may be due to the mesoporous structure of MSU-F which isolates the polymer in the mesopores. The reinforcements provided by carbon nanotubes and organo-clay are comparable with those achieved by MSU-F. However, the former two composites required complicated processing methods. For example, 10 cycles of extrusion and molding were needed to achieve good dispersion of CNT in PE.

In the PE - organo-clay system, both clay and polymer must be modified to enhance surface compatibility. Carbon fibers provided significant reinforcement to PE, but a loading as high as 50 vol% was required. Additionally, the carbon fibers had to be weaved and oriented in PE, making the composites anisotropic. In comparison to other particles, MSU-F is a good reinforcing agent for PE, and the composites can be made readily through conventional melt blending.

6.2 Future Directions

Synthetic saponite with an irregularly stacked morphology has proven to be an effective reinforcing agent for epoxy polymers. However, the composite preparation requires on the assistance of ultrasonication in solvent suspension to break down saponite particles to the nanoscale prior to composite preparation. Therefore, epoxy - saponite nanocomposite deserves further exploration to simplify the preparation procedures by avoiding the use of solvent and ultrasonication. Possible methods include saponite edge decoration to reduce the edge-face interactions between clay nanolayers.

The use of saponite for polymer reinforcement deserves further expansion into polymer systems other than epoxy. Preliminary studies on PE - saponite composites prepared through melt-blending showed no improvement in the strength of the composites, possibly due to (i) incompatibility between the saponite surfaces and the highly hydrophobic PE matrix; (ii) the presence of sub-

micron saponite particles. The first limitation may be solved by employing a small amount of maleic anhydride grafted PE into the system to enhance surface compatibility. Regarding the second limitation, a new technique has been reported that has a ultrasonic slit die attached to a compounding extruder [22]. This technique has been used in enhancing organo-clay dispersion in polyolefin, and may have a promising ability to disperse saponite in polyolefin as well.

One of the advantages of synthetic saponite is that it has an irregularly stacked layered morphology. Therefore, organic modification of the clay surfaces no longer is necessary to achieve delamination of the layers. It will be interesting to use saponite to form nanocomposites based on polymers that require high processing temperature, such as nylon, polystyrene, polyimides and poly(ethylene terephthalate). For these polymers, it has been reported that alkylammonium exchanged clays have the modifiers decomposed at the polymer processing temperatures [23]. Therefore, a completely inorganic reinforcing agent, such as synthetic saponite, can be a great advantage in developing polymer nanocomposites.

Mesocellular MSU-F foam has the ability to reinforce polyethylene without any surface modification. The questions remaining in this research are whether or not PE chains intercalate into MSU-F pores and, if so, whether the structure or crystallinity of the PE chains is altered in the MSU-F pores. Preliminary investigation has been carried out by measuring composite density. It is known

that pristine LDPE and silica have a density of 0.92 g/cc and 2.15 g/cc, respectively, and that MSU-F has a pore volume of 2.3 cc/g. The density of a 5.5 wt% LDPE - MSU-F mesocomposites should be either 0.95 g/cc or 0.85 g/cc, assuming that the porous region on MSU-F surfaces is filled with LDPE or empty, respectively. Experimentally, a 1 cm X 6 mm X 2 mm pristine LDPE block and a 5.5 wt% LDPE - MSU-F mesocomposite block were both emerged into ethanol in a 10 mL graduate cylinder, and the mass and volume of the material were recorded to calculate the density. The densities of LDPE and the 5.5 wt% LDPE - MSU-F mesocomposite were 0.93 g/cc and 0.95 g/cc, respectively, agreeing with the assumption that the mesopores on MSU-F were filled with LDPE chains. However, more elaborate evidence for pore filling is needed. Such evidence may be obtained by using positron annihilation lifetime spectroscopy for the measurement of free volume in the composite [24]. TEM-EDS line scan is a promising way to image the 3-D structure of the composites. Another approach is to use HF to etch the silica portion of the composite and image the remaining polymer portion. It may be possible to fill the silica voids with heavy scattering materials to enhance the contrast. However, maintaining empty pores during TEM sample preparation, particularly under microtome conditions, will be a challenging task.

Preliminary studies indicate that MSU-F provides little reinforcement benefit for polypropylene. Further exploration of the PP - MSU-F system will require the study of polymer structure in silica pores, as described above.

To conclude, this thesis research hopefully has demonstrated that inorganic particles with suitable surface properties can be used to make polymer nanocomposites that are as good, if not better, than those made from organically modified particles. Saponite and MSU-F are two examples. A wide range of inorganic nanoparticles, such as layered and fibrous alumina, layered and large pore zeolites, silica nanoparticles, carbon nanotubes, nano clay, makes the field of polymer nanocomposites research full of excitements and opportunities.

References

(1) Naous, W.; Yu, X. Y.; Zhang Q. X.; Naito, K.; Kagawa, Y. J. *Polym. Sci. Part B* **2006**, *44*, 1466.

(2) Vassileva, E.; Friedrich, K. *J. Appl. Polym. Sci.* **2006**, *101*, 4410.

(3) Liu, Y. L.; Lin, Y. L.; Chen, C. P.; Jeng, R. L. *J. Appl. Polym. Sci.* **2003**, *90*, 4047.

(4) Deng, S.; Ye, L.; Friedrich, K. *J. Mater. Sci.* **2007**, *42*, 2766.

(5) Zhang, H.; Zhang, Z.; Friedrich, K.; Eger, C. *Acta. Mater.* **2006**, *54*, 1833.

(6) Preghenella, M.; Pegoretti, A.; Migliaresi, C. *Polymer* **2005**, *46*, 12065.

(7) M. Moniruzzaman, K. I. Winey, *Macromolecules*, **2006**, *39*, 5194.

(8) Xiao J.; Gillespie, J. W. *Polym. Eng. Sci.* **2006**, *8*, 1051.

(9) Tseng, C.; Wang, C.; Chen, C. *Chem. Mater.* **2007**, *19*, 308.

(10) Ci, L.; Bai, J. *Comp. Sci. Tech.* **2006**, *66*, 599.

(11) Zhou, Y.; Pervin, F.; Rangari, V. K.; Jeelani, S. *Mater. Sci. Eng. A* **2006**, *426*, 221.

(12) Choi, Y.; Sugimoto, K.; Song, S.; Gotoh, Y.; Ohkoshi, Y.; Endo, M. *Carbon* **2005**, *43*, 2199.

(13) Lan, T.; Pinnavaia, T. J. *Chem. Mater.* **1994**, *6*, 2216.

(14) Miyagawa, H.; Foo, K. H.; Daniel, I. M.; Drzal, L. T. *J. Appl. Polym. Sci.* **2005**, *96*, 281.

(15) Park, J. H.; Jana, S. C. *Macromolecules* **2003**, *36*, 2758.

(16) Wang, K.; Wang, L.; Wu, J.; Chen, L.; He, C. *Langmuir* **2005**, *21*, 3613.

(17) Paesano, A.; Cohee, D.; Palmese, G. R. *J. Thermoplast. Compos. Mater.* **2003**, *16*, 139.

(18) Xiao, K. Q.; Zhang, L. C.; Zarudi, I. *Compos. Sci. Tech.* **2007**, *67*, 177.

(19) Van Dyke. J. D.; Gnatowski, M.; Burczyk, A. *J. Appl. Polym. Sci.* **2002**, *83*, 2562.

(20) Zhang, M. Q.; Rong, M. Z.; Zhang, H. B.; Friedrich, K. *Polym. Eng. Sci.* **2003**, *43*, 490.

(21) Hotta, S.; Paul, D. R. *Polymer* **2004**, *45*, 7639.

(22) Swain, S. K.; Isayev, A. I. *Polymer* **2007**, *48*, 281.

(23) He, A.; Hu, H.; Huang, Y.; Dong, J.-Y.; Han, C. C. *Macromol. Rapid Commun.* **2004**, *25*, 2008.

(24) Park, I.; Peng, H.-G.; Gidley, D. W.; Xue, S.; Pinnavaia, T. J. *Chem. Mater.* **2006**, *18*, 650.